UNIVERSITAT POLITÈCNICA DE CATALUNYA BARCELONATECH

Optimal sizing and operation planning of microgrids and operation analysis of charging stations for electric vehicles

by

Ioannis Zenginis

UNIVERSITAT POLITÈCNICA
DE CATALUNYA
BARCELONATECH

Departament de Teoria
del Senyal i Comunicacions

Centre
Tecnològic
de Telecomunicacions
de Catalunya

iquadrat

Optimal sizing and operation planning of microgrids and operation analysis of charging stations for electric vehicles

Doctoral Thesis

By

Ioannis Zenginis[1,3]

Submitted to the Universitat Politècnica de Catalunya (UPC)
in partial fulfillment of the requirements for the degree of
DOCTOR OF PHILOSOPHY

Supervisors:

Dr. Christos Verikoukis[2], Dr. John Vardakas[3] and Dr. Luis Alonso Zárate[1]

[1] Department of Signal Theory and Communications (TSC), Polytechnic University of Catalonia (UPC), Barcelona, Spain
[2] Catalan Telecommunications Technology Centre (CTTC), Barcelona, Spain
[3]Iquadrat Informatica, Barcelona, Spain

Barcelona, October 2018

Abstract

Energy and transportation sectors are going through major changes as a result of technological advances, depletion of fossil fuels and climate change. With regard to the energy sector, the future smart grid is expected to be an interconnected network of small-scale and self-contained microgrids, in addition to a large-scale electric power backbone. By utilizing microsources, such as renewable energy sources, energy storage systems and vehicle-to-grid systems, microgrids target to satisfy the customers' energy demands in a safe, reliable, economic and environmentally friendly way. With regard to the changes in the transportation sector, internal combustion engine vehicles are expected to be gradually replaced by electric vehicles, which are considered to be a promising solution for mitigating the impact of transportation sector on the environment. The presented thesis deals with two main topics; the first one refers to the optimal sizing and operation planning of microgrids comprising various urban building types, while the second one is related to the operation of fast charging stations for electric vehicles that are located in densely populated areas.

The first objective of the thesis is to examine the effect of energy exchanges among interconnected buildings with diverse load profiles on the sizes of power equipment to be installed at the buildings. To this end, a mixed integer linear programming optimization framework is presented that determines the optimal capacities of photovoltaic panels, energy storage systems, and inverters, as well as the optimum management of the generated power. As a first step, the benefits of cooperation among buildings that are already interconnected through an existing point of common coupling is examined. The cooperation benefits are derived by comparing the buildings' costs when they participate in the microgrid with their costs when they operate as separate entities. As a second step, a different microgrid topology is proposed where energy exchanges take place through a common DC bus. In this way, neighboring buildings that are not already physically connected can be members of the same microgrid. Moreover, the optimization results for the new topology are obtained by using the Nash bargaining method, through which the benefits of cooperation are equally distributed among the participating members. Finally, the possible integration of new buildings in the existing microgrid at a later time point is also examined.

The second objective of the thesis is to provide an accurate operation analysis of fast charging stations for electric vehicles. To this end, a novel queuing theory-based model is presented that classifies the various electric vehicles by their battery size. As a first step, it is analyzed a charging station that contains DC outlets, and the electric vehicles recharge their batteries up to the maximum possible level. The proposed model takes into account the arrival rates and state of charge of the electric vehicles' batteries when arriving at the station, in order to compute the maximum number of customers that can be served, subject to an upper bound for the waiting time in the queue. In addition, a charging strategy is proposed, which allows the charging station to serve more customers without any increase in

the queue waiting time. As a second step, it is considered that the charging station can serve both DC and AC electric vehicle classes, while a more flexible way is adopted for denoting the customers' recharging patterns. Based on these additional novelties, the overall profit margin of the charging station operator, and the queue waiting times of the DC and AC classes are calculated under two different pricing policies.

List of publications

Journals

I. Zenginis, J. S. Vardakas, N. Zorba and C. Verikoukis, "Analysis and quality of service evaluation of a fast charging station for electric vehicles," *Energy*, vol. 112, pp. 669-678, Oct. 2016.

I. Zenginis, J. S. Vardakas, N. Zorba and C. Verikoukis, "Performance Evaluation of a Multi-standard Fast Charging Station for Electric Vehicles," *IEEE Trans. Smart Grid,* 2017.

I. Zenginis, J. S. Vardakas, C. Echave, M. Morató, J. Abadal, and C. Verikoukis, "Cooperation in microgrids through power exchange: An optimal sizing and operation approach," *Appl. Energy,* vol. 203, pp. 972-981, Oct. 2017.

J. S. Vardakas, **I. Zenginis,** N. Zorba, C. Echave, M. Morató, and C. V. Verikoukis, "Electricity savings through efficient cooperation of urban buildings: the smart community case of Superblocks in Barcelona," to appear in *IEEE Com. Mag,* 2018.

I. Zenginis, J. S. Vardakas, C. Echave, M. Morató, J. Abadal, and C. Verikoukis, "Optimal power equipment sizing and management for cooperative buildings in microgrids," to appear in *IEEE Trans. Ind. Informat,* 2018

Book Chapters

I. Zenginis, J. S. Vardakas, P. V. Mekikis, and C. Verikoukis, "Cooperative Energy Management in Microgrids," Transportation and Power Grid in Smart Cities: Communication Networks and Services, John Wiley, UK, 2017.

International Conferences

J. S. Vardakas, and **I. Zenginis,** "A Survey on Short-Term Electricity Price Prediction Models for Smart Grid Applications," in Proc. WICON 2014, Lisbon, Portugal, 12-14 Nov. 2014.

J. S. Vardakas, **I. Zenginis,** and M. Oikonomakou, "Peak Demand Reduction Through Demand Control: A Mathematical Analysis," in Proc. ICTF 2016, 6-8 July, Patras, Greece.

Contents

List of Figures

List of Tables

List of abbreviations

CCS	combined coupler standard
CDF	cumulative distribution function
CHP	combined heat and power
CS	charging spot
EMS	energy management system
ESS	energy storage system
EV	electric vehicle
EVSE	electric vehicle supply equipment
FCS	fast charging station
FPP	flat-rate pricing policy
LAN	local area network
LC	load controller
MC	micro-source controller
MG	microgrid
MGCC	microgrid central controller
MILP	mixed integer linear programming
MPC	model predictive control
NPV	net present value
PCC	point of common coupling
PDF	probability distribution funtion
PV	photo-voltaic
QoS	quality of service
RES	renewable energy sources
SoC	state of charge
SoE	state of energy
SPP	scheduled pricing policy
TI	time interval
V2B	vehicle-to-building
V2G	vehicle-to-grid
V2H	vehicle-to-home

Nomenclature for chapters 3 and 4

$A_{PV}(b)$	building's b available surface for installing PVs (m^2)
B	number of buildings
B_U	number of additional buildings
$C(b)$	total annualized cost for building b (€)
$C'(b)$	total annualized cost for building b when it is separately optimized (€)
$C_A(b)$	equipment acquisition cost for building b (€)
$C_{ad}(b)$	annualized cost of additional building b (€)
$C_{ad,max}(b)$	maximum annualized cost of additional building b (€)
$C_{ad,min}(b)$	minimum annualized cost of additional building b (€)
c_{bus}	per unit installation cost of the DC bus (€/m)
$C_C(b)$	NPV of carbon emission taxes cost for building b (€/kg)
$C_{in}(b)$	annualized cost of initial building b (€)
$C_{in,max}(b)$	maximum annualized cost of additional building b (€)
$C_{in,min}(b)$	minimum annualized cost of additional building b (€)
c_j	per unit installation cost of technology j
$C_M(b)$	NPV of maintenance cost for building b (€)
$C_{max}(b)$	maximum annualized cost for building b (€)
$C_{min}(b)$	minimum annualized cost for building b (€)
$C_O(b)$	NPV of electricity supplying cost for building b (€)
$C_q(b)$	value of buildings' b annualized cost in the interval q (€)
$C_R(b)$	NPV of replacement cost for building b (€)
$Carb_{int}$	carbon intensity of the MG's region (kg/kWh)
$Carb_{tax}$	carbon emission taxes (€/kg)
CRF	capital recovery factor
CSV	coalition savings (€)
f	objective value
CSV_{nt}	savings of the new MG topology (€)
d	discount rate
$H_{c,EV}(v,t)$	EV's v charging power at time interval t (kW)
$H_{d,EV}(v,t)$	EV's v discharging power at time interval t (kW)
$H_{EV}^{ESS}(v,t)$	power provided to EV v by the ESS at time interval t (kW)
$H_L^{EV}(v,t)$	power provided by EV v for covering the load at time interval t (kW)
$H_{EV}^{G}(v,t)$	power provided to EV v by the main grid at time interval t (kW)
$H_{EV}^{MG}(v,t)$	power provided to EV v by the MG at time interval t (kW)
$H_{EV}^{PV}(v,t)$	power provided to EV v by the PVs at time interval t (kW)
$L_{bus}(b)$	length of the DC bus for building b (m)
$life_j$	lifetime of technology j (yr)
m	number of linearization intervals of the objective function
$n_{c,ESS}$	charging efficiency of the ESS
$n_{c,EV}$	charging efficiency of the EVs

$n_{d,ESS}$	discharging efficiency of the ESS
$n_{d,EV}$	discharging efficiency of the EVs
$N_{ESS}(b)$	capacity of building's b ESS (kW)
n_{INV}	efficiency of the inverter
$N_{INV}(b)$	capacity of building's b inverter (kW)
n_{PV}	efficiency of the PV array
$N_{PV}(b)$	capacity of building's b PV panels (kW)
$P_{c,ESS}(b,t)$	charging power of building's b ESS during time interval t (kW)
$P_{c,EV}(b,t)$	charging power of building's b EVs during time interval t (kW)
$P_{d,ESS}(b,t)$	discharging power of building's b ESS during time interval t (kW)
$P_{d,EV}(b,t)$	discharging power of building's b EVs during time interval t (kW)
$P_{EV}^{ESS}(b,t)$	power from building's b ESS used for charging EVs at time interval t (kW)
$P_{L}^{ESS}(b,t)$	power transferred from building's b ESS to the load at time interval t (kW)
$P_{MG}^{ESS}(b,t)$	power sold to the MG by building's b ESS at time interval t (kW)
$P_{L}^{EV}(b,t)$	power transferred from building's b EVs to the load at time interval t (kW)
$P_{G,buy}(b,t)$	power imported from the main grid by building b at time interval t (kW)
$P_{EV}^{G}(b,t)$	power imported from the main grid for charging building's b EVs at time interval t (kW)
$P_{L}^{G}(b,t)$	power imported from the grid by building b at time interval t (kW)
$P_{G,sell}(b,t)$	power sold to the main grid by building b at time interval t (kW)
$P_{L}(b,t)$	power demand of building b at time interval t (kW)
$P_{MG,buy}(b,t)$	power imported by the MG by building b at time interval t (kW)
$P_{ESS}^{MG}(b,t)$	power from the MG used for charging building's b ESS at time interval t (kW)
$P_{EV}^{MG}(b,t)$	power from the MG used for charging building's b EVs at time interval t (kW)
$P_{L}^{MG}(b,t)$	power imported from the MG for covering building's b load at time interval t (kW)
$P_{MG,sell}(b,t)$	power sold to the MG by building b at time interval t (kW)
$P_{ESS}^{PV}(b,t)$	power from building's b PV used for charging its ESS at time interval t (kW)
$P_{EV}^{PV}(b,t)$	power from building's b PVs used for charging the EVs at time interval t (kW)
$P_{G}^{PV}(b,t)$	power sold to the main grid by building b at time interval t (kW)
$P_{L}^{PV}(b,t)$	power generated by building's b PVs at time interval t and is used for self-consumption (kW)
$P_{MG}^{PV}(b,t)$	power generated by building's b PVs and sold to the MG at time interval t (kW)
$P^{PV,pro}(b,t)$	power generated by building's b PVs at time interval t (kW)
$P^{PV,unit}(b,t)$	building's b PV normalized power generation (kW)
r_1, r_2	price coefficients
$R_{G,buy}(t)$	price of buying power from the main grid at time interval t (€/kWh)
$R_{G,sell}(t)$	price of selling power to the main grid at time interval t (€/kWh)
$R_{MG,buy}(t)$	price of buying power from the MG at time interval t (€/kWh)
$R_{MG,sell}(t)$	price of selling power to the MG at time interval t (€/kWh)
rep_j	number of replacements of technology j

$SoE_{ESS}(b,t)$	state of energy of building's b ESS at time interval t (kWh)
$SoE_{ESS,max}$	maximum state of energy of the ESS (kWh)
$SoE_{ESS,min}$	minimum state of energy of the ESS (kWh)
$SoE_a(v)$	arrival state of energy of EV v (kWh)
$SoE_d(v)$	departure state of energy of EV v (kWh)
$SoE_{EV}(v,t)$	state of energy of EV v at time interval t (kWh)
$SoE_{ESS,max}$	maximum state of energy of the EV (kWh)
$SoE_{ESS,min}$	minimum state of energy of the EV (kWh)
$SV(b)$	savings of building b (€)
T	optimization horizon
$T_a(v)$	arrival time of EV v
$T_d(v)$	departure time of EV v
U	Time point that the additional buildings join the MG
$u_{ESS}(b,t)$	binary variable used for the definition of the ESS operation
$u_{EV}(b,t)$	binary variable used for the definition of the EV operation
$u_{ex}(b,t)$	binary variable used for the definition of the power exchanges in the MG
$u_{ESS}^{unit}(b,t)$	binary parameter, which is equal to 1 only for $t=t_0$
$u_{EV}^{unit}(v,t)$	binary parameter, which is equal to 1 only for $t=T_a(v)$
V_b	number of EVs in building b
w	Sum of the annualized costs of the buildings (€)
w'	sum of the buildings' annualized costs when they are separately optimized (€)
w_{nt}	sum of the annualized costs of the buildings in the new MG topology (€)
X	duration of participation of the additional buildings in the project (yr)
Y	lifetime of the project (yr)
$Yrep_j$	year of 1st replacement of technology j (yr)
z	objective value
Z_{ESS}	ESS's charging rate
$Z_{EV}(v)$	EV's charging rate
Greek symbols	
Δt	duration of time slot t (hour)
λ_{PV}	capacity of PV panels that can be installed per available surface (kW/m^2)
$\lambda_q(b)$	special ordered variables (only two adjacent $\lambda_q(b)$ can be non-zero)
Ξ	a very large number
$\Phi(b)$	revenue for building b (€)
μ_{bus}	per unit maintenance cost of the DC bus (€/m)
μ_j	per unit maintenance cost of technology j (€/kW or kWh)
Subscripts	
b	building index
j	technology index
t	time interval index
v	EV index
y	year index

Nomenclature for chapter 5

a	total load of the system
a_c	load of c-class EVs
a_{c1}	load of subclass c_1 EVs
a_{c2}	load of subclass c_2 EVs
$a_{\max}$	maximum load
B_c	battery capacity of c-class EVs (kWh)
C	number of EV classes
c_v	coefficient of variation of the superposed charging time distribution
d	discount offered to subclass c_1 EVs
E_{EVs}	mean energy supplied to the EVs (kWh)
F_c	arrival SoC CDF of c-class EVs
f_c	arrival SoC PDF of c-class EVs
G	CDF of the superposed charging time
g	PDF of the superposed charging time
G_c	CDF of c-class EVs charging time
g_c	PDF of c-class EVs charging time
h_c	market shares of EV classes
k_c	probability that a c-class EV enters a CS
k_{c1}	probability that a subclass c_1 EV enters a CS
k_{c2}	probability that a subclass c_2 EV enters a CS
$L_{M/D/s}$	mean number of customers waiting in the queue in an M/D/s system
$L_{M/G/s}$	mean number of customers waiting in the queue in an M/G/s system
$L_{M/M/s}$	mean number of customers waiting in the queue in an M/M/s system
m	mean superposed charging time (h)
m_c	mean charging time of c-class EVs (h)
m_{c1}	mean charging time of subclass c_1 EVs (h)
m_{c2}	mean charging time of subclass c_2 EVs (h)
P_{EVs}	mean power drawn by the EVs (kW)
P_{DC}	power rate of the CSs (kW)
R	operator's revenue (€)
$R^{'}$	operator's revenue when the charging strategy is activated (€)
r	energy price (€/kWh)
$r^{'}$	energy price for subclass c_1 EVs (€/kWh)

s	number of CSs
$SoCA_c$	arrival SoC of c-class EVs
$SoCD_c$	departure SoC of c-class EVs
$SoCD_{thr}$	departure SoC threshold when the charging strategy is activated
T	superposed charging time (h)
t	time (h)
T_c	charging time of c-class EVs (h)
v	variance of the superposed charging time distribution
W	mean queue waiting of the EVs (h)
W_q	QoS criterion for the queue waiting time (h)
x_c	residual SoC increase of c-class EVs
x_{c1}	residual SoC increase of subclass c_1 EVs
Greek symbols	
γ	increase in the arrival rate capacity when the charging strategy is activated
λ	superposed arrival rate (EVs/h)
λ_c	arrival rate of c-class EVs (EVs/h)
λ_{c1}	arrival rate of subclass c_1 EVs (EVs/h)
λ_{c2}	arrival rate of subclass c_2 EVs (EVs/h)
$\lambda_{c,\max}$	maximum arrival rate of c-class EVs (EVs/h)
$\lambda_{\max}$	maximum arrival rate capacity (EVs/h)
$\lambda'_{c,\max}$	maximum arrival rate of c-class EVs (EVs/h) (the charging strategy is activated)
$\lambda'_{\max}$	maximum arrival rate capacity (EVs/h) (the charging strategy is activated)
ρ	utilization rate of the system
σ_c	percentage of c-class EVs that accept the operator's offer
τ	time interval where the arrival rates are equal to their maximum values (h)
ψ	correction function used for the calculation of the queue waiting time
Subscripts	
c	c-class EVs
c_1	subclass c_1 EVs
c_2	subclass c_2 EVs

Nomenclature for chapter 6

$a_{c,\delta}$	load of c-class EVs during the interval I_δ
$a_{c1,\omega,j}$	load of subclass c_1 EVs during I_ω
$a_{c2,\omega,j}$	load of subclass c_2 EVs during I_ω
$a_{c3,\omega,j}$	load of subclass c_3 EVs during I_ω
a_δ	total load of the system during I_δ
B_c	battery capacity of c-class EVs (kWh)
C	number of EV classes
d_h	duration of interval Z_h (h)
E_c	amount of energy obtained by c-class EVs (kWh)
$E_{thr,j}$	energy threshold (kWh)
$E_{V,\delta}$	mean energy provided to the EVs during the interval I_δ (kWh)
E_{V,ω,j,R_j}	the amount of energy provided to the EVs at price R_j during the interval I_ω (kWh)
$E_{V,\omega,j,R_j^{'}}$	the amount of energy provided to the EVs at price $R_j^{'}$ during the interval I_ω (kWh)
EXP_{AC}	operator's daily expenses for the AC system when the FPP is activated during the whole day (€)
$EXP_{AC}^{'}$	operator's daily expenses for the AC system when the FPP and the SPP are activated during different parts of the day (€)
EXP_δ	operator's expenses during I_δ (€)
EXP_{DC}	operator's daily expenses for the DC system when the FPP is activated during the whole day (€)
$EXP_{DC}^{'}$	operator's daily expenses for the DC system when the FPP and the SPP are activated during different parts of the day (€)
$EXP_{\omega,j}$	operator's expenses during I_ω (€)
F_c	CDF of c-class EVs' recharging pattern
f_c	PDF of c-class EVs' recharging pattern
$f_{c1,j}$	PDF of subclass c_1 EVs' recharging pattern
$F_{c2,j}$	CDF of subclass c_2 EVs' recharging pattern
$f_{c3,j}$	PDF of subclass c_3 EVs' recharging pattern
$G_c(t)$	CDF of c-class EVs' charging time
$g_c(t)$	PDF of c-class EVs' charging time
$g_{c1,j}(t)$	PDF of subclass c_1 EVs' charging time
$G_{c2,j}(t)$	CDF of subclass c_2 EVs' charging time
$g_{c3,j}(t)$	PDF of subclass c_3 EVs' charging time
$G_\delta(t)$	CDF of the superposed charging time during I_δ
$g_\delta(t)$	PDF of the superposed charging time during I_δ
$H_\delta(t)$	number of time slots of interval I_δ characterized by constant energy price R_h

I_δ	time interval during which the FPP is activated
I_ω	time interval during which the SPP is activated
$L_{\delta,M/G/s}$	mean number of customers waiting in the queue in an M/G/s system during I_δ
$L_{\delta,M/M/s}$	mean number of customers waiting in the queue in an M/M/s system during I_δ
m_c	mean charging time of c-class EVs (h)
$m_{c1,j}$	mean charging time of subclass c_1 EVs when $E_{thr,j}$ is activated (h)
$m_{c2,j}$	mean charging time of subclass c_2 EVs when $E_{thr,j}$ is activated (h)
$m_{c3,j}$	mean charging time of subclass c_3 EVs when $E_{thr,j}$ is activated (h)
m_δ	mean superposed charging time during I_δ (h)
$N_{c1,j}$	percentage of c-class EVs belonging to subclass c_1 when $E_{thr,j}$ is activated
$N_{c2,j}$	percentage of c-class EVs belonging to subclass c_2 when $E_{thr,j}$ is activated
$N_{c3,j}$	percentage of c-class EVs belonging to subclass c_3 when $E_{thr,j}$ is activated
P_{AC}	power rate of the AC outlet (kW)
P_{DC}	power rate of the DC outlets (kW)
$P_{v,\delta}$	power transferred to the EVs under FPP (kW)
$P_{v,\omega,j}$	power transferred to the EVs under SPP when $E_{thr,j}$ is activated (kW)
R	price that the operator sells energy when the FPP is activated (€)
R_h	price that the operator buys energy during time slot Z_h (€)
$R_j^{'}$	price that the operator sells energy under SPP when $E_{thr,j}$ is activated (€)
RVN_{AC}	operator's daily revenue from the AC system when the FPP is activated during the whole day (€)
$RVN_{AC}^{'}$	operator's daily revenue from the AC system when the FPP and the SPP are activated during different parts of the day (€)
RVN_δ	operator's revenue during I_δ (€)
RVN_{DC}	operator's daily revenue from the DC system when the FPP is activated during the whole day (€)
$RVN_{DC}^{'}$	operator's daily revenue from the DC system when the FPP and the SPP are activated during different parts of the day (€)
$RVN_{\omega,j}$	operator's revenue during I_ω (€)
s	number of CSs
T_c	charging time of c-class EVs (h)
$T_{c,max}$	maximum value of T_c (h)
$T_{c,min}$	minimum value of T_c (h)
T_δ	superposed charging time of the system during I_δ (h)
T_L	specified time period for the definition of the tail of the queue waiting time (h)
$T_{Q,\delta}$	customers' waiting time in the queue during I_δ (h)
v_δ	variation of the superposed charging time distribution
$W_{AC,\delta}$	EVs' mean waiting time in the AC queue during I_δ (h)

$W_{DC,\delta}$	EVs' mean waiting time in the DC queue during I_δ (h)
$W_{l,j}$	mean queue waiting time values that define the activation of different $E_{thr,j}$ when the SPP is applied (h)
W_Q	QoS criterion for the mean waiting time in the queue (h)
W_ω	EVs' mean waiting time in the queue during I_ω (h)
Z_h	time slot belonging in the interval I_δ
Greek symbols	
Γ	operator's daily profit margin when the FPP is activated during the whole day
$\Gamma^{'}$	operator's daily profit margin when the FPP and the SPP are activated during different parts of the day
Δ	number of time intervals that a day consist of
ΔSoC_c	increase in the SoC of c-class EVs' batteries during fast charging
$\Delta SoC_{c,thr,j}$	threshold in the change of SoC of c-class EVs' batteries when $E_{thr,j}$ is activated
$\Delta SoC_{c,max}$	maximum increase in the SoC of c-class EVs' batteries during fast charging
$\Delta SoC_{c,min}$	minimum increase in the SoC of c-class EVs' batteries during fast charging
$\lambda_{c,\delta}$	mean arrival rate of c-class EVs during I_δ (EVs/h)
$\lambda_{c1,\omega,j}$	mean arrival rate of subclass c_1 EVs when $E_{thr,j}$ is activated (EVs/h)
$\lambda_{c2,\omega,j}$	mean arrival rate of subclass c_2 EVs when $E_{thr,j}$ is activated (EVs/h)
$\lambda_{c3,\omega,j}$	mean arrival rate of subclass c_3 EVs when $E_{thr,j}$ is activated (EVs/h)
λ_δ	aggregated mean arrival rate of EVs during I_δ (h)
$\Xi_{c,j}$	percentage of c-class EVs that quit the FCS without recharging when $E_{thr,j}$ is activated
ρ_δ	utilization rate of the system during I_δ
$\Sigma_{c,j}$	percentage of c-class EVs that obtain as much energy as the operator's energy threshold $E_{thr,j}$
τ_δ	duration of I_δ (h)
τ_ω	duration of I_ω (h)
Subscripts	
AC	AC system
c	c-class EVs
c_1	subclass c_1 EVs
c_2	subclass c_2 EVs
c_3	subclass c_3 EVs
DC	DC system
h	time slot index
j	defines the activated energy threshold
δ	time interval index
ω	time interval index

1 Introduction

The global energy consumption may increase more than 50% by 2030, if the current consumption pattern is maintained. Industry, transportation and buildings are the main energy consumers, while fossil fuels in the form of coal, oil and natural gas are the primary sources of energy nowadays [1]. Relying on fossil fuels for meeting the energy demands has two main disadvantages; firstly, they are finite and may be depleted, and secondly, they are one of the main contributors of greenhouse gas emissions, which accelerate climate change and global warming. Therefore, one of the main challenges of the 21st century is to limit the reliance of society on fossil fuels, as well as their impact on the environment. The necessity for reducing pollution, meeting the increased energy demands and improving peoples' quality of life are the driving forces behind the advent of smart cities. In brief, smart cities aim to deal with the problems generated by rapid urbanization and population growth, such as energy supply, waste management, and mobility by improving the present systems and implementing efficient and resource optimization solutions [2].

It is predicted that over 70% of the global population will be living in metropolitan areas by 2050. This continuous urbanization trend together with the globalized economy have initiated significant challenges for cities and restated their role as key national or even international economic engines. In this new environment, cities struggle to remain competitive in order to attract investments, increase their tourist appeal and provide better services to their habitants [3]. A variety of smart technologies and solutions have been proposed or even become available over the last years with the target to provide improved service delivery and reduced environmental impact to the citizens. Examples include mobility management and control [4], provision of health-care services [5], waste management [6], as well as green growth initiatives in the energy sector where the integration of intermittent renewable sources and the necessity for energy-efficient transportation systems, among other things, represent important challenges that are better addressed in a coordinated way [7].

Buildings account for the biggest proportion of global energy needs. For example, in European Union countries, energy consumption in buildings represents about 40% of the total energy consumption [8]. Therefore, predominantly strategic for the successful implementation of the vision of smart cities is the energy management sector. Urban communities are well-placed to identify local energy needs, take proper initiatives and bring people together in order to achieve common targets such as the reduction of energy supplying costs and CO_2 emissions, as well as the decrease of the energy dependence on the national grid. The traditional power grid can be transformed to a smart grid by incorporating the advantages of the information and communication technologies. This evolution, together with the significant reduction of the cost of renewable energy sources (RES) and energy storage systems (ESS) has stimulated the development of environment-friendly and cost-efficient solutions for small-scale power networks (microgrids) that interconnect urban buildings and

target to increase their self-sufficiency and sustainability. Microgrids (MGs) can be key components of the future smart cities that will facilitate the transition to a low-carbon energy system, contribute to the adoption of more rational energy consumption habits by consumers, as well as provide valuable flexibility in the energy market [6].

Electric vehicles (EVs) will be another key component of the future smart cities. The transportation sector accounts for about a quarter of the global energy-related greenhouse gas emissions being one of the main air polluters within cities and creating important health costs [7]. Due to the necessity of mitigating the impact of conventional vehicles on the environment, the penetration of EVs in the market is largely promoted. In 2015, the global stock exceeded one million EVs, while the target for 2020 has been set to 20 million EVs [9]. Growing EV market shares are expected to progressively reduce technology costs in the forthcoming years, thereby making EVs an increasingly attractive option. A review of national targets forecasts an annual production of over 100 million EVs by 2050 [10]. In a context of growing urbanization, EVs provide multiple advantages; they can contribute to the reduction of high noise levels in densely populated areas. They can support the integration of RES in the local MGs that will be developed in smart cities, and thus contribute to a more sustainable power generation mix [11]. Moreover, due to their high energy efficiency and zero tailpipe emissions, EVs represent a promising pathway to reduce air pollution, especially when they are coupled with a low-carbon power generation mix [12].

1.1 Main features of microgrids

The European Technology Platform of Smart Grids defines the smart grid as an electricity network that can intelligently integrate the actions of all users connected to it, i.e. producers, consumers and prosumers (participants that both produce and consume energy) in order to efficiently deliver sustainable, economic and secure electricity supplies [13]. MGs are considered as the building blocks of the future smart grids. They are small-scale energy networks, which include fixed and controllable loads, distributed energy resources (DER), energy storage systems, as well as energy management and control systems. MGs may appear in various sizes, such as a single building, a university or a military campus, an urban neighborhood or a rural village [14].

Figure 1.1 illustrates a MG example of an urban community. It consists of a group of buildings, which are equipped with their own energy resources. The local DERs involve conventional diesel generators, combined heat and power (CHP) units, which can satisfy both the electrical and thermal needs of the buildings, ESSs for storing the excess energy, as well as RES, such as PV systems and wind turbines. Power conversion equipment is also used as an interface between the DERs and the buildings' loads. For example, the PVs and the ESSs produce DC power, which is converted to AC power by using a DC/AC inverter. Micro-source controllers (MCs) are also necessary for controlling the output of the DERs

by regulating their frequency and voltage, while load controllers (LCs) are responsible for the regulation of controllable loads [15]. An EV is a typical controllable load, since it can be either curtailed or deferred. Moreover, by using the vehicle-to-grid (V2G) technology, EVs can provide power back to the MG, and thus operating as a storage system [16]. The local power network is also equipped with a microgrid central controller (MGCC), which is responsible for the co-ordination of the local micro-source and load controllers. The information exchange among the local controllers and the central one is achieved through a local area communication network (LAN) [17]. The MG is also connected with the main distribution grid in order to import electricity when the energy produced by the local DERs is not enough, while electricity is exported to the main grid when there is excess of energy.

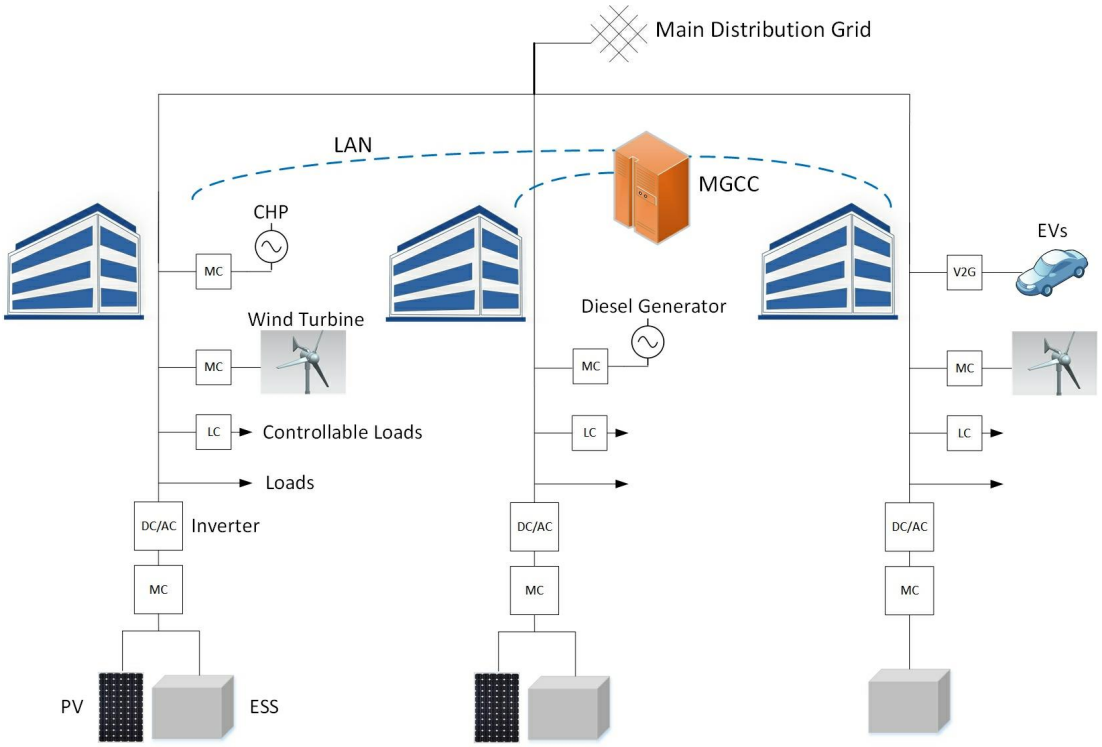

Figure 1.1: Typical architecture of an urban community microgrid.

MGs are promoted as the building blocks of the future smart grid for a number of reasons: They satisfy the energy demands of the consumers in a more reliable way. For example, in case of an emergency, such as a failure in the main grid, the MG can operate in an islanded mode (disconnected from the main grid). They also provide better power quality, since they are not affected by the voltage dips that may take place along the distribution lines [18]. Furthermore, MGs provide economic benefits because the consumers produce part of their needs at significantly lower costs. Due to the localized energy generation, power transmission costs are reduced, while the storage systems can contribute to the avoidance of peak power costs. Moreover, consumers may have additional revenues by selling their excess

power to the main grid, as well as by supplying auxiliary services to the main grid, such as voltage support. In addition, a great amount of the consumers' demands is satisfied by RES. The utilization of renewables provides environmental and economic benefits by reducing the carbon footprint of the consumers and costs associated with carbon emissions [15].

1.2 Main features of electric vehicles and charging infrastructure

The target of gradually replacing conventional vehicles with EVs, as well as achieving wide penetration rates of EVs in the automotive market is correlated with the availability of charging infrastructure. All EVs have an on-board charger, through which they can charge from a typical AC outlet. Depending on the provided power level, EV charging is classified into three categories. Level 1 refers to standard single-phase outlets that provide power rates up to 1.9 kW and it is appropriate for charging at workplaces or for night-time charging at home, since it is the slowest charging method; the charging duration may last up to 11 hours. Level 2 uses either home outlets or dedicated electric vehicle supply equipment (EVSE) and provides power rates up to 19.2 kW. Level 2 charging infrastructure can be used for charging at home or workplaces, while it is also appropriate for charging at public parking lots, shopping malls, cinemas etc., since the charging duration ranges between 1-6 hours. Level 3 is the fastest charging option. It uses specialized charging spots (CSs) that provide power rates up to 100 kW, while the duration of charging is less than 30 minutes. Level 3 charging infrastructure is usually installed in highway rest areas, as well as in city refueling points (gasoline and oil stations) [19].

The main concern over the EV technology is the confrontation of drivers' range anxiety, which refers to EVs' short driving ranges and long charging durations [28]. A selection of popular EV models and their basic characteristics, such as the the battery size, the energy consumption, the driving range, and the fast charging option they contain are summarized in Table 1.1. Fast charging stations (FCSs) are considered as an effective solution for mitigating range anxiety and strengthening the public acceptance of EVs [29]. For this reason, the vast majority of EV models contain inlets that are compatible with off-board fast charging equipment. Currently, the Japanese standard CHArge de MOve (CHAdeMO) is the most popular fast charging option and it is adopted by many EV manufacturers, such as Nissan Mitsubishi and Kia[30]. Another technology that is projected to gradually increase its market share is the combined coupler standard (CCS), which is promoted in Europe and North America. CCS has been adopted by manufacturers such as BMW and Volkswagen [31]. The operation of both the CHAdeMO and CCS standards is based on the utilization of DC power. On the other hand, Renault promotes AC as a fast charging option [32]. The adoption of three different fast charging standards has led manufacturers to design charging spots that include all of these options in a single cabinet, as illustrated in Figure 1.2 [33].

Table 1.1: Technical characteristics of popular EV models [20]-[27]

EV model	Battery (kWh)	Consumption (kWh/km)	Range (km)	Fast charging option
Nissan Leaf	24	0.186	135	CHAdeMO
Mitsubishi i-MiEV	16	0.186	100	CHAdeMO
Kia Soul	27	0.199	150	CHAdeMO
BMW i3	18.8	0.168	130	CCS
Volkswagen E-Golf	36	0.174	201	CCS
Renault Zoe	22	0.146	210	AC

Figure 1.2: Multi-standard charging spot.

1.3 Motivation and scope

Several factors, including climate change, economic restructuring, and urban population growth have generated interest in smart cities, which are expected to lead to economic development, improve sustainability, and enhance citizens' quality of life. Smart technologies and programs have been already implemented in various metropolitan areas around the world, such as in Southampton [34], Amsterdam [35] and Stockholm [36], while it is estimated that the global market for smart urban services will be 400$ billion per annum by 2020 [37]. The concept of smart cities is also highly promoted in Barcelona, Spain [38], where *Superblocks* are expected to be the basic cells for the organization of infrastructures and facilities, such as charging stations for EVs and small-scale power networks. The Superblock model goes beyond the traditional geographic and demographic principles for urban planning. As Figure 1.3 illustrates, it consists of nine city blocks where the inner part is mainly used by pedestrians and cyclists, while the typical urban traffic uses only the exterior roads.

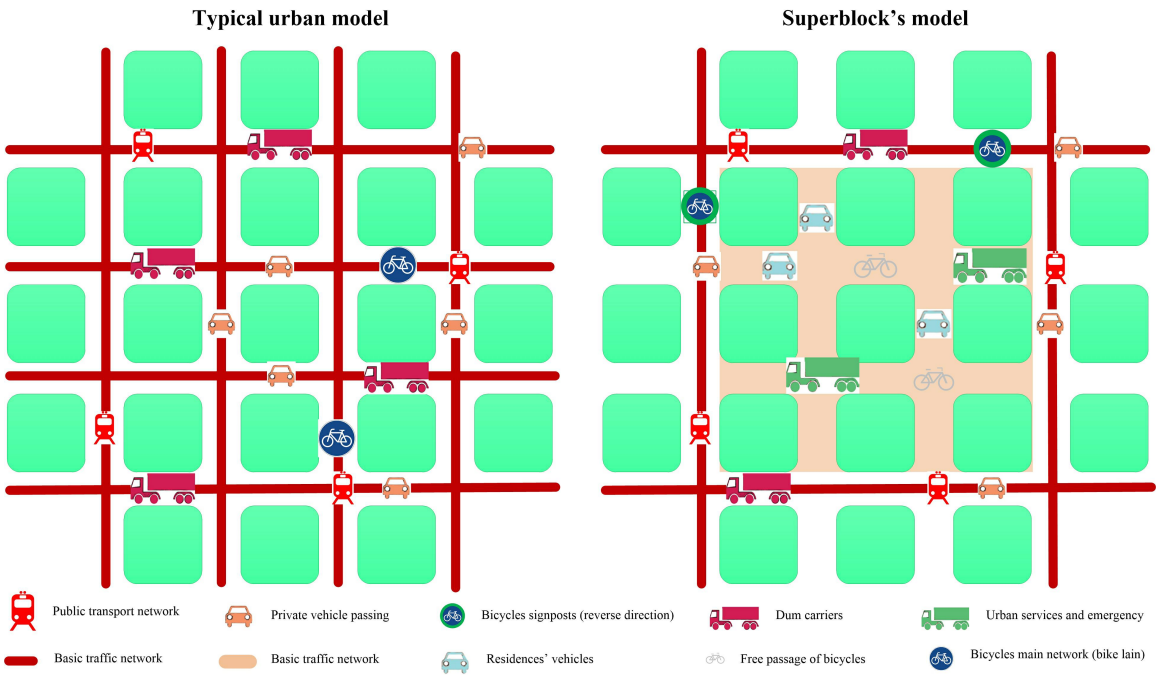

Figure 1.3: Superblock model

The Superblock, as an innovative smart-community model solution and an integrated ecosystem vision has set ambitious targets regarding the reduction of public and private buildings' dependence on the national grid (by 40 percent), as well as the reduction of electricity supplying costs (by 35 percent) [39]. A Superblock has the optimal dimensions to test innovative smart MG solutions and represents a good opportunity to apply ideas and projects that can be later applied in the entire city. This potential is also amplified by the fact that the Superblock model promotes the installation of renewable systems on

public buildings, while residential and commercial buildings' owners are encouraged to shift from fossil fuel based energy resources to green and sustainable solutions. Furthermore, the presence of different types of buildings in a relatively small coverage area together with a communication network may lead to a more efficient utilization of the installed energy resources. For example, consumers with high energy demands during the daytime (PV production hours), such as educational and office buildings, can be supplied with energy by neighboring residential buildings with energy surplus. On the other hand, the evening peak demand of residential buildings can be satisfied by discharging their owned storage systems or/and by discharging the storage systems installed in other buildings with low energy demands during the evening hours.

Motivated by the advantages provided by the Superblocks' structure and the ambitious energy dependence and cost reduction targets, in this thesis we propose an optimization model for determining the power equipment sizing of a MG containing cooperative buildings, located within the same Superblock. The proposed model obtains the optimum capacities of solar panels, storage systems and power inverters to be installed at the buildings by considering their acquisition, maintenance and replacement costs. The sizing process is correlated with the MG's operation plan over a yearly optimization horizon, which refers to the allocation of the generated PV power, the charge and discharge scheduling of the storage systems, as well as the energy exchanges taking place among the buildings. The operation plan is determined by taking into account the buildings' load profiles, the electricity prices and the carbon-related taxes. The proposed scheme targets to increase the buildings' self-sufficiency, through an effective energy exchange procedure, where the excess energy of buildings with energy surplus is locally consumed by buildings with energy deficit, instead of being sold back to the main grid. In addition, one of the main objectives of the proposed cooperative model is to investigate the effect of energy sharing on the equipment sizing.

Fast charging stations will also be an important component of smart cities, given the projected wide penetration of EVs in the automotive market. For EVs, the role of fast charging stations is similar to that of gasoline and oil stations for conventional vehicles. Although fast charging facilities provide high power levels, the duration (0.2-1 hour) of recharging an EV is considered to be long compared to the duration of refilling a conventional vehicle, which normally lasts for 1-3 minutes. This may result in the formation of queues and long waiting times. The problem may be more intense at stations located at densely populated areas where the number of customers' visits is expected to be high, especially during peak-traffic hours. In turn, long queue waiting times may cause EV drivers' discomfort and dissatisfaction.

It is therefore essential for charging station operators to develop realistic and accurate models in order to estimate the expected charging demand at fast charging stations and the quality of service (QoS) provided by their facilities. Equally important for the charging station operators, is the development of charging control strategies in order to deal with

problematic situations where long queues are built up. To this end, in this thesis, we develop a mathematical framework based on queuing theory, aiming to evaluate the performance of a fast charging station in terms of customers' waiting time in the queue, and operators' profits. The aforementioned performance evaluation metrics are calculated by taking into account the stochastic arrival and recharging patterns of the EVs, which are classified based on their battery size. Charging control strategies are also proposed, targeting to reduce the customers' waiting time in the queue, and hence improving the quality of service provided by the fast charging facilities.

1.4 Structure of the dissertation and main contributions

The remainder of the thesis consists of six chapters, the contents and the contributions of which are described in detail as follows:

Chapter 2. This chapter is divided into two main parts. The first part presents studies that deal with the optimal operation planning and sizing of MGs, as well as the main features of mixed integer linear optimization (MILP) technique, which is the basic tool for the formulation of both problems. The second part presents studies that deal with the mathematical analysis of charging stations' operation based on queuing theory models.

Chapter 3. This chapter presents a cooperative scheme for the optimum selection of power equipment components to be installed at MGs, as well as for the optimum management of the energy generated, stored and consumed. A MG topology is considered where buildings with diverse load profiles, equipped with PV systems and storage devises, are connected to the low voltage of the same distribution transformer. Through this point of common coupling the buildings are able to exchange energy so that an optimal utilization of the renewable energy sources and storage systems installed at the buildings is achieved. A MILP optimization model is developed that determines the optimal energy exchanges taking place, the optimal charge and discharge scheduling of the storage systems, as well as the amount of energy each building imports/exports from/to the main grid. Moreover, the proposed optimization model determines the optimal capacities of PV systems, energy storage devises and power inverters to be installed at each building. The impact of energy sharing on the equipment sizing, and hence on the implementation cost of the project, is demonstrated by comparing the proposed cooperative scheme with a non-cooperation scenario. The difference in the implementation costs of the two scenarios indicates the financial gains of the buildings' coalition. The contributions of this chapter have been published in:

I. Zenginis, J. S. Vardakas, P. V. Mekikis, and C. Verikoukis, "Cooperative Energy Management in Microgrids,"Transportation and Power Grid in Smart Cities: Communication Networks and Services, John Wiley, UK, 2017.

Chapter 4. This chapter extends the work of the previous one in four ways. The first enhancement refers to the MG topology, since it is considered that the various buildings are interconnected through a DC bus. This new architecture enables buildings that are fed by different distribution transformers to participate in the MG increasing the cooperation opportunities and benefits. Furthermore, in this chapter the buildings are equipped with vehicle-to-building (V2B) systems, which can operate as storage systems providing additional flexibility in the MG's energy management. Another major advantage of the optimization model presented in this chapter is the utilization of the Nash bargaining method for obtaining the optimal equipment sizes and power allocation in the system. This method guarantees that the coalition profits are equally distributed among the participants. Finally, the possible integration of new players, years after the initial establishment of the buildings' coalition is investigated. The contributions of this chapter have been published in part in 3 journals and 2 international conferences:

I. Zenginis, J. S. Vardakas, C. Echave, M. Morató, J. Abadal, and C. Verikoukis, "Cooperation in microgrids through power exchange: An optimal sizing and operation approach," *Appl. Energy,* vol. 203, pp. 972-981, Oct. 2017.

J. S. Vardakas, **I. Zenginis,** N. Zorba, C. Echave, M. Morató, and C. V. Verikoukis, "Electricity savings through efficient cooperation of urban buildings: the smart community case of Superblocks in Barcelona,"to appear in *IEEE Com. Mag,* 2018.

I. Zenginis, J. S. Vardakas, C. Echave, M. Morató, J. Abadal, and C. Verikoukis, "Optimal power equipment sizing and management for cooperative buildings in microgrids,"to appear in *IEEE Trans. Ind. Informat,* 2018

J. S. Vardakas, and **I. Zenginis,** "A Survey on Short-Term Electricity Price Prediction Models for Smart Grid Applications,"in Proc. WICON 2014, Lisbon, Portugal, 12-14 Nov. 2014.

J. S. Vardakas, **I. Zenginis,** and M. Oikonomakou, "Peak Demand Reduction Through Demand Control: A Mathematical Analysis," in Proc. ICTF 2016, 6-8 July, Patras, Greece.

Chapter 5. In this chapter, the operation of a FCS for EVs is analyzed by employing a novel multi-class M/G/s queuing model. The proposed analysis considers that the various EV models are classified by their battery size, and computes the customers' mean waiting time in the queue by taking into account the available charging spots, as well as the stochastic arrival process and the stochastic recharging needs of the various EV classes. The users' waiting time in the queue is the QoS criterion for the performance evaluation of the FCS. To

this end, the maximum number of served customers is determined, subject to a maximum queue waiting time value. The amount of efficiently served EVs is initially computed by assuming that their batteries are charged up to the maximum allowable state of charge (80% in fast charging). Furthermore, a charging strategy is proposed according to which the drivers are motivated to limit their energy demands. The implementation of the proposed strategy allows the charging station to serve more customers without any increase in the queue waiting time. The contributions of this chapter have been published in the following journal:

I. Zenginis, J. S. Vardakas, N. Zorba and C. Verikoukis, "Analysis and quality of service evaluation of a fast charging station for electric vehicles," *Energy*, vol. 112, pp. 669-678, Oct. 2016.

Chapter 6. This chapter extends the work of the previous one in three ways. First of all, EV classes that utilize AC fast charging resources are taken into account in the mathematical analysis. Therefore, the EVs are classified not only by their battery size, but also by their fast charging option (AC or DC). Moreover, the EVs' recharging patterns are denoted by the increase of their batteries' state-of-charge. This is a more realistic approach compared to the assumption of the previous chapter where the EVs recharge up to the maximum possible level. It also allows for the utilization of real-case statistical data regarding the amount of energy obtained during a fast charging session. Furthermore, it enables the formulation of a pricing policy, which targets to mitigate the long queue built-ups during peak demand periods. According to this policy, fixed energy thresholds are set by the FCS operator, and the customers that request to obtain more energy than the arranged thresholds are asked to pay higher rates. The implementation of the proposed policy alleviates the pressure on the FCS because the customers either adjust their demands or search for satisfying their initial requirements to nearby stations. The contributions of this chapter have been published in the following journal:

I. Zenginis, J. S. Vardakas, N. Zorba and C. Verikoukis, "Performance Evaluation of a Multi-standard Fast Charging Station for Electric Vehicles," *IEEE Trans. Smart Grid,* 2017.

Chapter 7. This chapter concludes the dissertation by providing a summary of our major contributions, together with some potential lines for future investigation.

2 Literature overview on microgrids' optimization and electric vehicles' charging stations' operation analysis

This chapter is organized as follows. In section 2.1, the concept of MGs' optimal operational planning is introduced, while works that consider different MG topologies and components are discussed. In addition, the problem of optimal MG sizing is defined and some of the most important works in the literature are discussed. Section 2.2 contains the state-of-the-art on the analysis of charging stations' operation. Several queuing theory models are presented that have been used for the estimation of charging stations' load and profits, as well as for the derivation of QoS metrics, such as the customers' waiting time in charging stations' queues, and the probability of customers' blocking due to lack of waiting space or/and available energy resources.

2.1 State-of-the-art on optimization of microgrids

Studies on MGs are generally classified into two groups; those dealing with the problem of optimal operation planning and those dealing with the optimal sizing and design of MGs. Both problems are commonly formulated as a MILP one. MILP is the optimization problem of minimizing an objective function that consists of a linear combination of integral and continuous decision variables, subject to a set of linear equality and inequality constraints. A typical MILP problem is formulated as follows:

$$\begin{aligned} \text{minimize} \quad & c^T x, \\ \text{subject to} \quad & Ax \leq b \\ & A_{eq} x = b_{eq} \end{aligned}$$

where x is the n-dimensional vector of the decision variables to be calculated and c is the n-dimensional vector of coefficients. Furthermore, A and A_{eq} are the coefficients' matrices for the p linear inequality and the q linear equality constraints, respectively, while b and b_{eq} are the right-hand side vectors for the p linear inequality and the q linear equality constraints, respectively.

The MILP optimization technique is appropriate for modeling MGs, since continuous and discrete-valued dynamics interact in a such systems. For example, physical quantities, such as the amount of imported/exported energy can be represented by continuous variables, while the discrete features of MGs' components, such as the charging/discharging state of the storage systems can be modeled by using binary decision variables.

2.1.1 Optimal operation planning of microgrids

The operation plan refers to the short term (a day or a week) management of the system's load and generated power with the objective to satisfy the energy demand of the MG in the most economic and/or environment friendly way. More precisely, the optimal operation planning consists in taking decisions over an optimization horizon that is divided into several time slots. At every time slot the MGCC determines: 1) The amount of energy that should be imported or exported to the main grid. 2) The amount of energy that should be transferred to the storage systems or discharged from the storage systems. 3) The amount of energy that should be generated by each of the dispatch-able distributed generators. 4) The optimal scheduling of controllable loads over the optimization horizon. All these decisions are taken by considering the MG topology, the capacity of conventional or/and RES, the capacity of energy storage systems, the local energy demand, as well as the energy prices.

Kriett et al. [40], present a MILP model for determining the optimal operation plan of a single, grid-connected residential building, which is equipped with PVs, thermal solar panels, CHP units, boilers, as well as electrical and thermal energy storage units. The residential building also contains controllable loads, such as dishwashers, washing machines and EVs and non-controllable loads, such as lighting and entertainment machines. Given the electricity and natural gas prices, the technical specifications of the considered technologies and the building's energy demands (electrical and thermal), the proposed optimization scheme determines the generators' optimal production levels, the optimal charge and discharge scheduling of the storage systems, the time scheduling of the controllable loads, as well as the optimal energy exchanges between the building and the main grid. The objective function minimized in order to obtain the aforementioned decisions consists of the daily operating costs of the residential building (i.e. electricity and natural gas supplying costs).

The optimal operation plan in [40] is obtained based on day ahead predictions for the RES production, the building's energy demands and the energy prices. On the other hand, authors in [41] and [42] integrate the MILP problem formulation into an model predictive control (MPC) framework, which makes the system more robust against the prediction errors. This is achieved through the utilization of a feedback mechanism, which provides updated information for the the RES' output, the time-varying load and the time-varying energy prices. Authors in [42] conclude that the utilization of the MPC framework reduces the building's daily operational cost by 60% compared to the traditional day-ahead method.

The works in [40]-[42] deal with the optimization of a single residential building. On the other hand, Paterakis et al. [43] obtain the optimal operation plan of a neighborhood consisting of multiple smart homes. The dwellings are interconnected at the low voltage part of a distribution transformer, while they are also equipped with vehicle-to-home (V2H) systems, controllable appliances, energy storage systems and PVs, as depicted in Figure 2.1. Furthermore, it is considered that they can exchange energy with each other through their point of common coupling (PCC), while they also sell energy back to the main grid. The

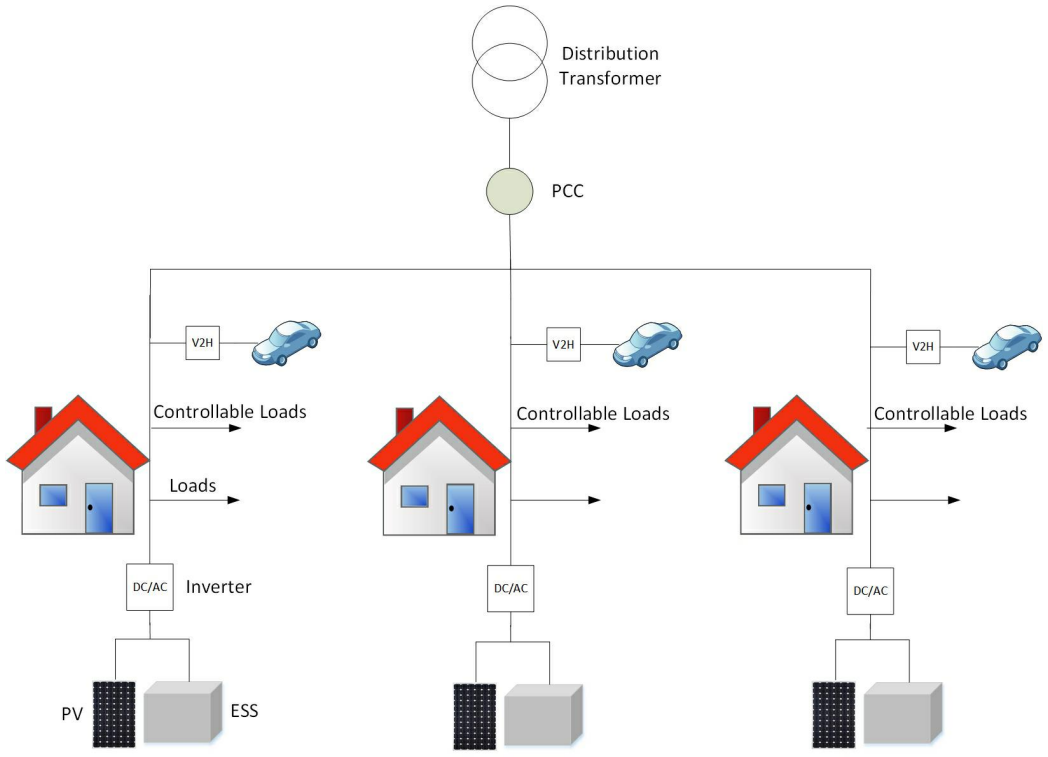

Figure 2.1: Smart homes connected at the low voltage of a distribution transformer

operation plan of the considered MG is obtained by using the MILP technique with the objective to minimize the daily electricity supplying cost. Moreover, a demand response strategy is proposed, which targets to fairly allocate the energy delivered by the main grid by mitigating the homes' competitive behavior when the price of the supplied energy is low.

A cooperative network of large residential MGs is presented in [44] where a MPC-MILP optimization scheme is applied for the determination of the energy exchanges taking place among the various sites. The MGs are equipped with RES, such as wind turbines and PVs, as well as with storage systems, while they are assumed to be interconnected through a PCC. The optimal energy exchanges among the MGs, and the optimal charge and discharge scheduling of the MGs' storage systems are obtained by maximizing the total profit of the network. More precisely, the objective function to be maximized consists of the sum of each MG's profit, which is expressed as the difference between the income due to power exports (to the main grid and to the other MGs in the network) minus the expenses due to power imports (from the main grid and from the other MGs in the network). Furthermore, the authors highlight the benefits of cooperation among multiple MGs compared to the non-cooperation case. As Figure 2.2 illustrates, the amounts of energy that the considered MGs purchase by the main grid under the cooperation scenario are smaller than the corresponding amounts under the non-cooperation scenario.

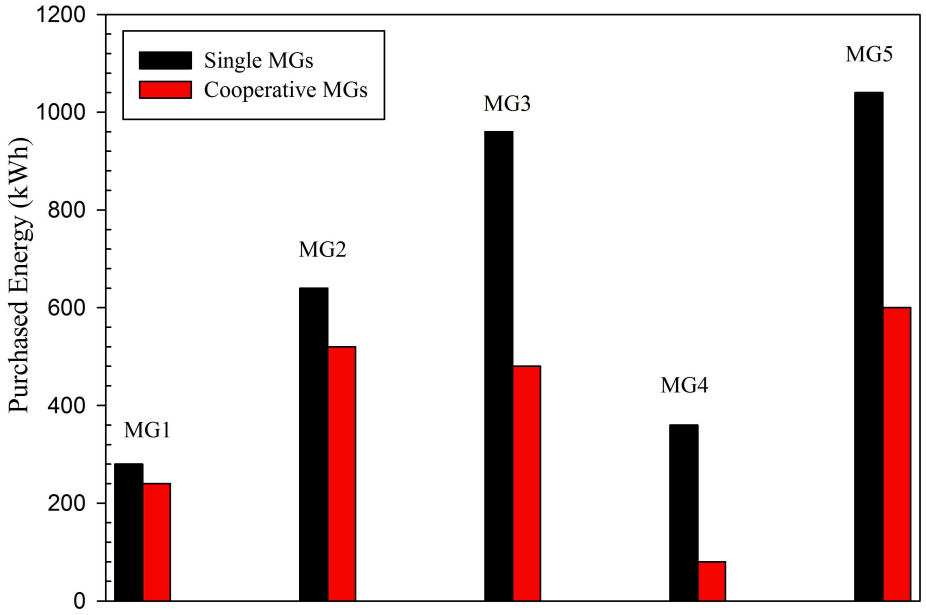

Figure 2.2: Energy purchased from the main grid under single and cooperative MGs.

2.1.2 Optimal sizing and design of microgrids

System design is a long-term planning activity, which involves the determination of the optimal capacities of power technologies to be installed in the MG. The MILP optimization technique is extensively used for the formulation of this type of problems. For the optimal equipment sizing, the specific characteristics of the candidate technologies to be installed are taken into account, such as the acquisition cost, the lifetime, as well as the maintenance and operating costs. The energy tariffs and the energy demands of the MG participants are also considered, while yearly load profiles are commonly used as input parameters because the loads' seasonal variability affects the optimal solution in this type of problems.

Erdinc et al. [45], deal with selecting the optimal PV and energy storage system sizes for a smart home, which is also equipped with a V2H system. The whole problem is formulated as a MILP optimization one. The objective function to be minimized contains terms that are related to the equipment sizes, such as the equipment acquisition cost, as well as the net present values (NPVs) of the equipment maintenance and replacement costs. In addition, the objective function contains terms that are related to the operation plan of the smart home, such as the NPV of the cost of importing electricity from the main grid and the NPV of the profit of exporting electricity to the main grid. The optimal equipment sizing of a large residential MG is also the topic in [46], where the objective function is formulated in the same way as in [45]. Besides the PV and energy storage sizes, the optimal capacity of wind turbines and AC/DC inverters are also determined in [46]. A MILP model is also proposed by Mehleri et al. [47] for the optimal capacity sizing of PVs, CHP units and boilers

that satisfy the electrical and heating demand of multiple neighboring residential buildings. An additional objective of the proposed model in [47] is the designing of a heating pipeline network that allows heat exchanges among the various buildings.

Optimization models other than MILP have also been used in the literature for the optimal sizing problem. Authors in [48] determine the capacities of PVs, storage systems and inverters, as well as the sizes of wind and biomass turbines for an isolated MG, which is located in a village. The optimization problem is solved by using an artificial bee colony algorithm, while an operational strategy is also proposed for determining the MG's operation plan. Authors in [49] obtain the equipment sizing of a community consisting of a set of residential apartments. The problem is formulated based on a multi-objective function, where both the total cost of the system and the energy availability are taken into account, while a set of optimal solutions is obtained by using a multi-objective genetic algorithm. Di Silvestre et al. [50] apply a multi-objective glow-worm swarm optimization algorithm for optimizing a MG located in the low voltage of a distribution transformer. The optimal capacities of PVs, ESSs and micro-turbines are obtained by minimizing the objective function, which contains the system's yearly power losses, power production cost and CO_2 emissions.

In the aforementioned studies, either a single residential building or a set of residential buildings are taken into account. On the other hand, authors in [51] demonstrate the benefits of cooperation among different building types. A MG topology is considered where electricity can be transferred among a residential building, an office building, a school, a hotel and a restaurant. The buildings are equipped with boilers and thermal storage systems, which satisfy their thermal demands, as well as with CHP units, which satisfy both the electrical and thermal demands. The problem of selecting the optimal CHP units', boilers' and thermal storage systems' sizes, as well as of determining the price levels of energy transactions among the participants and the MG's operation plan is formulated as a MILP one. The operation plan in this case refers to the amounts of electrical and thermal power generated by the CHP units, the amount of thermal power generated by the boilers, the charge/discharge scheduling of the thermal storage units, as well as the amount of energy exchanges among the buildings. However, the presence of RES and electrical storage systems is neglected.

2.2 State-of-the-art on charging stations' mathematical modeling and analysis

EVs and public charging facilities will be key components towards a more sustainable and energy efficient transportation sector. Therefore, the operation of charging stations, the estimation of their load, the QoS providing to their customers, as well as their economic feasibility are topics that has drawn the attention of the research community. For the stochastic modeling of the EVs' arrival and charging process at public facilities, various probabilistic models have been proposed based on queuing theory.

M/M/s is the most commonly used queuing model. As Figure 2.3 illustrates the first M denotes that the EVs arrive at a charging station by following a Poisson process, while the second M denotes that the EVs' charging duration follows an exponential distribution function. The M/M/s model also assumes that the charging station contains s identical charging spots that can simultaneously serve equal number of EVs, as well as infinite waiting space where the not served EVs are queued. On the contrary, another commonly used model (M/M/s/c) assumes that the maximum number of EVs that can be present in the charging station is c (where s EVs are being charged, and $c-s$ EVs are waiting in the queue). Finally, the M/M/s/s queuing model considers that there is no available waiting space.

Li et al. [62] determine the overall charging demand of EVs at a FCS that consists of AC outlets. Based on the derived charging demand, authors then examine the impact of uncontrolled EV charging on the distribution network by performing probabilistic power flow calculations. The FCS is modelled as an M/M/s queue where the probability p_n that n EVs are present at the charging station is given by the following relation:

$$p_n = \begin{cases} \left(\sum_{i=0}^{s-1} \frac{(s\rho)^i}{i!} + \frac{(s\rho)^s}{s!}\frac{1}{1-\rho}\right)^{-1}, & n = 0 \\ \frac{(s\rho)^n}{n!}p_0, & n = 1, 2, ..., s \end{cases} \tag{2.1}$$

where ρ is the utilization rate of the queuing system, and it is calculated as follows, given the EVs' mean arrival rate λ and mean charging rate μ:

$$\rho = \frac{\lambda}{s\mu} \tag{2.2}$$

The M/M/s queue is also applied in [63] for estimating the charging demand of a FCS located on a highway, as well as in [64] for calculating the charging load of a network of FCSs.

The aforementioned studies ([62]-[64]) aim at investigating the impact of EVs' load on the grid, which is a crucial issue for distribution system operators. The M/M/s queuing model is also applied for the calculation of QoS metrics, such as the EVs' queue waiting time in a parking lot consisting of level 2 outlets [65], or in a network of FCSs [66]. More

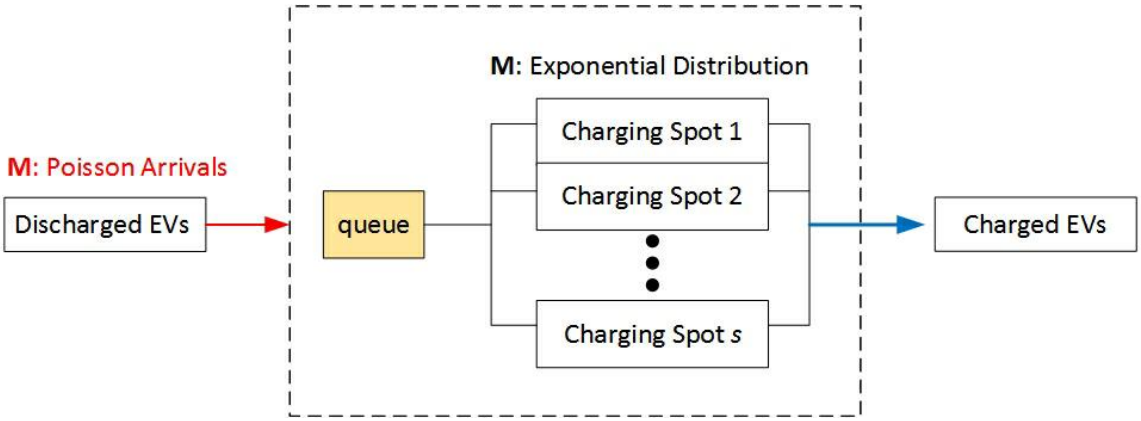

Figure 2.3: Charging station modeled as an M/M/s queuing system.

specifically, the mean waiting time of customers in the queue of the charging station is given by the following relation:

$$W_{M/M/s} = \frac{\rho(\frac{\lambda}{\mu})^s}{s!\lambda(1-\rho)^2}\left(\sum_{i=0}^{s-1}\frac{(s\rho)^i}{i!} + \frac{(s\rho)^s}{s!}\frac{1}{1-\rho}\right)^{-1} \tag{2.3}$$

Furthermore, the M/M/s/c queue is used for modeling a parking lot with finite waiting space in [67]. In this case, the QoS metrics under evaluation are both the queue waiting time and the blocking probability, which denotes the percentage of EVs that arrive at the charging station requesting to be served, but they are not allowed to enter because all charging spots are occupied and there is no available waiting space.

Queuing models are useful tools not only for describing the operation of charging stations and evaluating QoS metrics, but also for formulating charging control strategies to improve the operability of charging stations. Gong et al. [65] propose a charging control strategy aiming at minimizing the loss of life of the distribution transformer that supplies a parking lot. The customers' queue waiting time is also taken into account in order to evaluate the effectiveness of the proposed strategy in terms of customers' QoS. Gusrialdi et al. [68] propose a higher level distributed scheduling algorithm together with a lower level cooperative control policy for individual EVs in order to optimize the operation of a network of FCSs on a highway. The proposed methodology aims at adjusting the percentage of the EVs to be charged at individual FCSs so that all the FCSs are uniformly utilized and the total waiting time is minimized. This is achieved by optimally routing the drivers within the network. Customer routing is also employed in [69] in order to reduce the number of blocked EVs among a network of FCSs.

The works in [70]-[72] consider the operation of networks of FCSs where each station draws a certain amount of power form the distribution grid. This configuration assures the reliable operation of the grid, however when the EVs' charging demands are higher than

the available power, an amount of customers is blocked. In order to mitigate this problem, authors in [70] introduce a decentralized control mechanism where the network operator offers price incentives, so that customers accept being routed to stations less busy than others. In this way more customers are served with the same amount of grid resources and the revenue of the operator is maximized. A pricing based control mechanism is also proposed in [71] aiming at ensuring that only a small percentage of EVs is blocked. This is achieved by incentivizing EV drivers to shift their charging requests from peak to less congested periods. The charging management scheme proposed in [72] targets the reduction of customers' blocking probability by motivating EV drivers who are blocked by their preferred station to visit a nearby station which provides lower power levels.

A key assumption in all aforementioned queuing models is that the EVs' charging times are exponentially distributed random variables. In real life though, charging times do not seem to follow any specific probability distribution, since they are mainly influenced by the EVs' battery capacities and the batteries' state of charge (SoC) when the EVs arrive at the charging station [73]. Therefore, the assumption of exponentially distributed charging times may not describe the charging behavior effectively.

A more sophisticated queuing model is employed in [74], where the charging times are generally distributed random variables (M/G/∞). This model is useful for distribution system planners who need to estimate the EVs' charging demands, however it is not appropriate for evaluating QoS metrics since the number of CSs is assumed to be infinite, and therefore the EVs are neither queued nor blocked. Generally distributed charging times are also considered in [75] where the EVs' charging time depends on the power level provided by the charging spots and on the arrival SoC of the EVs' batteries, which is considered to be a generally distributed random variable. Specifically, authors in [75] model a FCS as an M/G/s/c queue and derive the operator's profits, as well as the customers' mean waiting time in the queue and the blocking probability. Nevertheless, the aforementioned analysis considers that only one EV class is served by the FCS (all EVs have the same battery size). The concept of classifying the EVs by their different battery sizes is only considered in [62], where despite this realistic approach, the EVs' charging load is calculated by applying the M/M/s queue, and hence the EVs' charging time is assumed to be an exponentially distributed random variable.

3 Cooperation among buildings with diverse load profiles in microgrids

The benefits of cooperation among different types of buildings are examined in this chapter in terms of power equipment sizing and operation planning. The idea of forming MGs that consist of neighboring buildings with diverse load profiles stems from Barcelona's superblocks where schools, residential and office buildings, etc coexist in a relatively small coverage area. To this end, a MILP model is presented for determining the optimal sizes of PVs, ESSs and DC/AC inverters to be installed in each building. The sizing process is correlated with the MG's operation plan over a yearly optimization horizon, which refers to the optimal allocation of the produced PV power, the ESSs' charge and discharge scheduling, the energy exchanges taking place among the buildings, as well as the amount of energy each building buys or/and sells to the main grid. The benefits of forming buildings' coalitions are demonstrated by comparing the proposed cooperation scenario with the baseline scenario and the non-cooperation scenario. The baseline scenario refers to the case where all buildings are supplied with energy by the main grid only, while the non-cooperation scenario considers that the buildings are equipped with PVs, ESSs and inverters, but they do not exchange energy with each other.

This chapter is organized as follows. Section 3.1 presents the MG's architecture and the formulation of the optimal sizing and operation planning problem. Section 3.2 presents the economic analysis and the objective function that is used for deriving the optimization results. The equations that describe the MG's operation are formulated in section 3.3, while section 3.4 contains the examined case study and the corresponding results.

3.1 Microgrid architecture and problem formulation

The cooperative scheme is applied to a MG topology consisting of neighboring buildings that are connected to the main distribution grid through a common distribution transformer, as depicted in Figure 3.1. The various buildings will be equipped with PV panels, ESSs and DC/AC inverters, which are used for the connections of the PVs and the ESSs with the buildings' loads, and the main distribution grid. In addition, it is assumed that the MG contains a MGCC, local controllers and a LAN that can provide an optimal power operation plan.

The proposed MILP optimization model is formulated as follows: Given 1) a yearly optimization horizon y, divided into $t = (1, ..., T)$ time intervals of equal duration Δt, 2) the load of the buildings and the normalized PV production for each time interval, 3) the buildings' available surface for installing PVs, 4) the open market electricity tariffs, 5) the energy buying and selling prices from and to the other MG users, respectively, 6) the energy selling price to the main grid, 7) the carbon intensity and the carbon taxes at the MG's

location, and 8) the acquisition and maintenance costs, as well as the lifetimes and the efficiency factors of the PVs, ESSs and inverters, determine the 1) optimal PVs', ESSs' and inverters' sizes to be installed at each building, and 2) the optimal power operation plan in the MG, in order to satisfy the buildings' energy demands at minimum cost.

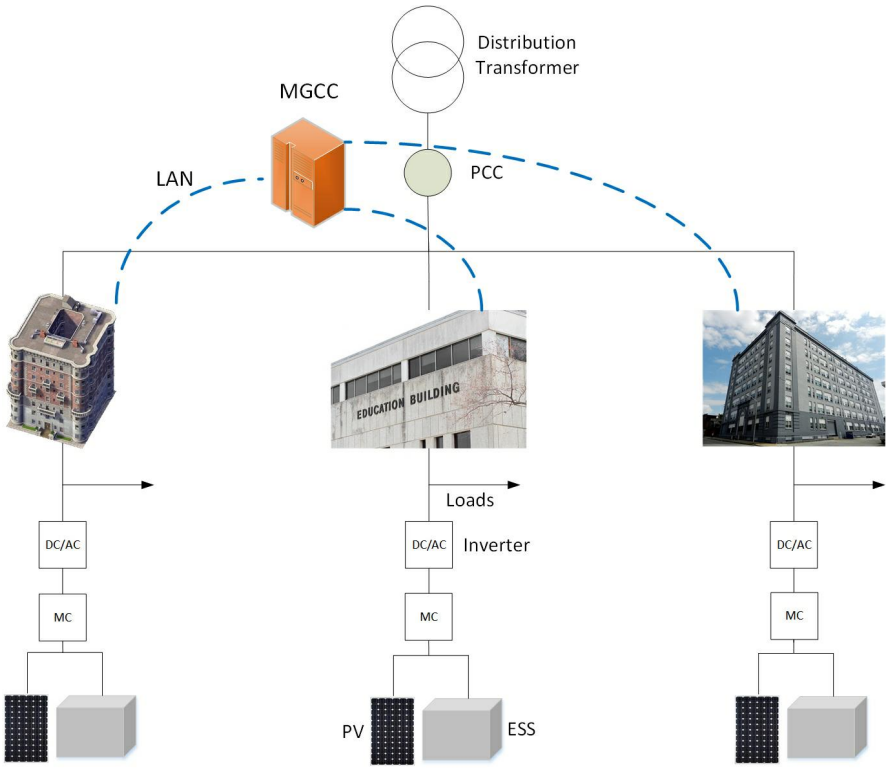

Figure 3.1: Microgrid architecture.

3.2 Economic analysis

The optimal power equipment sizing and operation planning of the considered MG are determined by minimizing the total cost w of all buildings $b \in \{1, ..., B\}$ participating in the coalition:

$$w = \sum_{b} C(b) \tag{3.1}$$

where $C(b)$ denotes the overall annualized cost of each building, which involves the equipment acquisition cost $C_A(b)$, the NPVs of the equipment maintenance and replacement costs, $C_M(b)$ and $C_R(b)$, respectively, the NPVs of the electricity supplying and carbon emissions-related costs, $C_E(b)$ and $C_C(b)$, respectively, as well as the NPV of each building's revenue $R_E(b)$ due to electricity exports to the other buildings and the main grid. The overall annualized cost $C(b)$ is obtained by multiplying the sum of the aforementioned costs with

the capital recovery factor $CRF(d, Y)$:

$$C(b) = CRF(d, Y)[C_A(b) + C_M(b) + C_R(b) + C_E(b) + C_C(b) - R_E(b)] \tag{3.2}$$

$$CRF(d, Y) = \frac{d(1+d)^Y}{(1+d)^Y - 1} \tag{3.3}$$

where d the discount rate and Y the lifetime of the project. The equipment acquisition cost is derived by multiplying the size N_j by the per unit cost c_j of each technology $j = (PV, ESS, INV)$:

$$C_A(b) = \sum_j N_j(b) c_j. \tag{3.4}$$

Likewise, the maintenance cost is obtained by multiplying the equipment sizes by the annual per unit maintenance cost μ_j of each technology. Given the discount rate d and the lifetime of the project Y, the NPV of the maintenance cost is derived by the following relation:

$$C_M(b) = \sum_{y=1}^{Y} \frac{\sum_j N_j(b) \mu_j}{(1+d)^y} \tag{3.5}$$

while, the NPV of the equipment replacement cost is obtained by:

$$C_R(b) = \sum_{i=1}^{rep_j} \frac{\sum_j N_j(b) c_j}{(1+d)^{iYrep_j}} \tag{3.6}$$

where $Yrep_j$ indicates the year of first replacement of technology j, and $rep_j = int[Y/life_j]$ denotes the number of replacements required for each technology, which is obtained by the integer part of the division between the project lifetime and the lifetime of each technology $life_j$.

On the one hand, the acquisition, maintenance and replacement costs depend are correlated with the aspect of the optimization problem that refers to equipment sizing. On the other hand, the electricity supplying and carbon emissions-related costs, as well as the revenue derived due to electricity exports depend on the power operation plan of the MG. Specifically, the NPV of the electricity supplying cost is determined by:

$$C_E(b) = \sum_{y=1}^{Y} \frac{\sum_{t=1}^{T} [P_{G,buy}(b,t) R_{G,buy}(t) + P_{MG,buy}(b,t) R_{MG,buy}(t)] \Delta t}{(1+d)^y} \tag{3.7}$$

where $P_{G,buy}(b,t)$ and $P_{MG,buy}(b,t)$ denote the amounts of power imported by the main grid and the MG at each time interval t, respectively, while $R_{G,buy}(t)$ and $R_{MG,buy}(t)$ denote the corresponding electricity prices. Furthermore, the NPV of the carbon emissions-related cost depends on the power imported by the main grid, the carbon intensity $Carb_{int}$ of the area

where the MG is located, and the carbon taxes $Carb_{tax}$:

$$C_c(b) = \sum_{y=1}^{Y} \frac{\sum_{t=1}^{T} P_{G,buy}(b,t) Carb_{int} Carb_{tax} \Delta t}{(1+d)^y} \tag{3.8}$$

Finally, the NPV of each building's revenue $R_E(b)$ due to the electricity exports to the MG ($P_{MG,sell}(b,t)$) and to the main grid ($P_{G,sell}(b,t)$) is calculated as follows, where $R_{G,sell}(t)$ and $R_{MG,sell}(t)$ are the prices of selling power to the main grid and to the other MG users, respectively:

$$R_E(b) = \sum_{y=1}^{Y} \frac{\sum_{t=1}^{T} [P_{G,sell}(b,t) R_{G,sell}(t) + P_{MG,sell}(b,t) R_{MG,sell}(t)] \Delta t}{(1+d)^y} \tag{3.9}$$

Regarding the prices of energy transactions among the MG users and the price of selling energy to the main grid, the following relations hold:

$$R_{MG,buy}(t) = R_{MG,sell}(t) = r_1 R_{G,buy}(t) \tag{3.10}$$

$$R_{G,sell}(t) = r_2 R_{G,buy}(t) \tag{3.11}$$

where $r_1 > r_2$. The proposed pricing scheme promotes the cooperation among the MG participants for two reasons. The first one is that for buildings with power deficit is cheaper to import electricity from other participants than from the main grid. The second reason is that for buildings with power excess is more profitable to export to other MG users than to the main grid.

3.3 Operation plan of the MG

The objective function of the considered optimization problem, which is described by equation (3.1), is minimized subject to the following set of relations and constraints that describe the operation of the MG at each time interval of the optimization horizon.

3.3.1 Power balance

The power demand $P_L(b,t)$ of each building at any time interval is satisfied by importing power from the main grid $P_L^G(b,t)$, by the power $P_L^{PV}(b,t)$ produced by the PVs, by the power $P_L^{ESS}(b,t)$ discharged from the ESS, as well as by the power $P_L^{MG}(b,t)$ imported from neighboring buildings with power excess:

$$P_L(b,t) = P_L^G(b,t) + P_L^{PV}(b,t) + P_L^{ESS}(b,t) + P_L^{MG}(b,t) \tag{3.12}$$

3.3.2 PV operation

The produced PV power $P^{PV,pro}(b,t)$ is given by:

$$P^{PV,pro}(b,t) = N_{PV}(b)P^{PV,unit}(t) \tag{3.13}$$

where $N_{PV}(b)$ is the installed capacity of the PV array and $P^{PV,unit}(t)$ is the normalized PV production, which is obtained by considering the optimal PV panels' tilt angle and orientation for the MG's geographical location. The size of the PV array is bounded by the building's available surface $A_{PV}(b)$ and the amount of PV capacity λ_{PV} that can be installed per available surface:

$$N_{PV}(b) \leq A_{PV}(b)\lambda_{PV} \tag{3.14}$$

Part of the power at the output of the PV array (i.e. the produced power multiplied by the overall efficiency n_{PV} of the PV system) is transferred though the inverter to the AC side for covering the building's load $P_L^{PV}(b,t)$, and for being sold to other MG participants and to the main grid ($P_{MG}^{PV}(b,t)$ and $P_G^{PV}(b,t)$, respectively). In addition, part of the produced power is used for charging the ESS ($P_{ESS}^{PV}(b,t)$):

$$P^{PV,pro}(b,t)n_{PV} = \frac{P_L^{PV}(b,t) + P_{MG}^{PV}(b,t) + P_G^{PV}(b,t)}{n_{INV}} + P_{ESS}^{PV}(b,t). \tag{3.15}$$

It should be noted that the power conversion losses at the inverter are denoted by dividing power transferred from the DC to the AC side ($P_L^{PV}(b,t)$, $P_{MG}^{PV}(b,t)$ and $P_G^{PV}(b,t)$) by the inverter's efficiency n_{INV}.

3.3.3 ESS operation

The state of energy of each building's ESS at any time interval $SoE_{ESS}(b,t)$ depends on the state of energy of the previous time interval, and the charging power $P_{c,ESS}(b,t)$, if the ESS is being charged, or the discharging power $P_{d,ESS}(b,t)$, if the ESS is being discharged, during the current time interval:

$$SoE_{ESS}(b,t) = SoE_{ESS}(b,t-1) + P_{c,ESS}(b,t)\Delta t - P_{d,ESS}(b,t)\Delta t + u_{ESS}^{init}(b,t)SoE_{ESS}(b,t_0) \tag{3.16}$$

where, $SoE_{ESS}(b,t_0)$ denotes the state of energy of the ESS at the beginning of the optimization horizon, and $u_{ESS}^{init}(b,t)$ is a binary parameter, which is equal to 1 only for the first time interval and equal to 0 for any other interval. In order to ensure that the final solution of the optimization problem is not conditioned by the initial storage level, the state of energy $SoE_{ESS}(b,T)$ at the end of the optimization horizon should be higher than or

equal to state of energy at the beginning of the optimization horizon:

$$SoE_{ESS}(b,T) \geq SoE_{ESS}(b,t_0). \tag{3.17}$$

Moreover, as constrain (3.18) denotes, the ESS's state of energy at any time interval ranges between a minimum and a maximum value ($SoE_{ESS,\min}$ and $SoE_{ESS,\max}$, respectively):

$$SoE_{ESS,\min} \leq SoE_{ESS}(b,t) \leq SoE_{ESS,\max} \tag{3.18}$$

The ESS's charging power $P_{c,ESS}(b,t)$ consists of the power $P_{ESS}^{PV}(b,t)$ provided by the PVs and by the power $P_{ESS}^{MG}(b,t)$ that is imported by the neighboring buildings, while the ESS's discharging power $P_{d,ESS}(b,t)$ is used for satisfying the local load $P_L^{ESS}(b,t)$, as well as for being sold to other MG buildings ($P_{MG}^{ESS}(b,t)$):

$$P_{c,ESS}(b,t) = [P_{ESS}^{PV}(b,t) + P_{ESS}^{MG}(b,t)]n_{c,ESS} \tag{3.19}$$

$$P_{d,ESS}(b,t)\ n_{d,ESS}\ n_{INV}{=}P_L^{ESS}(b,t){+}P_{MG}^{ESS}(b,t) \tag{3.20}$$

The parameters $n_{c,ESS}$ and $n_{d,ESS}$ define the ESS's charging and discharging efficiency, respectively, while equations (3.21) and (3.22) define the upper limit of the ESS's charging and discharging power, which depends on the charging rate Z_{ESS} and the capacity N_{ESS}. The ESS cannot be charged and discharged simultaneously. This is ensured by constraints (3.23) and (3.24) where $u_{ESS}(b,t)$ is a binary variable and Ξ is a very large number:

$$P_{c,ESS}(b,t) \leq Z_{ESS}N_{ESS}(b) \tag{3.21}$$

$$P_{d,ESS}(b,t) \leq Z_{ESS}N_{ESS}(b) \tag{3.22}$$

$$P_{c,ESS}(b,t) \leq \Xi u_{ESS}(b,t) \tag{3.23}$$

$$P_{d,ESS}(b,t) \leq \Xi[1 - u_{ESS}(b,t)] \tag{3.24}$$

3.3.4 Power exchanges

At any time interval there may be users that buy power from other MG participants or/and from the main grid. As described by relation (3.25), the power bought from the MG is used for satisfying the load or/and for charging the ESS, while as described by relation (3.26),

the power bought from the main grid is used only for satisfying the load:

$$P_{MG,buy}(b,t) = P_L^{MG}(b,t) + \frac{P_{ESS}^{MG}(b,t)}{n_{INV}} \tag{3.25}$$

$$P_{G,buy}(b,t) = P_L^{G}(b,t) \tag{3.26}$$

Furthermore, at any time interval there may be users that sell power to other MG participants or/and to the main grid. As described by relation (3.27) the power sold to the MG is provided by the PVs and the ESS, while as described by relation (3.28) the power sold to the main grid is provided only by the PVs:

$$P_{MG,sell}(b,t) = P_{MG}^{PV}(b,t) + P_{MG}^{ESS}(b,t) \tag{3.27}$$

$$P_{G,sell}(b,t) = P_{G}^{PV}(b,t) \tag{3.28}$$

The following constraints ensure that the buildings cannot sell and buy power at the same time:

$$P_{MG,buy}(b,t) + P_{G,buy}(b,t) \leq \Xi u_{ex}(b,t) \tag{3.29}$$

$$P_{MG,sell}(b,t) + P_{G,sell}(b,t) \leq \Xi[1 - u_{ex}(b,t)] \tag{3.30}$$

where $u_{ex}(b,t)$ is a binary variable. In addition, the total amount of power bought from the MG by the buildings belonging to the subset $B^{'} \subseteq B$ (left side of (3.31)) equals the total amount of power sold to the MG by the buildings belonging to the subset $B^{''} \subseteq B$(right side of (3.31)):

$$\sum_{b \in B'} P_{MG,buy}(b,t) = \sum_{b \in B''} P_{MG,sell}(b,t) \tag{3.31}$$

3.3.5 Inverter operation

The following constraints denote that the power transferred from the DC to the AC side through each building's inverter, as well as the power that follows the opposite direction are bounded by the inverter's nominal capacity $N_{INV}(b)$:

$$\frac{P_L^{PV}(b,t) + P_L^{ESS}(b,t) + P_{MG,sell}(b,t) + P_{G,sell}(b,t)}{n_{INV}} \leq N_{INV}(b) \tag{3.32}$$

$$\frac{P_{ESS}^{MG}(b,t)}{n_{INV}} \leq N_{INV}(b) \tag{3.33}$$

Table 3.1: Specifications of power equipment [48], [77]

Parameter	Value
ESS charging efficiency coefficient ($n_{c,ESS}$)	0.95
ESS discharging efficiency coefficient ($n_{d,ESS}$)	0.95
Power rate of the ESS (Z_{ESS})	0.5
ESS minimum value of the SoE ($SoE_{ESS,\min}$)	0.2
ESS maximum value of the SoE ($SoE_{ESS,\max}$)	1
PV efficiency coefficient (n_{PV})	0.95
Inverter efficiency coefficient (n_{INV})	0.9

3.4 Numerical results

The proposed optimization model is evaluated by considering a MG located in Barcelona, Spain, which comprises of a multi-apartment residential building, a school and a municipality administrative building. The buildings' hourly power consumptions for one year are provided by the municipality of Barcelona, while the available surfaces for installing PV panels are: i) for the residential building 750 m^2, ii) for the school 900 m^2, and, iii) for the administrative building 1000 m^2. By assuming that 1 kW is installed for every 7 m^2 of available surface, the maximum PV capacity that can be installed at the residential building, the school and the administrative building are 107 kW, 128.6 kW and 143 kW, respectively. In addition, the normalized hourly PV production profile for one year is obtained by considering the optimal PV panels' tilt angle and orientation for the area of Barcelona (31°, south) in the PVWatt calculator [60].

The input parameters regarding the technical specifications of the power equipment, such as the PVs' and inverters' efficiency, the ESSs' charge and discharge efficiency and power rate, as well as the ESSs' minimum and maximum state of energy are summarized in Table 3.1. Furthermore, Table 3.2 contains the input parameters that are taken into account for the buildings' cost calculations, such as the acquisition and maintenance costs of the PVs, the ESSs and the inverters, the ESS's replacement year, the project lifetime, the discount rate, the carbon intensity and the carbon tax. In addition, Table 3.3 reports the applied time-of-use electricity rates of a Spanish retailer [61], which differ between winter and summer months. In both cases, the lower rate is from 00:00-08:00, while during the winter months, the higher rate is between 18:00 and 22:00, and the peak price period for the summer months is between 11:00 and 15:00. For the remaining hours the medium rate is activated. Finally, as Table 3.4 reports, the rates of energy transactions among the MG users is considered to be 40 percent lower than the corresponding rates provided by the energy retailer, while the price of selling energy back to the main grid is 90 percent lower than the corresponding buying prices.

Table 3.2: Economic data [48], [76], [77]

Parameter	**Value**
Project Lifetime (Y)	20 (yr)
Discount rate (d)	3%
Carbon Intensity ($Carb_{int}$)	0.455 (kg/kW)
Carbon Tax ($Carb_{tax}$)	0.03 (€/kg)
ESS acquisition cost (c_{ESS})	208 (€/kWh)
ESS annual maintenance cost (μ_{ESS})	(2.1 €/kWh/yr)
ESS replacement year	15
PV acquisition cost (c_{PV})	1000 (€/kW)
PV annual maintenance cost (μ_{PV})	3.3 (€/kWh/yr)
Inverter acquisition cost (c_{INV})	106 (€/kW)
Inverter annual maintenance cost (μ_{INV})	(0.8 €/kWh/yr)

Table 3.3: Open market energy tariffs $R_{G,buy}(t)$.

	November - March	**April - October**
00:00-08:00	0.079 €/kWh	0.079 (€/kWh)
00:80-11:00	0.109 €/kWh	0.109 (€/kWh)
11:00-15:00	0.109 €/kWh	0.135 (€/kWh)
15:00-18:00	0.109 €/kWh	0.109 (€/kWh)
18:00-22:00	0.135 €/kWh	0.109 (€/kWh)
22:00-00:00	0.109 €/kWh	0.109 (€/kWh)

Table 3.4: Energy prices for the transactions among the MG users and the main grid.

Parameter	**Value**
Price of buying energy by other MG users	$R_{MG,buy}(t) = 0.6R_{G,buy}(t)$ (€/kWh)
Price of selling energy to other MG users	$R_{MG,sell}(t) = 0.6R_{G,buy}(t)$ (€/kWh)
Price of selling energy to the main grid	$R_{G,sell}(t) = 0.1R_{G,buy}(t)$(€/kWh)

Table 3.5: Results for the three evaluation scenarios.

	Residential	**School**	**Public Building**	**Total**
Main Grid Scenario				
Annualized Cost (€)	26,690	39,245	42,641	108,576
No Energy Exchange Scenario				
Annualized Cost (€)	21,831	26,905	28,023	76,759
$N_{PV}(b)$ (kW)	71.6	128.6	143	343.2
$N_{ESS}(b)$ (kWh)	28.3	0	67	95.3
$N_{INV}(b)$ (kW)	38.5	72.5	79	190
Energy Exchange Scenario				
Annualized Cost (€)	18,108	22,775	24,729	65,612
$N_{PV}(b)$(kW)	107	128.6	143	378.6
$N_{ESS}(b)$(kWh)	98	120	77.5	295.5
$N_{INV}(b)$(kW)	50	65	73	188

In order to highlight the advantages of the proposed cooperative scheme, we present cost results for three different scenarios: the main grid scenario assumes that all buildings obtain the required energy exclusively from the main distribution network; therefore, no PVs, ESSs and inverters are installed. The no energy exchange scenario assumes that all buildings are equipped with PVs, ESSs and inverters, but, they are not able to exchange energy with each other. Finally, the energy exchange scenario applies the cooperative model. As Table 3.5 reveals, the application of the proposed cooperative scheme results in a significant cost reduction compared to the other two scenarios. Precisely, the application of the cooperative scheme results in 39.5% total cost savings compared to the main grid scenario and 14.5% compared to the no energy exchange scenario. This is achieved despite the fact that the sizes of the PVs, inverters and ESSs are higher under the cooperative scheme.

We also present the results of the case study regarding the optimal operation plan of the three considered buildings. Figure 3.2 illustrates the hourly power allocation during a Sunday in February, while Figure 3.3 shows the corresponding results for the case of a Monday in the same month. In addition, Figure 3.4 and Figure 3.5 present the corresponding results for a Sunday and a Monday in July, respectively. The comparison of these figures reveals that the energy exchange procedure is highly affected by the type of the day and the season. The residential building mainly buys energy on Sundays, while it provides its excess energy on Mondays when its demands are low and the PV production high. Furthermore, in both months the residential building uses the energy generated by its PV panels during the light-day hours, while during the high energy consumption evening hours, the building uses the energy stored in its ESS, as well as the energy bought from the other two buildings. On the other hand, the school buys energy on Mondays during their peak load, while it sells energy in any other case during low-load periods. Finally, the administrative building sells energy to the MG during the winter months, while on the contrast, buys great amounts of energy during its peak load, which takes place on weekday evenings of summer months.

Figure 3.2: Operation plan of the three buildings during a weekend day in February

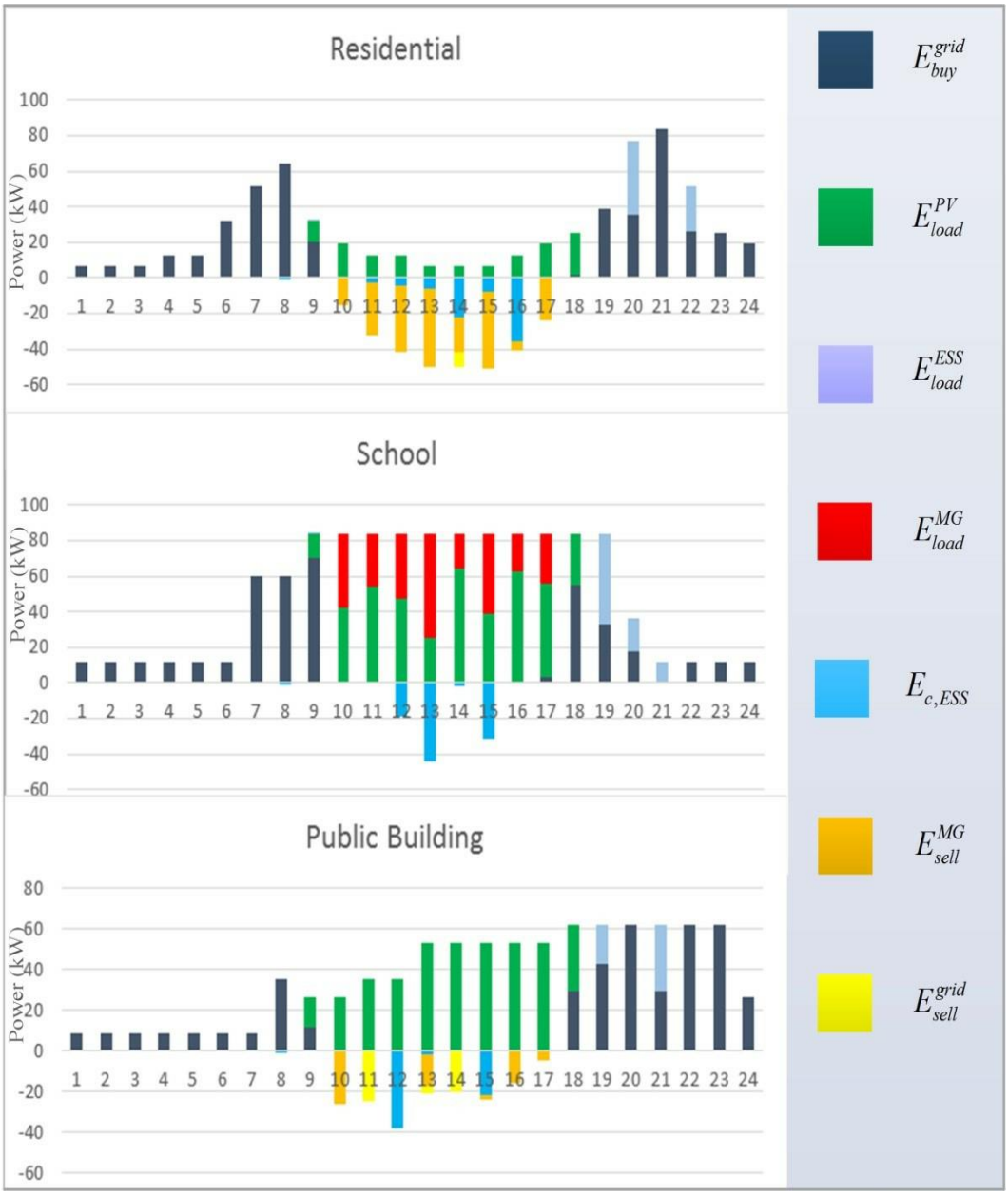

Figure 3.3: Operation plan of the three buildings during a week day in February

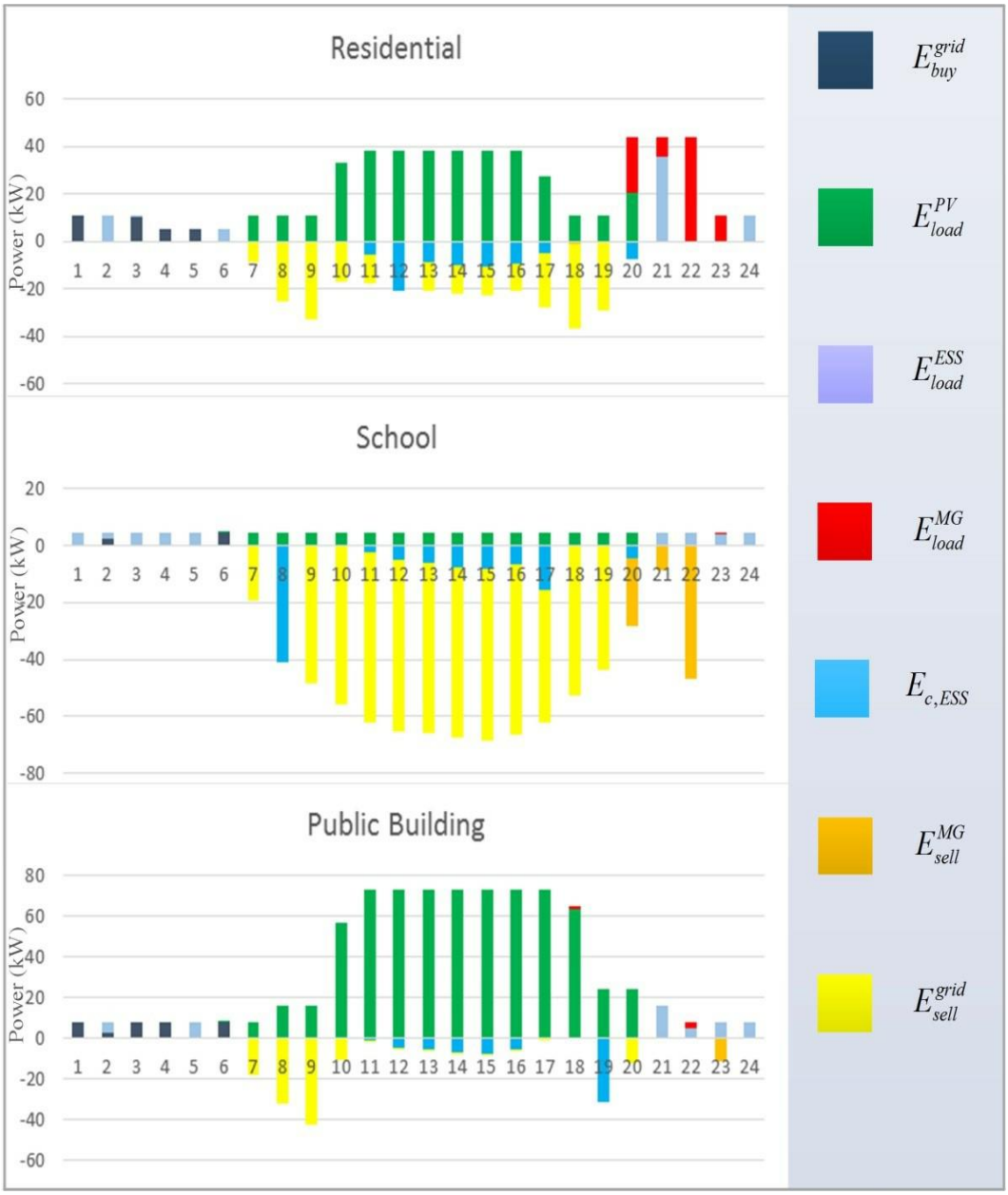

Figure 3.4: Operation plan of the three buildings during a weekend day in July

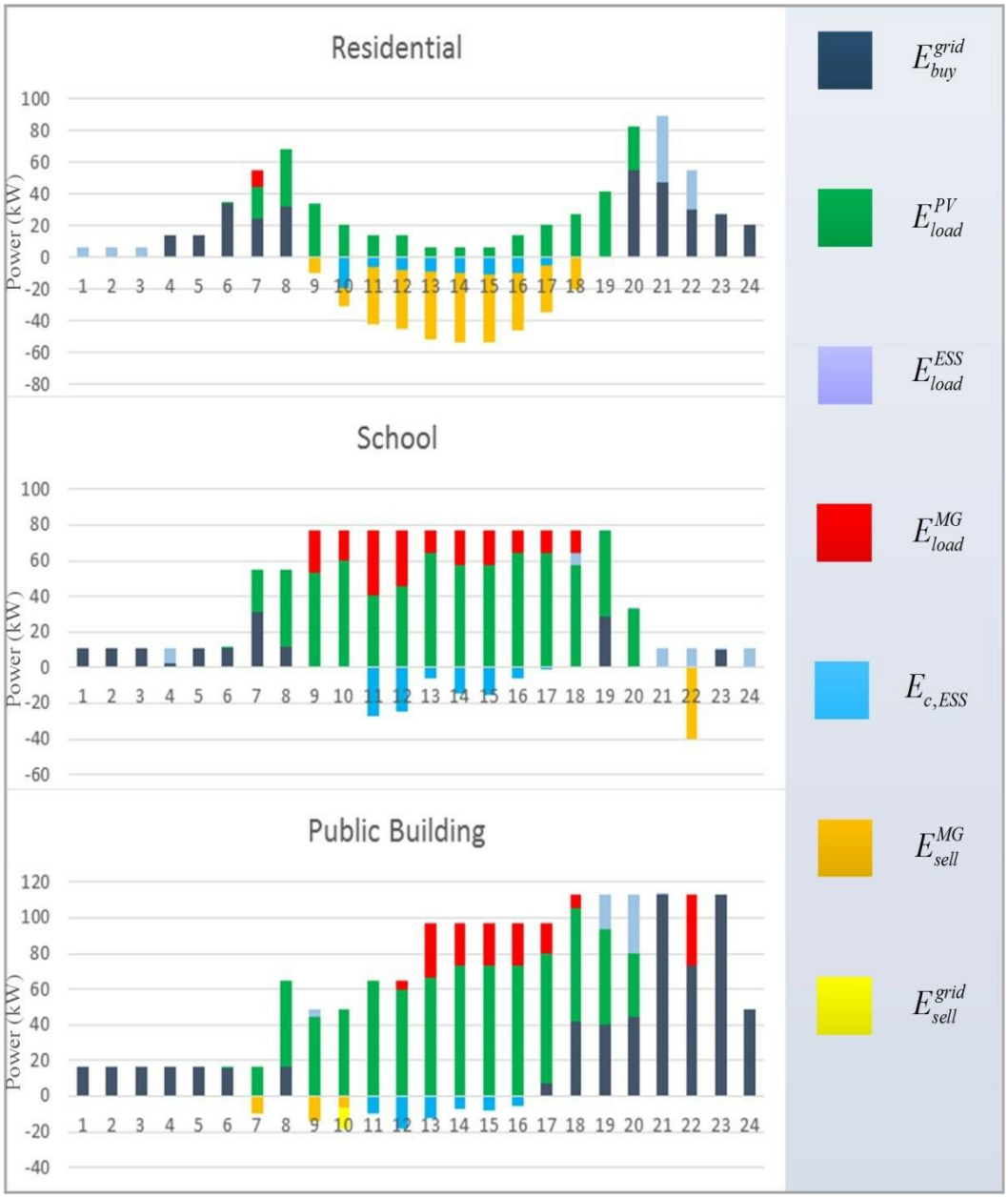

Figure 3.5: Operation plan of the three buildings during a week day in July

4 Buildings' cooperation in microgrids: an optimal equipment sizing and operation planning approach based on the Nash bargaining method

The benefits of cooperation among neighboring buildings with diverse load profiles are highlighted in the previous chapter in terms of power equipment sizing and operation planning. The system architecture presented in chapter 3 refers to a MG topology where the various buildings are fed by a common distribution transformer and the energy exchanges among the participants take place through a PCC, which is the low voltage side of the distribution transformer. However, there may be neighboring buildings that are willing to participate in the coalition, but they are fed by different distribution transformers. In that case, the only way for the buildings to exchange energy is through the medium voltage distribution line, which means that the decisions for the optimal power flows are taken by the distribution system operator, and not by the MG operator. The power losses taking place both at the seller's and buyer's distribution transformer is another disadvantage of exchanging energy through the medium voltage lines.

A MG topology that removes the aforementioned disadvantages is proposed in this chapter. Specifically, it is considered that the various buildings are connected to a common DC bus through which the energy exchanges take place. Moreover, this chapter considers that V2B systems are installed in the buildings. The smart charge and discharge scheduling of the EVs, which is not taken into account in the previous chapter's model, provides additional power scheduling flexibility. Another advantage of the present analysis is that the MG's optimal sizing and operation planning are determined by applying the Nash bargaining method. The superiority of this method compared to the traditional one (minimization of the aggregated cost of all participants as in equation 3.1) is that the savings achieved due to the buildings' cooperation are equally distributed among the MG's users. On the contrary, with the traditional method, some participants may achieve higher savings than others. Finally, in all works of the state-of-the-art dealing with the MGs' optimal sizing and operation planning problem, it is considered that the system's topology is the same for the whole lifetime of the project (it consists of the same set of buildings from the beginning till the end of the project). A significant contribution of the present analysis is that investigates the possible integration of additional buildings, years after the initial coalition's establishment.

This chapter is organized as follows. Section 4.1 presents the MG's architecture and the equations that describe its operation. Section 4.2 presents the economic analysis and the formulation of the objective function based on the Nash bargaining method. The integration of additional buildings in the initial coalition is described in section 4.3, while the considered case study is presented in section 4.4.

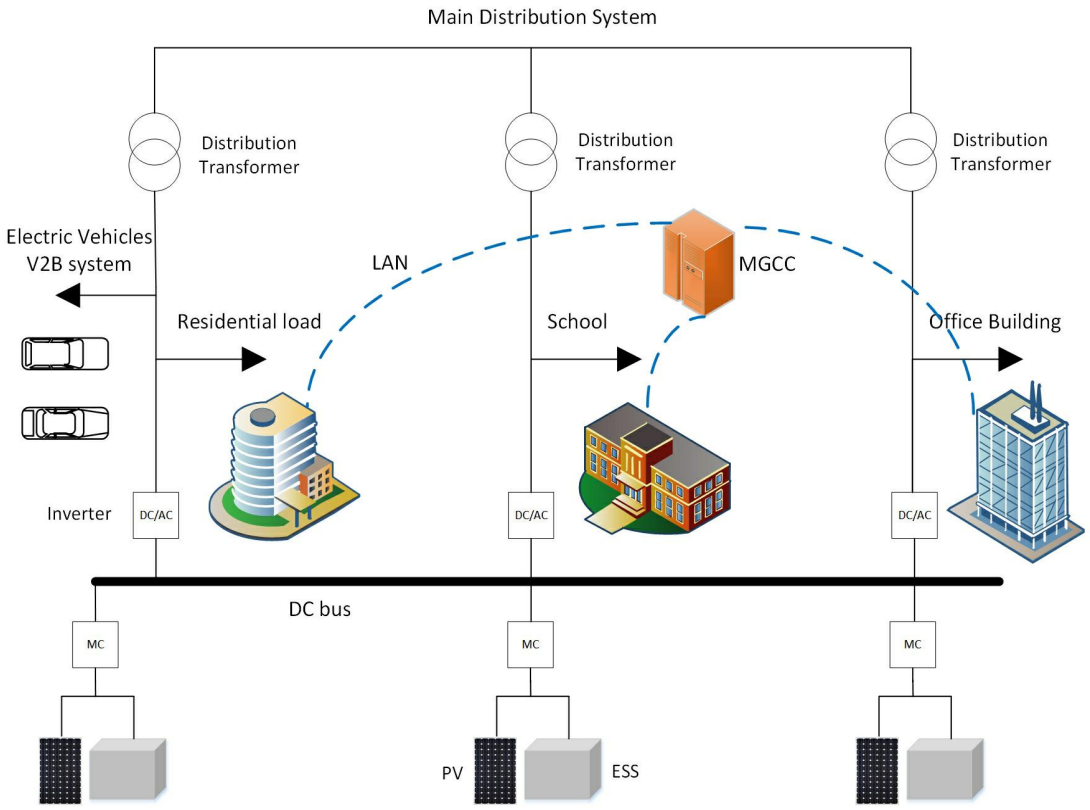

Figure 4.1: Microgrid architecture.

4.1 MG architecture and modeling

The proposed MG architecture is presented in Figure 4.1. The buildings' PVs and ESSs are installed on a DC bus, which interconnects the whole set of participating members. The V2B systems are installed at the AC side of the buildings, while the inverters are the interfaces between the DC and the AC side. Furthermore, a LAN interconnects the buildings' local controllers with the MGCC.

4.1.1 Power balance

At any time interval, the power balance at each building is described by equation (4.1):

$$P_L(b,t) = P_L^G(b,t) + P_L^{PV}(b,t) + P_L^{ESS}(b,t) + P_L^{MG}(b,t) + P_L^{EV}(b,t) \tag{4.1}$$

As in the corresponding power balance relation of chapter 3, $P_L^G(b,t)$ denotes the power imported from the main grid, $P_L^{PV}(b,t)$ the PV power that is used for self-consumption, $P_L^{ESS}(b,t)$ the power discharged from the ESS, and $P_L^{MG}(b,t)$ the power imported from the other MG users. It should also be noted that in the present analysis part of the load is satisfied by the EVs' discharging power, which is denoted as P_L^{EV} (b,t).

4.1.2 PV operation

As in chapter 3, the produced PV power $P^{PV,pro}(b,t)$ is determined based on the size $N_{PV}(b)$ of the PV array and the normalized PV production $P^{PV,unit}(t)$ at the MG's location:

$$P^{PV,pro}(b,t) = N_{PV}(b)P^{PV,unit}(t) \tag{4.2}$$

while the size of the PV array is bounded by each building's available surface $A_{PV}(b)$ and the amount λ_{PV} of PV capacity that can be installed per available surface:

$$N_{PV}(b) \leq A_{PV}(b)\lambda_{PV} \tag{4.3}$$

The following relation describes the way the produced PV power is utilized:

$$P^{PV,pro}(b,t)n_{PV}=\frac{P_L^{PV}(b,t)+P_{EV}^{PV}(b,t)+P_G^{PV}(b,t)}{n_{INV}}+P_{ESS}^{PV}(b,t)+P_{MG}^{PV}(b,t). \tag{4.4}$$

There are two main differences between (4.4) and the corresponding r (3.15) of chapter 3. The first difference is that part of the produced PV power is transferred through the inverter to the EVs ($P_{EV}^{PV}(b,t)$). The power $P_L^{PV}(b,t)$ that is used for the local load, as well as the power $P_G^{PV}(b,t)$ that is sold to the main grid are also transferred from the DC to the AC side. The power converion losses are denoted by dividing the aforementioned terms by the efficiency of the inverter n_{INV}. On the other hand, the power $P_{ESS}^{PV}(b,t)$ that is used for charging the ESS, and the power $P_{MG}^{PV}(b,t)$ that is sold to the other MG users are injected to the common DC bus. The fact that $P_{MG}^{PV}(b,t)$ is transferred to the other buildings through the DC bus is the second difference between the present approach and that of chapter 3.

4.1.3 ESS operation

The ESS operation is described by the same relations as in chapter 3. The only difference is noticed in the equation that refers to the ESS' discharging power (4.9):

$$SoE_{ESS}(b,t)=SoE_{ESS}(b,t-1)+P_{c,ESS}(b,t)\Delta t-P_{d,ESS}(b,t)\Delta t+u_{ESS}^{init}(b,t)SoE_{ESS}(b,t_0) \tag{4.5}$$

$$SoE_{ESS}(b,T) \geq SoE_{ESS}(b,t_0). \tag{4.6}$$

$$SoE_{ESS,\min} \leq SoE_{ESS}(b,y,t) \leq SoE_{ESS,\max} \tag{4.7}$$

$$P_{c,ESS}(b,t) = [P_{ESS}^{PV}(b,t) + P_{ESS}^{MG}(b,t)]n_{c,ESS} \tag{4.8}$$

$$P_{d,ESS}(b,t)n_{d,ESS}=\frac{P_L^{ESS}(b,t)+P_{EV}^{ESS}(b,t)}{n_{INV}}+P_{MG}^{ESS}(b,t) \tag{4.9}$$

$$P_{c,ESS}(b,t) \leq Z_{ESS}N_{ESS}(b) \tag{4.10}$$

$$P_{d,ESS}(b,t) \leq Z_{ESS}N_{ESS}(b) \tag{4.11}$$

$$P_{c,ESS}(b,t) \leq \Xi u_{ESS}(b,t) \tag{4.12}$$

$$P_{d,ESS}(b,t) \leq \Xi[1-u_{ESS}(b,t)] \tag{4.13}$$

According to equation (4.5), the state of energy $SoE_{ESS}(b,t)$ at the current time interval is determined by the state of energy of the previous interval $SoE_{ESS}(b,t-1)$ plus the energy that is transferred to the ESS (if it is being charged during the current time interval), or minus the discharged energy (if it is being discharged during the current time interval). Δt is the duration of the optimization intervals, $SoE_{ESS}(b,t_0)$ denotes the state of energy at the beginning of the optimization horizon, while the binary parameter u_{ESS}^{init} is equal to 1 for the first time interval and equal to 0 for any other time interval. Constraint (4.6) ensures that the state of energy at the beginning of the optimization horizon is higher than or equal to the state of energy at the end of the optimization horizon, while constraint (4.7) sets the minimum and the maximum state of energy of the ESS. According to equation (4.8), the charging power $P_{c,ESS}(b,t)$ is provided by the PVs ($P_{ESS}^{PV}(b,t)$) and by imports from other MG users through the DC bus ($P_{ESS}^{MG}(b,t)$). According to (4.9), part of the ESS's discharging power $P_{d,ESS}(b,t)$ is transferred to the AC side through the inverter for covering part of the building's load ($P_L^{ESS}(b,t)$), as well as part of the building's EVs needs ($P_{EV}^{ESS}(b,t)$). Furthermore, part of the ESS's discharging power is transferred to other MG users through the DC bus ($P_{MG}^{ESS}(b,t)$). The parameters $n_{c,ESS}$ and $n_{d,ESS}$ define the ESS's charging and discharging efficiency, respectively. Furthermore, constraints (4.10) and (4.11) define the upper limit of the ESS's charging/discharging power, which is a function of the charging rate Z_{ESS} and the capacity N_{ESS}. Finally, constraints (4.12) and (4.13) ensure that the ESS is not charged and discharged at the same time. This is mathematically modeled by using the parameter Ξ, which is a very large number, and the binary variable $u_{ESS}(b,t)$.

4.1.4 EVs' operation

One of the main differences between the MG topology of chapter 3 and the present one is the assumption that the buildings are equipped with the V2B technology. Specifically, it is considered that each building b, $(b=1,...,B)$ comprises a set of V_b EVs. Relations

(4.14)-(4.20) describe the operation of each single EV, while relations (4.21)-(4.26) describe the way the charging and discharging procedures of the whole set of EVs are scheduled.

As equation (4.14) denotes, the EVs' charging power $H_{c,EV}(v,t)$, where (v=(1,..., V_b)), is provided by the PVs, the ESS, as well as by the imports from the MG and the main grid ($H_{EV}^{PV}(v,t)$, $H_{EV}^{ESS}(v,t)$, $H_{EV}^{MG}(v,t)$ and $H_{EV}^{G}(v,t)$, respectively). According to equation (4.15), the EVs' discharging power $H_{d,EV}(b,t)$ is only used for satisfying part of the local load $P_L^{EV}(b,t)$. In (4.14) and (4.15), the parameters $n_{c,EV}$ and $n_{d,EV}$ define the charging and discharging efficiency of the EVs. Constraints (4.16) and (4.17) ensure that the EVs are not charged and discharged at the same time, while they also define the upper limit of the charging and discharging power. Additionally, in the aforementioned relations, Z_{EV} denotes the EVs' charging and discharging rate, while $u_{EV}(v,t)$ is a binary variable. The EVs' state of energy $SoE_{EV}(v,t)$ at any time interval t is described by equation (4.18). Similar to the ESSs' case, $SoE_{EV}(v,t)$ is equal to the state of energy of the previous time interval $SoE_{EV}(v,t-1)$ plus the energy that is transferred to the EV, or minus the discharged energy. Constraint (4.19) defines the EVs' minimum and the maximum state of energy, while (4.20) defines the EVs' arrival and departure state of energy.

$$H_{c,EV}(v,t)=[H_{EV}^{PV}(v,t)+H_{EV}^{ESS}(v,t)+H_{EV}^{MG}(v,t)+H_{EV}^{G}(v,t)]n_{c,EV} \tag{4.14}$$

$$H_{d,EV}(v,t)n_{d,EV} = H_L^{EV}(v,t) \tag{4.15}$$

$$H_{c,EV}(v,t) \leq Z_{EV}(v)u_{EV}(v,t) \tag{4.16}$$

$$H_{d,EV}(v,t) \leq Z_{EV}(v)[1-u_{EV}(v,t)] \tag{4.17}$$

$$SoE_{EV}(v,t)=SoE_{EV}(v,t-1)+H_{c,EV}(v,t)\Delta t - H_{d,EV}(v,t)\Delta t+u_{EV}^{init}(v,t)SoE_a(v,T_a(v)) \tag{4.18}$$

$$SoE_{EV,\min} \leq SoE_{EV}(v,t) \leq SoE_{EV,\max} \tag{4.19}$$

$$SoE_{EV}(v,T_a(v))=SoE_a(v), SoE_{EV}(v,T_d(v))=SoE_d(v) \tag{4.20}$$

The aforementioned relations ((4.14) - (4.20)) hold for $T_a(v) \leq t \leq T_d(v)$, where $T_a(v)$ and $T_d(v)$ define the EVs' arrival and departure times, respectively. Also, the parameter $u_{EV}^{init}(v,t)$ equals 1 for t=$T_a(v)$ and 0 in any other case. The charging power for the whole

set of the EVs is provided by the PVs, the ESS, the MG and the main grid:

$$P_{c,EV}(b,t)=P_{EV}^{PV}(b,t)+P_{EV}^{ESS}(b,t)+P_{EV}^{MG}(b,t)+P_{EV}^{G}(b,t) \tag{4.21}$$

where

$$P_{EV}^{PV}(b,t) = \sum_{v \in V_b} H_{EV}^{PV}(v,t) \tag{4.22}$$

$$P_{EV}^{ESS}(b,t) = \sum_{v \in V_b} H_{EV}^{ESS}(v,t) \tag{4.23}$$

$$P_{EV}^{MG}(b,t) = \sum_{v \in V_b} H_{EV}^{MG}(v,t) \tag{4.24}$$

$$P_{EV}^{G}(b,t) = \sum_{v \in V_b} H_{EV}^{G}(v,t) \tag{4.25}$$

In addition, as equation (4.26) denotes, the total amount of the EVs' discharging power is used for satisfying the local load only.

$$P_{d,EV}(b,t) = P_{L}^{EV}(b,t) = \sum_{v \in V_b} H_{L}^{EV}(v,t) \tag{4.26}$$

4.1.5 Power exchanges

At any time interval there may be users that buy power from other MG participants or/and from the main grid. As described by relation (4.27), the power bought from the MG is used for satisfying the load, part of the EVs' needs and for charging the ESS. Note that the power bought from the MG for the load and the EVs is transfered from the common DC bus to the AC side of the buildings through the inverter. The power losses at the inverter are denoted by dividing the terms $P_{L}^{MG}(b,t)$ and $P_{EV}^{MG}(b,t)$ by the inverter's efficiency. On the other hand, the power bought from the MG for charging the ESS is directly transferred to the ESS without any power conversion losses. Furthermore, as described by relation (4.28), the power bought from the main grid is used for satisfying the load and the EVs' needs:

$$P_{MG,buy}(b,t) = \frac{P_{L}^{MG}(b,t) + P_{EV}^{MG}(b,t)}{n_{INV}} + P_{ESS}^{MG}(b,t) \tag{4.27}$$

$$P_{G,buy}(b,t) = P_{L}^{G}(b,t) + P_{EV}^{G}(b,t). \tag{4.28}$$

Moreover, at any time interval there may be users that sell power to other MG participants or/and to the main grid. As described by relation (4.29) the power sold to the MG is provided by the PVs and the ESS, while according to (4.30) the power sold to the main grid is provided

by the PVs only:

$$P_{MG,sell}(b,t) = P_{MG}^{PV}(b,t) + P_{MG}^{ESS}(b,t) \tag{4.29}$$

$$P_{G,sell}(b,t) = P_{G}^{PV}(b,t) \tag{4.30}$$

The following constraints describe the fact that the buildings cannot sell and buy power at the same time:

$$P_{MG,buy}(b,t) + P_{G,buy}(b,t) \leq \Xi u_{ex}(b,t) \tag{4.31}$$

$$P_{MG,sell}(b,t) + P_{G,sell}(b,t) \leq \Xi[1 - u_{ex}(b,t)] \tag{4.32}$$

where $u_{ex}(b,t)$ is a binary variable. In addition, at any time interval, the total amount of power bought from the MG by the buildings belonging to the subset $B^{'} \subseteq B$ (left side of (4.33)) is equal to the total amount of power sold to the MG by the buildings belonging to the subset $B^{''} \subseteq B$ (right side of (4.33)):

$$\sum_{b \in B'} P_{MG,buy}(b,t) = \sum_{b \in B''} P_{MG,sell}(b,t) \tag{4.33}$$

4.1.6 Inverter operation

Finally, constraint (4.34) ensures that the power transferred from the DC bus to the AC side of each building is bounded by the inverter's nominal capacity $N_{INV}(b)$. It should also be noted that in contrast with the analysis of the corresponding section 3.3.5 of the previous chapter 3, in the present case no power is transferred from the AC side to the DC side of the buildings.

$$\frac{P_{L}^{PV}(b,t)+P_{EV}^{PV}(b,t)+P_{L}^{ESS}(b,t)+P_{EV}^{ESS}(b,t)+P_{L}^{MG}(b,t)+P_{EV}^{MG}(b,t)+P_{G,sell}(b,t)}{n_{INV}} \leq N_{INV}(b) \tag{4.34}$$

4.2 Economic analysis and Nash bargaining method

As in section 3.2, the overall annualized cost of each building is defined by:

$$C(b) = CRF(d,Y)[C_A(b)+C_M(b)+C_R(b)+C_E(b)+C_C(b)-R_E(b)] \tag{4.35}$$

while the NPVs of the equipment acquisition, maintenance and replacement costs, the NPVs of the electricity supplying and carbon-emissions related costs, as well as the NPV of each building's revenue from electricity exports are obtained by the following equations, respectively:

$$C_A(b) = \sum_j N_j(b) c_j + L_{bus}(b) c_{bus}. \tag{4.36}$$

$$C_M(b) = \sum_{y=1}^{Y} \frac{\sum_j N_j(b)\mu_j + L_{bus}(b)\mu_{bus}}{(1+d)^y} \tag{4.37}$$

$$C_R(b) = \sum_{i=1}^{rep_j} \frac{\sum_j N_j(b)c_j}{(1+d)^{iYrep_j}} \tag{4.38}$$

$$C_E(b) = \sum_{y=1}^{Y} \frac{\sum_{t=1}^{T}[P_{G,buy}(b,t)R_{G,buy}(t) + P_{MG,buy}(b,t)R_{MG,buy}(t)]\Delta t}{(1+d)^y} \tag{4.39}$$

$$C_c(b) = \sum_{y=1}^{Y} \frac{\sum_{t=1}^{T} P_{G,buy}(b,t)Carb_{int}Carb_{tax}\Delta t}{(1+d)^y} \tag{4.40}$$

$$R_E(b) = \sum_{y=1}^{Y} \frac{\sum_{t=1}^{T}[P_{G,sell}(b,t)R_{G,sell}(t) + P_{MG,sell}(b,t)R_{MG,sell}(t)]\Delta t}{(1+d)^y} \tag{4.41}$$

where L_{bus} is the length of the DC bus required for the interconnection of each building to the MG, and c_{bus} and μ_{bus} are the per unit acquisition cost and maintenance costs, respectively of the DC bus. The considered pricing scheme is the same as in the previous chapter's analysis:

$$R_{MG,buy}(t) = R_{MG,sell}(t) = r_1 R_{G,buy}(t) \tag{4.42}$$

$$R_{G,sell}(t) = r_2 R_{G,buy}(t) \tag{4.43}$$

where $r_1 > r_2$.

A common approach that is used for optimizing a MG consisting of multiple members is the minimization of the aggregated annualized costs of the participants, as in the previous chapter:

$$w = \sum_b C(b) \tag{4.44}$$

The MG's equipment sizing and operation planning are obtained by minimizing (4.44) subject to (4.1) -(4.34). This method indicates the coalition savings compared to the case where each building is separately optimized. The coalition savings are defined as:

$$CSV = w' - w \tag{4.45}$$

where $w^{'}$ is the sum of the costs of each building when the buildings are separately optimized:

$$w^{'} = \sum_b C^{'}(b) \tag{4.46}$$

The cost $C^{'}(b)$ of each building's separate optimization is obtained by minimizing (4.44)

subject to (4.1) -(4.34). It should be noted that the terms in (4.1) -(4.34) that refer to the existence of the MG (terms that contain either a 'MG' subscript or a 'MG' superscript) are equal to zero when this problem is solved.

The motivation for buildings to participate in a coalition is to share part of the savings CSV in order to achieve lower costs compared to the separate optimization case ($C(b) \leq C^{'}(b)$). However, this is not guaranteed by implementing the traditional approach of minimizing the objective function in (4.44). For example, the optimal solution obtained through the traditional method may propose that the cost of some buildings is reduced ($C(b) = C^{'}(b) - \Psi_1(b), \Psi_1(b) > 0$), whereas the cost of other buildings is increased ($C(b) = C^{'}(b) + \Psi_2(b), \Psi_2(b) > 0$), so that $CSV = |\sum_b \Psi_1(b) - \sum_b \Psi_2(b)|$. The amount of coalition savings is derived to be the same when the Nash bargaining method is used. Moreover, the Nash bargaining method not only guarantees that the participants' costs will be lower than $C^{'}(b)$, but also that they attain the same amount of savings $SV(b) = C^{'}(b) - C(b) = CSV/B$. This is achieved by maximizing the following objective function that consists of the product of buildings' savings:

$$f = \prod_{b=1}^{B} SV(b) = \prod_{b=1}^{B} [C^{'}(b) - C(b)] \tag{4.47}$$

The objective function in (4.47) is non-linear, and therefore, it is linearized via logarithmic differentiation as $z = \ln f = \sum_{b=1}^{B} \ln[C^{'}(b) - C(b)]$, which is a sum of strictly concave functions $M(C(b)) = \ln[C^{'}(b) - C(b)]$ involving only one variable. When such a function is to be maximized, it can be approximated over an interval as a piecewise linear function $M_q(C_q(b)) = \ln[C^{'}(b) - C_q(b)])$ using m grid points [51]. The approximation is described by the following relations:

$$M(C(b)) \approx \sum_{q=1}^{m} M_q(C_q(b))\lambda_q \tag{4.48}$$

$$\sum_{q=1}^{m} \lambda_q = 1 \tag{4.49}$$

$$\lambda_q \geq 0. \tag{4.50}$$

λ_q are special ordered variables, and only two adjacent λ_q can be non-zero. Constraints (4.49) and (4.50) and the concavity requirement guarantee that two adjacent nodes out of the total m take non-zero values. Based on the logarithmic differentiation and the aforementioned approximation, the problem of maximizing (4.47) can be written as:

$$\max z \approx \sum_{b=1}^{B} \sum_{q=1}^{m} M_q(C_q(b))\lambda_q(b) \tag{4.51}$$

$$\sum_{q=1}^{m} \lambda_q(b) = 1 \tag{4.52}$$

$$\lambda_q(b) \geq 0 \tag{4.53}$$

where

$$\sum_{q=1}^{m} C_q(b)\lambda_q(b) = C(b) \tag{4.54}$$

$$C_{min}(b) \leq C(b) \leq C_{max}(b). \tag{4.55}$$

The maximum cost $C_{max}(b)$ is set to be equal to the annualized cost $C^{'}(b)$ of each building when it is separately optimized, while the minimum cost $C_{min}(b)$ is obtained by considering that each building reaps the whole amount of the coalition savings: $C_{min}(b)$=$C^{'}(b)$–CSV. The interval [$C_{max}(b)$, $C_{min}(b)$] is divided into m equal intervals where the value of interval q is assigned to the parameter $C_q(b)$. Based on (4.54), when the problem is solved, $C(b)$ is determined by the two adjacent intervals that have non-zero $\lambda_q(b)$ i.e. $C(b)$=$C_q(b)\lambda_q(b)$+ $C_{q+1}(b)\lambda_{q+1}(b)$. Recall that the total annualized cost $C(b)$ is given by (4.35) where the costs referring to the sizing aspect of the problem (acquisition, maintenance, replacement) are obtained by (4.36)-(4.38), respectively, and the costs referring to the operational planning aspect (electricity supplying, carbon emissions, electricity exports) are obtained by (4.39)-(4.41), respectively. The optimal MG sizing and operation planning are determined by maximizing (4.51) subject to (4.1)-(4.34) and (4.52)-(4.55).

4.3 Integration of additional buildings

The aforementioned economic analysis refers to the case where there is a set of B buildings that participate in the MG from the beginning of its establishment till the end of the project lifetime Y. In this section, we describe the concept of optimizing the MG when additional buildings join the coalition U years after the initial establishment. The equipment sizes for the initial set of building have already been determined, and hence, in this case the optimization process refers to the equipment sizes of the new buildings, as well as the operation plan of the new MG topology.

The NPVs of the equipment maintenance and replacement costs for the additional buildings are obtained by (4.37)-(4.38), respectively, by replacing Y with X=$Y-U$. This is due to the fact that the additional buildings will participate in the coalition for the remaining X years. For the same reason, the NPVs of the electricity supplying cost, the carbon emissions-related cost, and the buildings' revenue from electricity exports, are obtained by (4.39)-(4.41), respectively, by replacing Y with X. Under the new MG topology, the NPVs of the electricity supplying cost, the carbon emissions-related cost, and the revenue

of each building belonging to the initial set are given by relations (4.39)-(4.41), respectively by setting $y = U$ instead of $y = 1$. This is due to the fact that those costs depend on the operation plan, which in turn depends on the current MG topology. Based on the aforementioned analysis, the overall annualized cost of each building belonging to the initial set is:

$$C_{in}(b) = crf(d, Y)[C_A(b) + C_M(b) + C_R(b)] + crf(d, X)[C_E(b) + C_c(b) - R_E(b)] \tag{4.56}$$

while the overall annualized cost of each of the additional buildings is:

$$C_{ad}(b) = crf(d, X)[C_A(b) + C_M(b) + C_R(b) + C_E(b) + C_c(b) - R_E(b)] \tag{4.57}$$

Therefore, the total annualized cost of the system is:

$$w_{nt} = \sum_{b \in B} C_{in}(b) + \sum_{b \in B_U} C_{ad}(b) \tag{4.58}$$

The chart of Figure 4.2 summarizes the process of selecting the optimal equipment sizes for the additional buildings, as well as of obtaining the optimal operation plan of the new MG topology. The process consists of four steps. The first step refers to the optimization of the initial MG topology, which determines the equipment sizes and the total annualized cost of the initial set of buildings B. The obtained equipment sizes are used as input parameters in the fourth step, while the obtained annualized cost is used as the maximum cost $C_{in,max}$ of the initial set of buildings B when the Nash bargaining method is implemented in the fourth step. The second step refers to the separate optimization of the additional buildings. This step is necessary for obtaining the maximum annualized cost $C_{ad,max}$ of the additional buildings, which is also used in the fourth step. Note that the problem of optimizing the additional buildings separately is the same as the separate optimization of the initial buildings. The third step optimizes the new MG topology through the traditional method (minimization of the aggregated annualized costs of the participants). This step is necessary for obtaining the savings CSV_{nt} of the new MG topology, which are derived by the summation of the total cost of the initial coalition with the costs of the additional buildings' separate optimization, minus the total cost of the new MG topology. CSV_{nt} is then used in the fourth step for obtaining the minimum annualized costs of the initial and additional buildings ($C_{in,min}$ and $C_{ad,min}$, respectively). At this point it should be noted that the profitability of the new coalition depends on how many years after the establishment of the initial coalition the additional members join. If the savings calculated in the third step are negative, the integration of new participants should be avoided. Finally, the fourth step refers to implementation of the Nash bargaining method for obtaining the equipment sizes for the additional buildings, as well as the operation plan of the new MG topology.

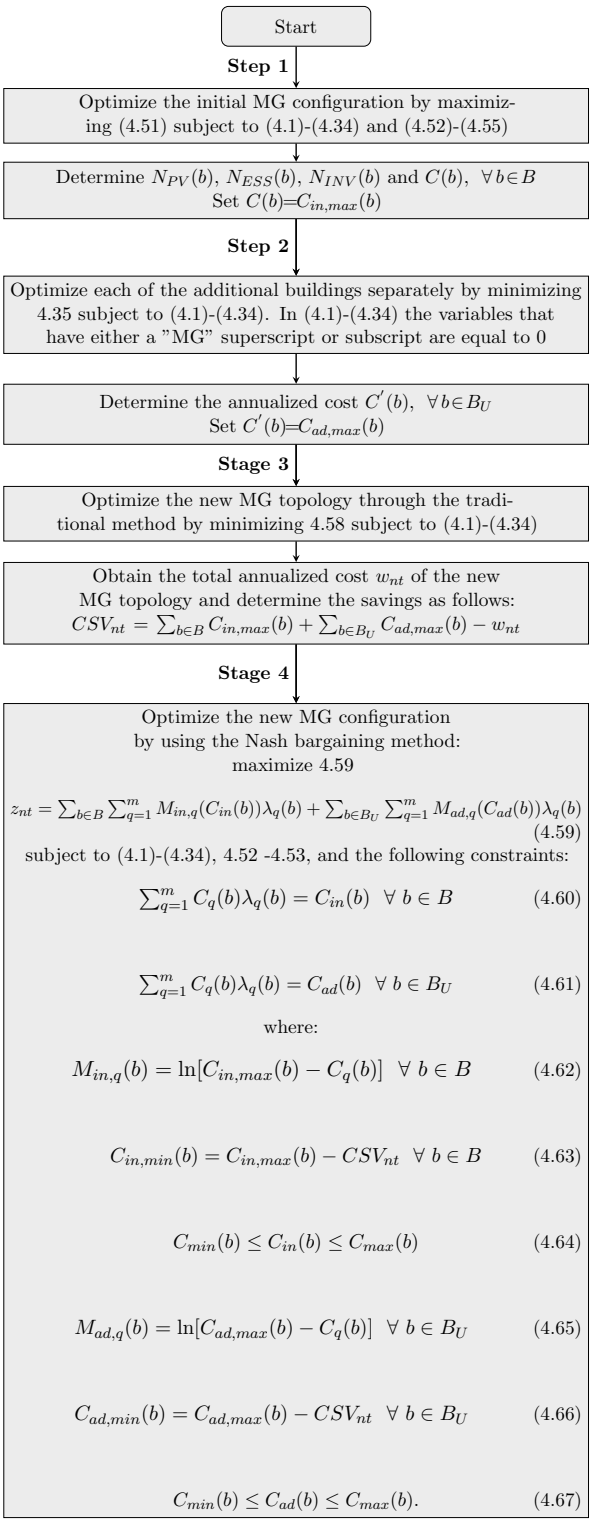

Figure 4.2: Process for the optimization of the additional buildings.

4.4 Numerical results

4.4.1 Input data

The proposed model is evaluated by considering the hourly load profile for one year of two residential buildings, two schools, a civic center and an office building, which are located in the Poblenou superblock, Barcelona, Spain. The one-year duration load profiles are composed of different daily profiles depending on the month and the day type (weekday-weekend). For example, Figure 4.3 illustrates the load profiles of the civic center and the office, as well as the load profile of one residential building and one school for a weekday in June, while Figure 4.4 shows the load profiles for a weekend day in January. In the first case (Figure 4.3), the school mainly consumes energy during the day time and the office during the working hours; the residential building has one peak early in the morning and another peak in the evening, while the civic center has larger energy needs than the other buildings, especially over the period 13:00-23:00. In the second case (Figure 4.4), the load of the civic center is significantly lower in the winter during the weekends, where the peak in the energy consumption is from 10:00 to 18:00. The peak load of the residential buildings is also lower in the weekend, taking place during 10:00-17:00 and 20:00-22:00. Finally, the loads of the school and the office are quite low and flat over the weekend.

The normalized hourly PV production profile for one year is obtained by considering the optimal PV panels' tilt angle and orientation for the area of Barcelona (31^{o}, south) in the PVWatt calculator [60]. Furthermore, each building's available surface for installing PVs is given in Table 4.1, while it is also considered that 1kW can be installed for every 7 m^2 of available surface. Table 4.1 also reports the length of the DC bus required for the interconnection of the buildings, while Table 4.2 contains the input data regarding the PVs, the inverters [48] and the ESSs [77]. It is also considered that the residential building I contains 18 EVs, and the residential building II contains 12 EVs. Nissan Leaf is the most popular EV model in Spain ([78]), and hence the specifications ([20]) of this model are taken into account as input parameters for the whole set of EVs (Table 4.3). $SoE_a(v)$ is calculated to be 15 kWh. The $SoE_a(v)$ value is derived by taking into account the Leaf's consumption ([79]), the average covered distance between two consecutive charging events and by assuming that the EVs fully recharge their batteries before departing from the residential buildings. Finally, the arrival and departure times are reported in Table 4.4, and they are assumed to be the same for all EVs.

The electricity rates $R_{G,buy}(t)$ for winter and summer months are reported in Table 4.5 ([61]). In winter months, the highest rate is activated between 18:00-22:00, whereas in summer months between 11:00-15:00. The lowest rate is activated between 00:00-08:00 in both cases, while for the remaining hours the medium rate is activated. Regarding the prices of intra MG energy transactions, it is assumed that $R_{MG,buy}(t)$ and $R_{MG,sell}(t)$ are 40% lower than $R_{G,buy}(t)$, while the price $R_{G,sell}(t)$ of selling energy back to the grid is 90% lower

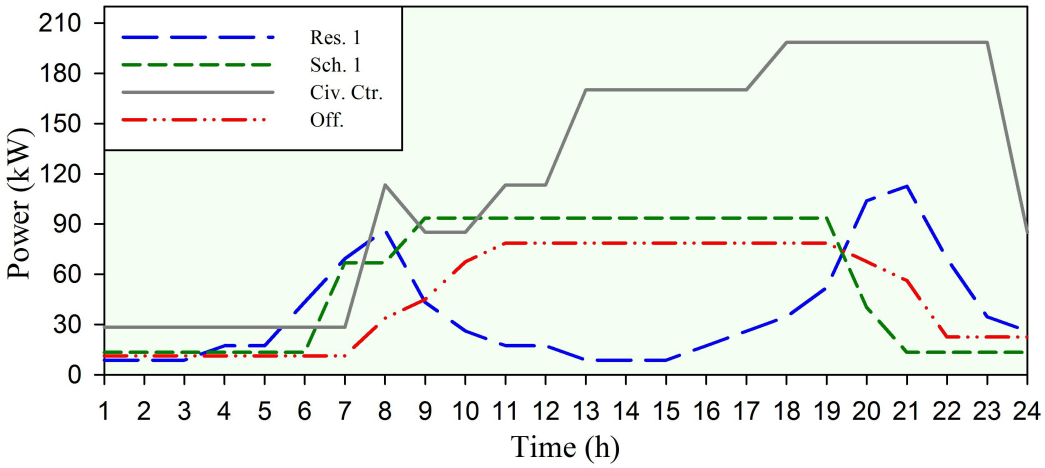

Figure 4.3: Buildings' load profiles for a June weekday

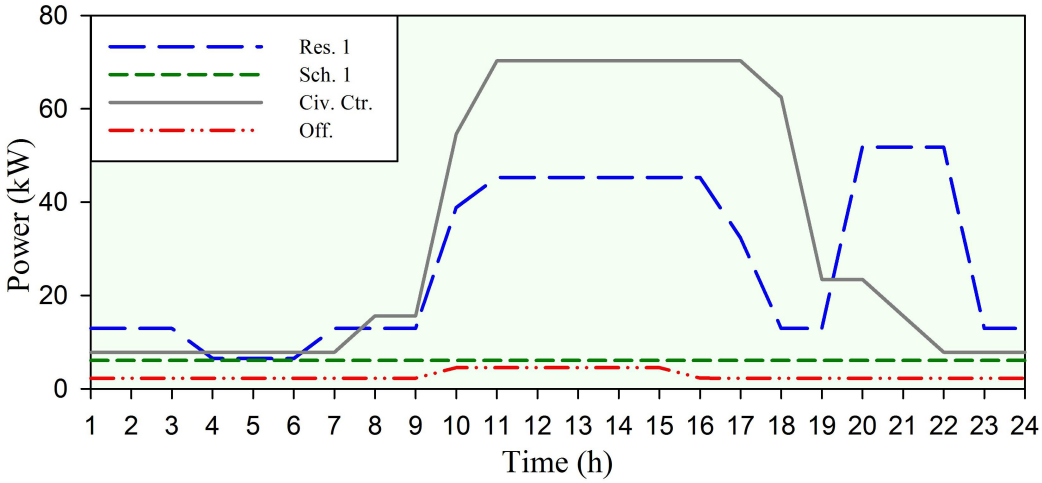

Figure 4.4: Buildings' load profiles for a January weekend day

than $R_{G,buy}(t)$ (Table 4.6). The input data for the equipment acquisition and maintenance costs, the ESSs' year of first replacement, as well as the project lifetime and the considered discount rate are presented in Table 4.7. The value of carbon intensity $Carb_{int}$ in Spain [80]) is also reported in Table 4.7, while for the carbon taxes, it is considered that $Carb_{tax}$=0.03 €/Kg [81]).

4.4.2 Results for the initial set of buildings

The sizing results and the annualized costs for the six buildings are reported in Table 4.8 for two cases. In the first case, the buildings are separately optimized, while in the second case their cooperative operation is optimized based on the proposed Nash bargaining method. Table 4.8 also compares the annual savings and the reduction in CO_2 emissions of the two optimization scenarios compared to the baseline case where the buildings are supplied with

Table 4.1: Buildings' surfaces and DC bus lengths

Building	School1	School2	Public	Office	Residential1	Residential2
Tot. surf. (m^2)	4,374	3,300	5,254	1,350	5,670	3,570
A_{PV}(m^2)	1,458	1,100	1,751	450	945	595
$L_{BUS}(b)$ (m)	85	45	170	30	100	75

Table 4.2: Specifications of power equipment [48], [77]

Parameter	**Value**
ESS charging efficiency coefficient ($n_{c,ESS}$)	0.95
ESS discharging efficiency coefficient ($n_{d,ESS}$)	0.95
Power rate of the ESS (Z_{ESS})	0.5
ESS minimum value of the SoE ($SoE_{ESS,\min}$)	0.2
ESS maximum value of the SoE ($SoE_{ESS,\max}$)	1
PV efficiency coefficient (n_{PV})	0.95
Inverter efficiency coefficient (n_{INV})	0.9

Table 4.3: Specifications of the EVs [20] [79]

EV charging efficiency coefficient $n_{EV,c}$	0.95
EV discharging efficiency coefficient $n_{EV,d}$	0.95
EV battery capacity N_{EV}	24 (kWh)
EV power rate Z_{EV}	6 (kW)
EV minimum value of the SoE $SoE_{EV,min}$	7.2 (kWh)
EV maximum value of the SoE $SoE_{EV,max}$	24 (kWh)
EV arrival SoE $SoE_a(v)$	15 (kWh)

Table 4.4: EVs' arrival and departure times

	Departure time: T_d	Arrival time: T_a
Weekday	08:00	18:00
Saturday	20:00	00:00
Sunday	11:00	18:00

Table 4.5: Open market electricity tariffs $R_{G,buy}(t)$.

	November - March	**April - October**
00:00-08:00	0.079 €/kWh	0.079 (€/kWh)
00:80-11:00	0.109 €/kWh	0.109 (€/kWh)
11:00-15:00	0.109 €/kWh	0.135 (€/kWh)
15:00-18:00	0.109 €/kWh	0.109 (€/kWh)
18:00-22:00	0.135 €/kWh	0.109 (€/kWh)
22:00-00:00	0.109 €/kWh	0.109 (€/kWh)

Table 4.6: Energy prices for the transactions among the MG users and the main grid.

Parameter	**Value**
Price of buying energy by other MG users	$R_{MG,buy}(t) = 0.6R_{G,buy}(t)$ (€/kWh)
Price of selling energy to other MG users	$R_{MG,sell}(t) = 0.6R_{G,buy}(t)$ (€/kWh)
Price of selling energy to the main grid	$R_{G,sell}(t) = 0.1R_{G,buy}(t)$(€/kWh)

Table 4.7: Economic data [48], [76], [77]

Parameter	**Value**
Project Lifetime (Y)	20 (yr)
Discount rate (d)	3%
Carbon Intensity ($Carb_{int}$)	0.455 (kg/kWh)
Carbon Tax ($Carb_{tax}$)	0.03 (€/kg)
ESS acquisition cost (c_{ESS})	208 (€/kWh)
ESS annual maintenance cost (μ_{ESS})	(2.1 €/kWh/yr)
ESS replacement year	15
PV acquisition cost (c_{PV})	1000 (€/kW)
PV annual maintenance cost (μ_{PV})	3.3 (€/kWh/yr)
Inverter acquisition cost (c_{INV})	106 (€/kW)
Inverter annual maintenance cost (μ_{INV})	(0.8 €/kWh/yr)
DC Bus acquisition cost (c_{BUS})	30 (€/km)
DC Bus maintenance cost (μ_{BUS})	0.3 (€/km/yr)

Table 4.8: Sizing results

		Separate Building Optimization						
	An. Base Cost (€)	N_{PV} (kW)	N_{ESS} (kWh)	N_{INV} (kW)	An. Cost (€)	An. Savings (€)	Payback (yr)	CO_2 red. (%)
Res1	38,110	97.2	51	52.4	32,336	5,775	6.6	31.5
Res2	24,161	60.2	27.8	32.9	20,532	3,629	6.6	30.5
Sch1	47,694	208.3	30	130.4	29,992	17,701	2.7	66.6
Sch2	35,983	157.1	22.6	98.4	22,628	13,355	2.7	66.6
Civic	75,755	248.4	141.6	151.8	49,622	26,133	2.9	61.6
Office	28,223	64.3	0	40.2	21,650	6,572	4.3	38.8
		Cooperative Optimization						
Res1	38,110	133.6	151.2	96.8	30,322	7,788	4.9	44.4
Res2	24,161	85	145.7	62.9	18,566	5,595	4.3	51.5
Sch1	47,694	208.3	52	130.4	27,979	19,715	2.4	70.7
Sch2	35,983	149.4	32.4	93.6	20,614	15,368	2.3	71
Civic	75,755	250.1	255.6	189	47,659	28,097	2.7	70
Office	28,223	64.3	101.5	87.3	19,674	8,548	3.3	73.6

electricity only by the main grid. The annual savings are obtained as the difference between the annualized cost of the baseline case (second column of Table 4.8) and the annualized costs of the two optimization approaches. Furthermore, the payback period for each building is obtained by dividing the annualized cost of the baseline case with the buildings' annual savings under the two optimization scenarios. The results of Table 4.8 indicate the benefits of energy exchanges on the PV, ESS and inverter sizing, as well as on the cost reduction; despite the fact that the equipment sizes are derived to be larger in the cooperation case, the buildings achieve higher savings and lower payback periods compared to the separate optimization case. The CO_2 emissions are calculated by multiplying the buildings' electricity imports from the main grid with the carbon intensity in Spain. Hence, the reduction of CO_2 emissions indicates the reduction of the buldings' dependence on the main grid under the two optimization scenarios compared to the baseline case. Moreover, due to the higher equipment sizes and the energy exchange process, the buildings import lower amounts of energy from the main grid under the cooperation scenario compared to the separate optimization case; this in turn results in lower CO_2 emissions.

Table 4.9 highlights the superiority of the Nash bargaining method over the traditional method for optimizing the MG. The annual savings are obtained by the difference between the annualized cost of the separate optimization case and the annualized costs of the two cooperative optimization approaches. Both methods achieve the same amount of total savings for the MG coalition (11,946 €/yr). However, when the traditional method is applied, the savings are not fairly distributed among the buildings; for example, the first residential buildings achieves almost three times higher savings than the two schools. By

Table 4.9: Traditional Optimization vs Nash Bargaining Method

	Res1	Res2	Sch1	Sch2	Civic	Office	Total
Separate Building Optimization							
Annualized Cost (€)	32,336	20,532	29,992	22,628	49,622	21,650	176,760
Cooperative Optimization (Traditional Method)							
Annualized Cost (€)	28,579	18,246	28,821	21,516	47,587	20,065	164,814
Annual Savings (€)	3,912	2,286	1,171	1,112	2,035	1,585	11,946
Cooperative Optimization (Nash bargaining method)							
Annualized Cost (€)	30,322	18,566	27,979	20,614	47,659	19,674	164,814
Annual Savings (€)	2,014	1,966	2,013	2,014	1,963	1,976	11,946

solving the optimization problem with the Nash bargaining method, the coalition savings are almost equally shared (about 2,000 €/yr for each building).

The power operation plans of one of the residential buildings, of the civic center, as well as of one of the schools and the office building are shown in Figures 4.5-4.8, respectively. The charts refer to a summer weekday and indicate the high energy exchange potential due to the variability of the buildings' load profiles and PVs' capacity. The school and the residential building have energy surplus over the period 10:00-17:00, and the civic center during 09:00-12:00. A portion of the excess energy is exported to the common DC bus, while another portion is used for charging the ESSs. The energy stored to the ESSs is later used for covering part of the buildings' evening demands. It should also be noted that the residential building and the school export to the DC bus a great amount of the energy stored to their ESSs over the periods 18:00-19:00 and 20:00, respectively. The aforementioned amount is imported by the office and the civic center in order to satisfy part of their evening peak demands, while the peak demand of the residential building is mainly satisfied by the EVs' discharging (21:00). It is also observed that the office covers a significant amount of its energy demands over the period 09:00-17:00 by importing energy from the DC bus, while at the same time using the power produced by its own PVs for charging the local ESS. The same process is followed by the civic center in the period 14:00-16:00. The stored energy is later used to cover part of the evening demands of the two buildings (at 18:00 and 21:00 for the office, at 20:00 and 23:00 for the civic center). Finally, over the night hours, when the electricity tariffs are low, the buildings' energy demands are mainly covered by imports from the main grid.

Figures 4.9-4.12 present the power operation plans of the four buildings during a Sunday in January. As in the previous case (summer weekday), over the night (01:00-08:00), the electricity prices are low, while all buildings have low energy demands, which are satisfied by imports from the main grid. During the PV production hours (09:00-18:00) the civic center, the school and the office have great amounts of excess energy because the demand is low compared to the produced PV power. Part of the excess energy is sold to the main grid and to the residential buildings for charging their EVs (09:00-11:00), while a significant

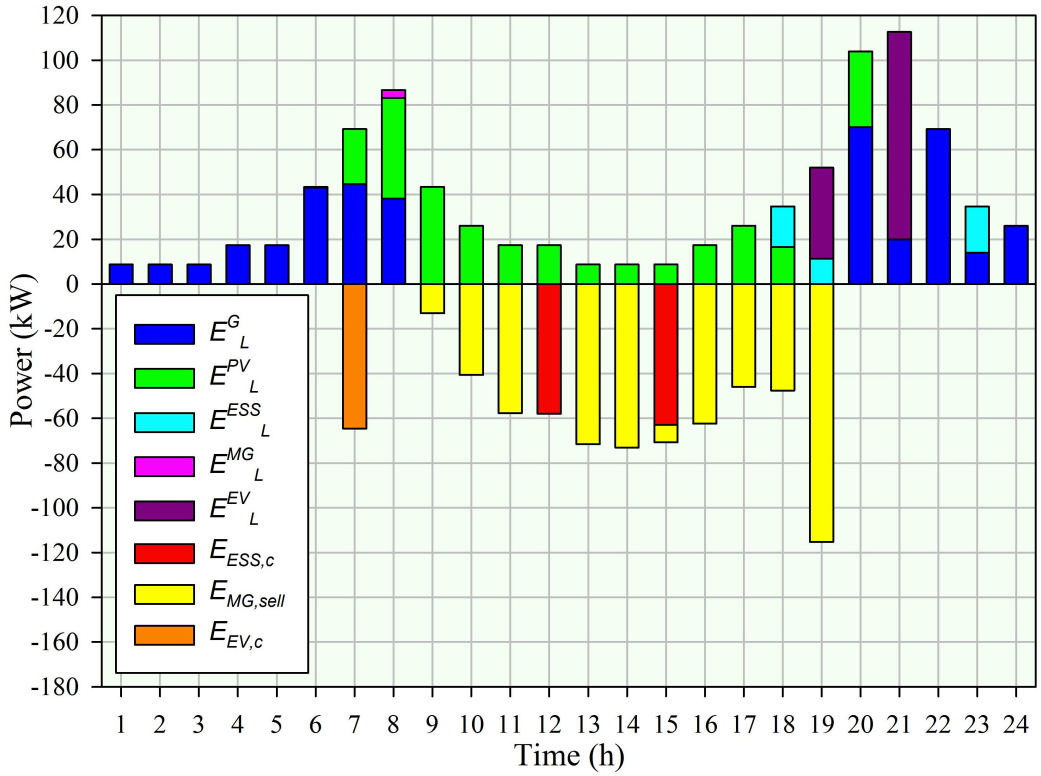

Figure 4.5: Power operation plan of residential building I (June, weekday)

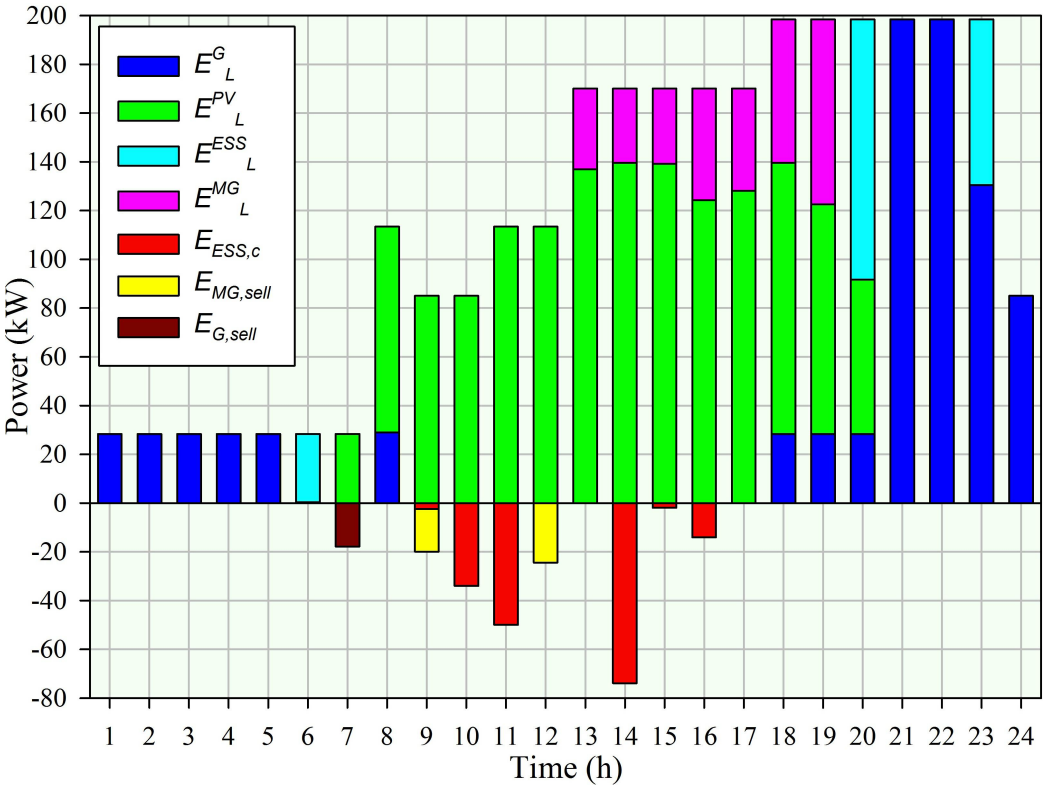

Figure 4.6: Power operation plan of the civic center (June, weekday)

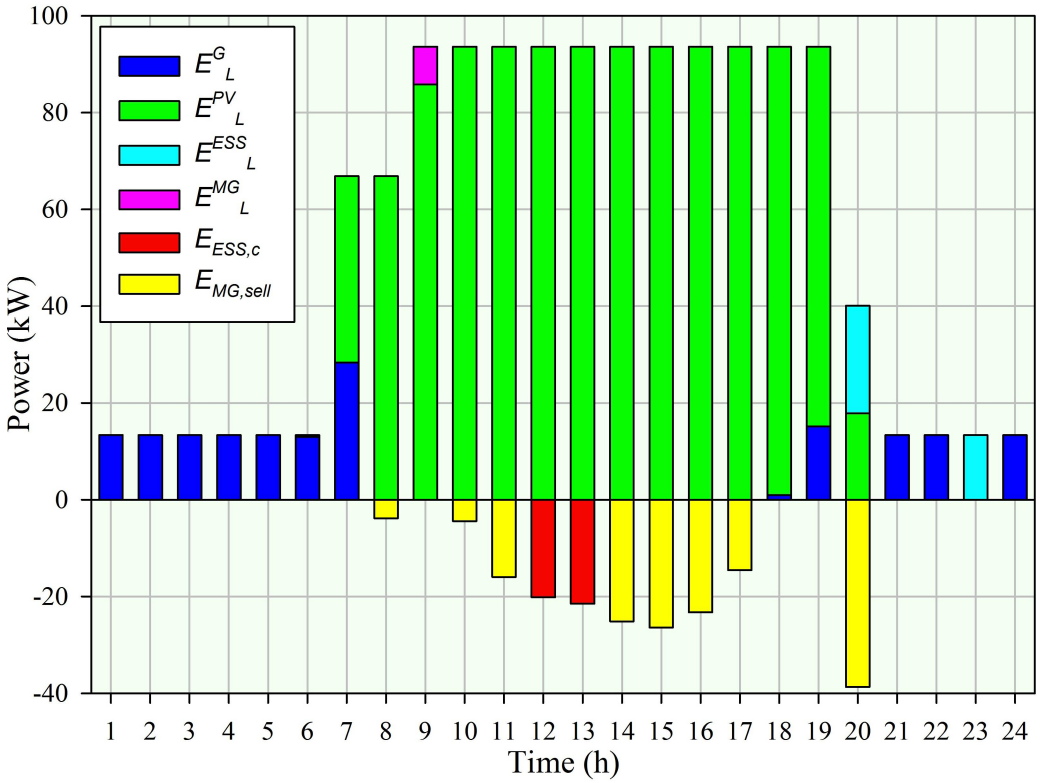

Figure 4.7: Power operation plan of school I (June, weekday)

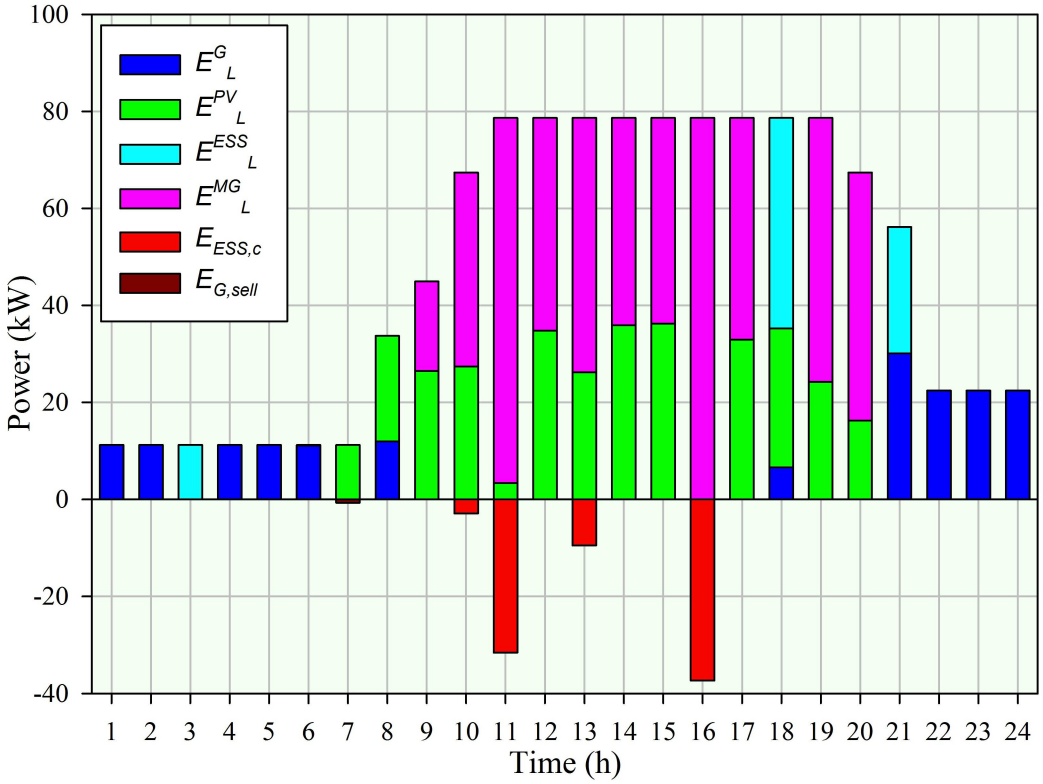

Figure 4.8: Power operation plan of the office building (June, weekday)

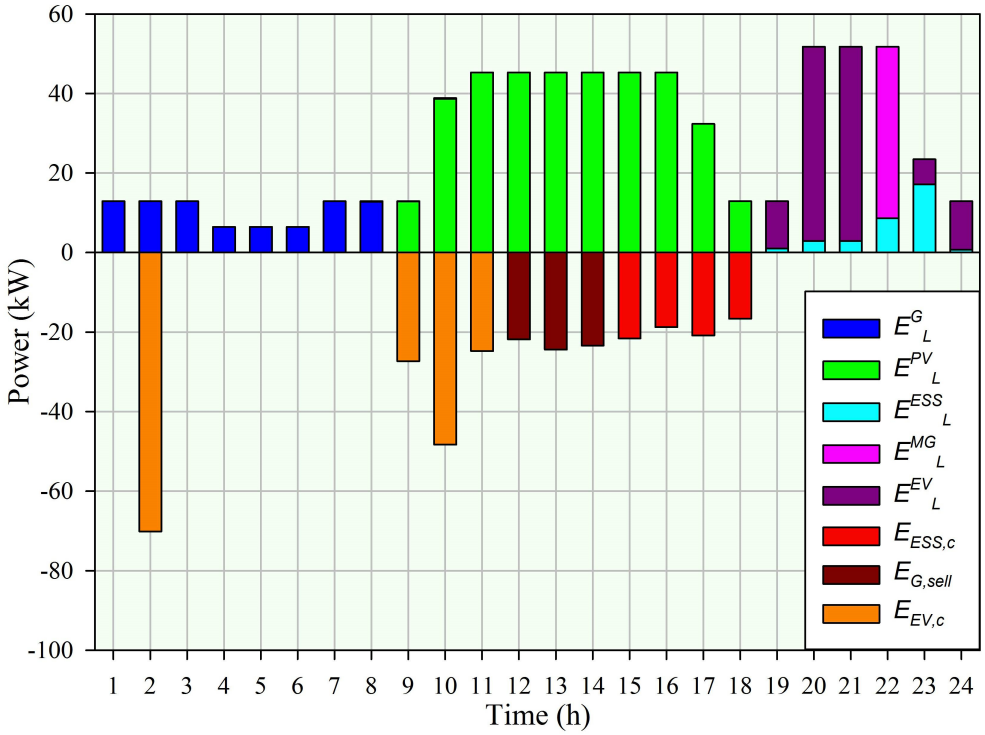

Figure 4.9: Power operation plan of residential building I (January, weekend)

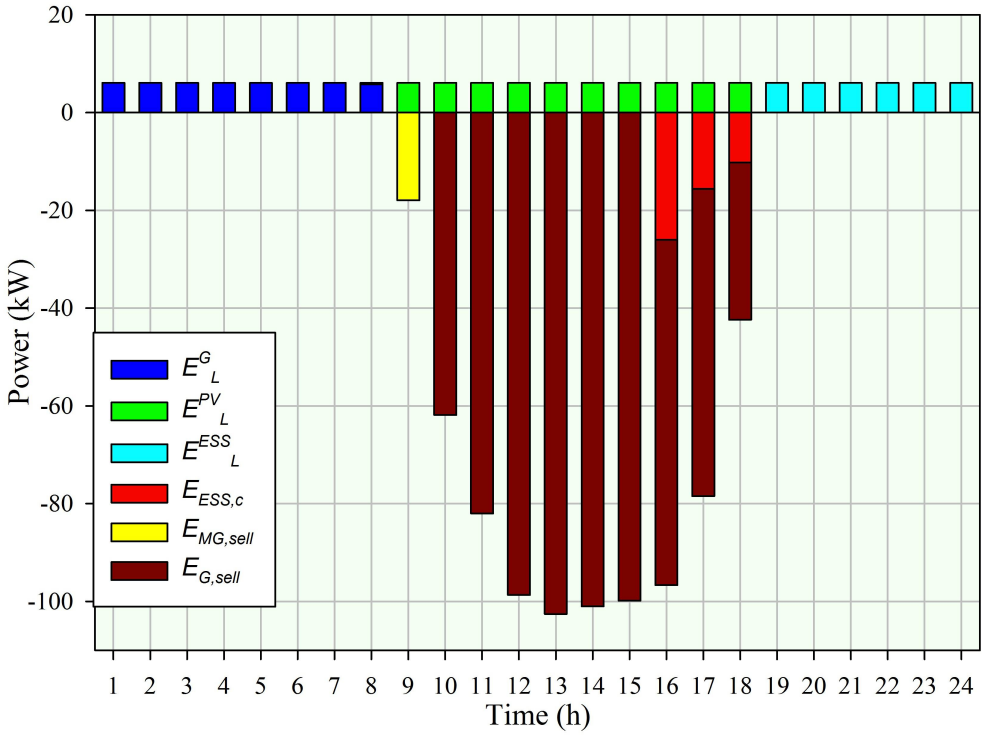

Figure 4.10: Power operation plan of the civic center (January, weekend)

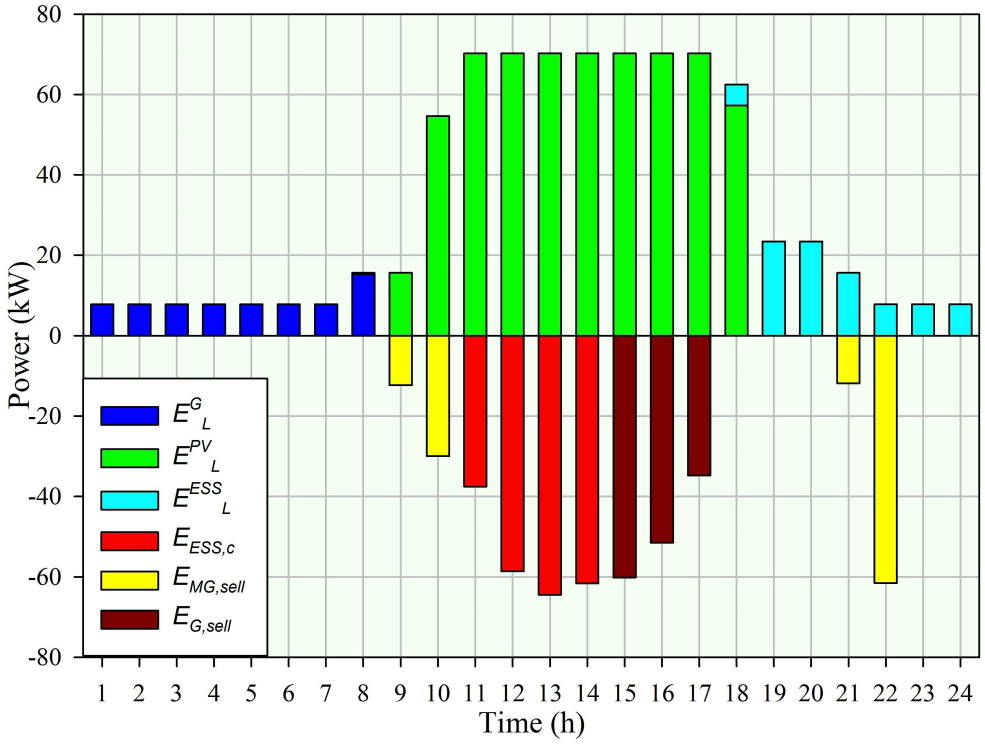

Figure 4.11: Power operation plan of school I (January, weekend)

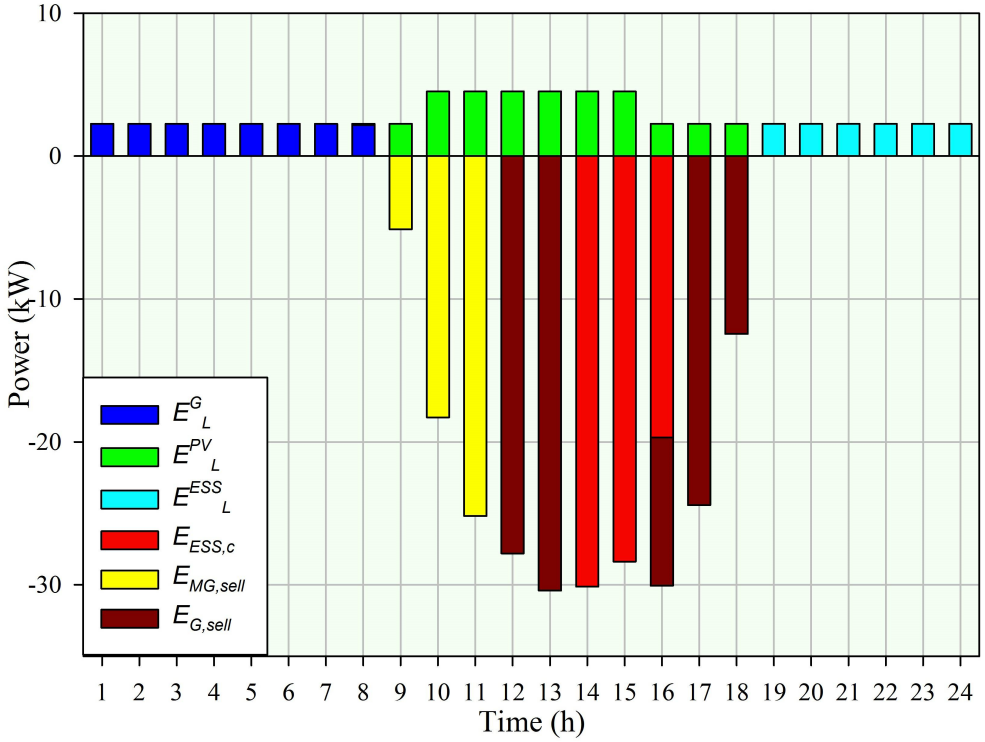

Figure 4.12: Power operation plan of the office building (January, weekend)

amount is also used for charging the ESSs. The stored energy is later used for covering the demand during the evening, which coincides with the peak price period of winter months (18:00 - 22:00). The residential building charges the EVs during the night low-price period by importing energy from the main grid, as well as before the EVs' departure (11:00) by importing energy from the other buildings. In turn, the EVs contribute to the peak load satisfaction (20:00-21:00). In addition, part of the peak load is covered by importing energy from the ESS of the civic center (22:00). The ESS of the residential building also contributes to the evening demand by providing energy that has been stored during 15:00 -18:00.

4.4.3 Participation of additional buildings

The aforementioned results refer to the case where the initial set of six buildings is optimized over a 20-year project lifetime. In this section, it is considered that two additional buildings join the MG coalition 5 years after the initial establishment. For comparison purposes, it is assumed that the two additional buildings have exactly the same characteristics with the initial civic center and office building. Therefore, the annualized cost of the additional civic center and office when they are separately optimized is the same with the annualized cost of the corresponding initial buildings i.e. 48,622 €/yr and 21,650 €/yr, respectively.

By implementing the Nash bargaining method, the obtained optimal PVs', ESSs' and inverters' sizes for the additional civic center are N_{PV}=250.1 kW, N_{ESS}=133.7 kWh and N_{INV} =189 kW, respectively, while for the additional office the corresponding sizes are N_{PV}= 64.3 kW, N_{ESS}=76 kWh and N_{INV}=72.2 kW. The participation of new buildings increases the energy exchange potential. Figure 4.13 compares the buildings' annual energy exchanges under the initial and under the new MG topology. In the second case, all of the initial buildings sell greater amounts of energy, while they also import greater amounts of cheap energy from the MG. The additional buildings also participate in the energy exchange process, however, the amounts of imported and exported energy are lower than the corresponding initial buildings. This fact implies that it is more benefiting to participate in the MG from the beginning than joining it at a later point.

Due to the higher energy exchange potential that is created, the participation of the new buildings leads to lower annualized costs for the initial buildings; the savings for each of the initial buildings are further increased by 1900€/year compared to the initial MG topology. The additional buildings achieve equal amount of savings. However, in their case the savings refer to the difference between the annualized costs of their separate optimization and the annualized cost when they participate in the coalition. This fact also indicates that joining the MG from the beginning is a more profitable choice than joining it some years after its initial establishment. It is also found that the new coalition is unprofitable, if the additional buildings join 8 years after its initial establishment because the savings of the new topology are found to be negative. This is determined in step 3 of the flowchart of Figure 4.2; the total cost of new coalition is higher than the summation of the total cost of the initial coalition

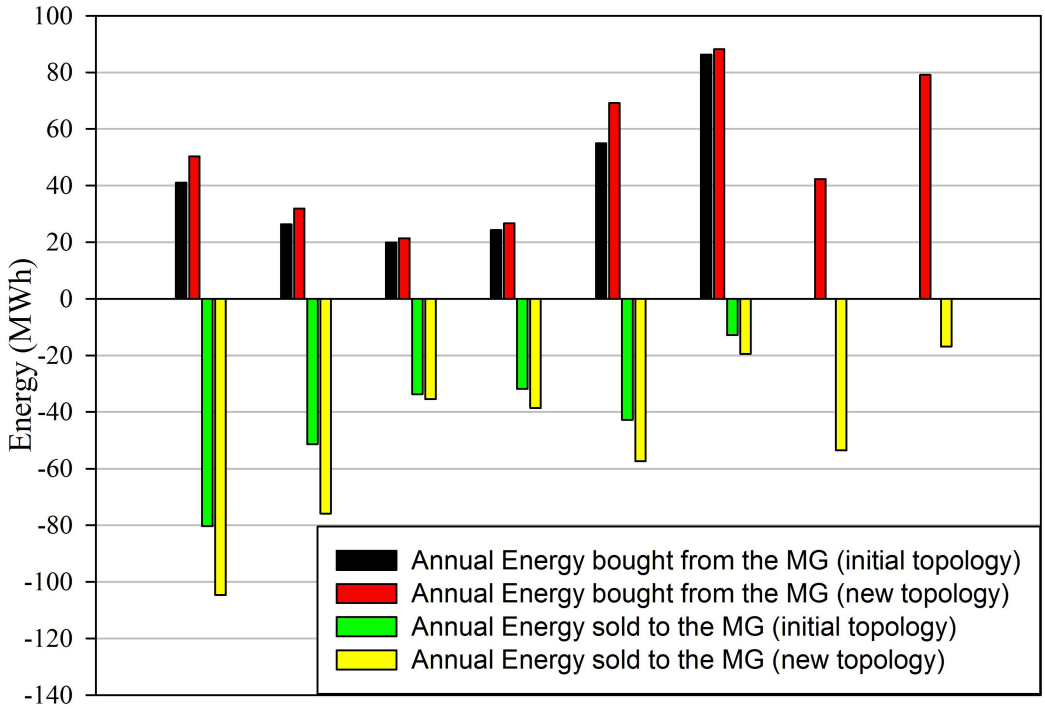

Figure 4.13: Energy exchanges of the MG participants

plus the annualized cost of the additional buildings when they are separately optimized.

5 Analysis and quality of service evaluation of a fast charging station for electric vehicles

In this chapter a novel multi-class M/G/s queuing model is presented for analyzing the operation of a FCS. Two features differentiate the present analysis and make it more realistic for describing the charging process of EVs over other approaches adopted in the literature. The first feature refers to the classification of the various EV models by their different battery sizes. The second feature refers to the fact that the charging time of each EV class is derived based on a random distribution function that describes the batteries' SoC when the EVs arrive at the FCS, as well as based on the charging power provided by the CSs. The proposed model is used in order to calculate the customers' queue waiting time, as well as the maximum amount of EVs that can be served subject to a QoS criterion for the queue waiting time. Moreover, a charging strategy is proposed, which aims at controlling the energy demands of the various EV classes. The FCS operator provides financial incentives to the customers so that they charge their batteries up to a predefined departure SoC level, instead of the maximum possible. As a result, the charging time of the users accepting the offer is reduced, and the FCS operator can serve more EVs, while providing a certain level of QoS, in terms of waiting time in the queue.

This chapter is organized as follows: Section 5.1 presents the FCS architecture, the EVs' classification, as well as the way the charging time distribution of each class is derived. Section 5.2 presents the analysis for the derivation of the EVs' mean waiting time in the queue based on the proposed multi-class M/G/s queuing model. In section 5.3, the upper bound of the EVs' arrival rates is derived given a corresponding upper bound for the waiting time in the queue. The charging strategy that allows the FCS operator to accommodate even greater arrival rates is formulated in section 5.4. The proposed model is evaluated in section 5.5, where both analytical and simulation results are presented and discussed.

5.1 Fast charging station's architecture and modeling

The considered FCS is depicted in Figure 5.1 It consists of s CSs each containing both a CHAdeMO and a CCS outlet that provide the same power rate P_{DC}. The two outlets of the same CS cannot operate simultaneously [82], and hence a single EV is served by each CS at a time. As a consequence, in case all CS are occupied, a newly arrived EV waits in the queue regardless the fast charging inlet it contains (CHAdeMO or CCS).

The EVs are divided into C classes depending on the rated capacity of their batteries B_c, where $c = (1, 2, ...C)$. It is considered that c-class EVs arrive at the FCS by following a Poisson process with mean arrival rate λ_c, while the charging time T_c of c-class EVs is derived by the following relation:

$$T_c = (SoCD_c - SoCA_c)\frac{B_c}{P_{DC}} = (0.8 - SoCA_c)\frac{B_c}{P_{DC}}. \tag{5.1}$$

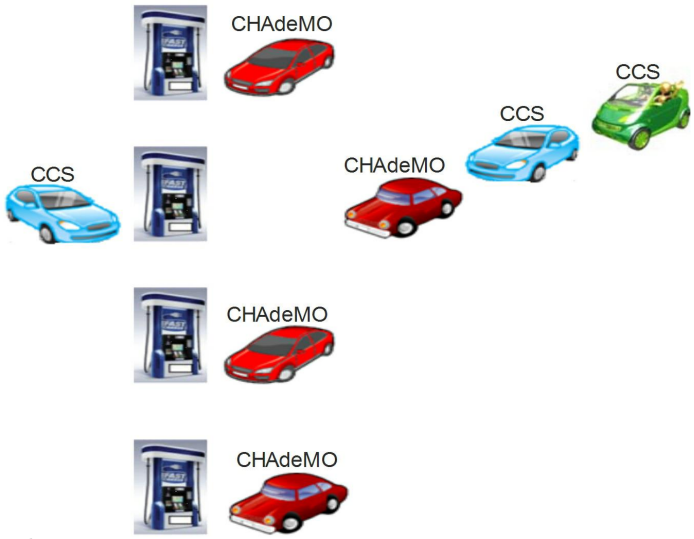

Figure 5.1: FCS architecture.

The derivation of the EVs' charging time T_c is based on the assumption that the power rate P_{DC} is constant during a fast charging session [83]. $SoCD_c$ denotes the state of charge of the battery when c-class EVs depart from the FCS, while $SoCA_c$ when they arrive. It is also assumed that all customers recharge their batteries up to $SoCD_c$=0.8, which is the maximum possible level during a fast charging session [73], while $SoCA_c$ is considered to be a random variable that follows a cumulative distribution function (CDF) $F_c(x)$=$P(SoCA_c \leq x)$. Based on equation (5.1) and the aforementioned considerations, T_c is also a random variable. The CDF G_c, the probability distribution function (PDF) g_c and the mean m_c of c-class EVs' charging time T_c are derived by the following equations, respectively:

$$\begin{aligned} &G_c(t) = P(T_c \leq t) = P[(0.8 - SoCA_c)\tfrac{B_c}{P_{DC}} \leq t] = \\ &= P(SoCA_c > 0.8 - \tfrac{P_{DC}}{B_c}t) = 1 - F_c(x_c(t)) \end{aligned} \tag{5.2}$$

$$g_c(t) = \frac{d}{dt}G_c(t) \tag{5.3}$$

$$m_c = \int t g_c(t) dt \tag{5.4}$$

where

$$x_c(t) = 0.8 - (P_{DC}/B_c)t. \tag{5.5}$$

Furthermore, in a multi-class queuing system, the load a_c of each class represents the mean number of CSs occupied by the corresponding class, and it is given by [85]:

$$a_c = \lambda_c m_c. \tag{5.6}$$

5.2 Determination of the EVs' waiting time in the queue

The determination of the mean waiting time of the EVs in the queue is based on the derivation of the superposed arrival process, the superposed charging time distribution, as well as the total load and the utilization rate of the system. This procedure is based on the aggregation of all C classes into a single class [85].

The superposed arrival process of the system is determined as a Poisson process, since the arrival process of each EV class is also Poisson [86]. Therefore, the mean superposed arrival rate is of the system is:

$$\lambda = \sum_{c=1}^{C} \lambda_c. \tag{5.7}$$

The analytical expression of the superposed charging time distribution is derived as follows: Let T be a random variable that denotes the charging duration at an arbitrary CS, given that an EV of any class enters for service. The probability that a c-class EV enters for service at the aforementioned arbitrary CS is [85]:

$$k_c = \frac{\lambda_c}{\lambda}. \tag{5.8}$$

As a result, the charging time CDF $G(t)$=$P(T \leq t)$ is equivalent to the probability $[k_1 P(T_1 \leq t) \bigcup k_2 P(T_2 \leq t) \bigcup ... \bigcup k_C P(T_C \leq t)]$. The events $k_c P(T_c \leq t)$ where $c = (1, 2, ...C)$ are mutually exclusive because only one EV is being charged at a time in the arbitrary CS. Therefore, $G(t)$ is determined as follows:

$$G(t) = \sum_{c=1}^{C} k_c G_c(t). \tag{5.9}$$

The expression of the CDF is used for the derivation of the PDF $g(t)$, the mean m and the variance v of the charging time distribution through the following relations, respectively:

$$g(t) = \frac{d}{dt} G(t) \tag{5.10}$$

$$m = \int t g(t) dt \tag{5.11}$$

$$v = \int t^2 g(t) dt - m^2 \tag{5.12}$$

Due to the fact that the arrival process of each EV class is Poisson, the total load of the

system a equals to the sum of the loads of each class [86]:

$$a = \sum_{c=1}^{C} a_c \tag{5.13}$$

The total load represents the mean number of busy CSs in the steady state condition of the system [84], while as noted in the previous section, the load a_c of each EV class represents the mean number of CSs occupied by c-class EVs. In addition, the following ratio defines the utilization rate of a multi-server queuing system:

$$\rho = \frac{\lambda m}{s} = \frac{a}{s}. \tag{5.14}$$

It should be noted that for a queuing system to be stable i.e. to have a finite queue in the steady state $\rho < 1$ is a necessary condition [84].

The derivation of the superposed arrival rate and the charging time distribution, as well as the determination of the total load and the utilization rate of the system enables the simplification of the considered multi-class system into a single-class M/G/s system. Consequently, the mean waiting time W of the EVs in the queue can be determined by using the analysis presented in [87].

Initially, the mean number of customers $L_{M/G/s}$ waiting in the queue in a single-class M/G/s system is approximated by [87]:

$$L_{M/G/s} \approx \frac{1 + c_v^2}{\frac{2c_v^2}{L_{M/M/s}} + \frac{1-c_v^2}{L_{M/D/s}}} \tag{5.15}$$

where $L_{M/M/s}$ and $L_{M/D/s}$ denote the mean number of customers waiting in the queue in the corresponding M/M/s and M/D/s systems, respectively, while c_v^2 is the square of the coefficient of variation of the service time PDF:

$$c_v^2 = \frac{v}{m^2}. \tag{5.16}$$

The mean number $L_{M/M/s}$ of customers waiting in the queue in an M/M/s system is obtained by [84]:

$$L_{M/M/s} = \frac{\rho \alpha^s}{s!(1-\rho)^2} \left[\sum_{r=0}^{s-1} \frac{\alpha^r}{r!} + \frac{\alpha^s}{s!} \left(1 - \frac{\alpha}{s}\right)^{-1} \right]^{-1} \tag{5.17}$$

while $L_{M/D/s}$ is approximated using the following equations [87]:

$$L_{M/D/s} \approx \psi(s, \rho) L_{M/M/s} \tag{5.18}$$

$$\psi(s,\rho)=\frac{1}{2}\left[1+\Phi(\theta)\zeta(\rho)\left(1-\exp\left\{-\frac{\theta}{\Phi(\theta)\zeta(\rho)}\right\}\right)\right] \tag{5.19}$$

$$\zeta(\rho)=\frac{1-\rho}{\rho} \tag{5.20}$$

$$\Phi(\theta)=\frac{\theta}{8(1+\theta)}\Big(\sqrt{\frac{9+\theta}{1-\theta}}-2\Big),\ \ with\quad \theta=\frac{s-1}{s+1} \tag{5.21}$$

Finally, the mean number of customers $L_{M/G/s}$ waiting in the queue in the single-class M/G/s system is used for the determination of the mean waiting time of customers in the queue through Little's law [84]:

$$W=\frac{L_{M/G/s}}{\lambda}. \tag{5.22}$$

5.3 Maximum arrival rate capacity of the fast charging station

The main advantage of fast charging compared to slow charging at home is the short duration of the charging session, due to the high power rates provided by the FCSs. However, for a FCS to provide high QoS, the EVs' waiting time in the queue should be kept to low levels; otherwise, the aforementioned advantage is pointless. In this section, the EVs' maximum arrival rates are initially computed, subject to a maximum queue waiting time value W_q. Moreover, in both cases, the operator's mean revenue during a time interval τ is computed, by taking into account that the EVs' mean arrival rates are equal to their maximum values.

As analyzed in the previous section, the mean waiting time of the EVs in the queue depends on the superposed arrival rate and the superposed charging time distribution of the system. In turn, the superposed charging time distribution is derived based on the charging time distribution of each single class, as well as on the probabilities k_c. In the following analysis it is assumed that the values of k_c can be approximated based on the market shares h_c of the EV classes in the region where the FCS is located, so that k_c=h_c. The aforementioned consideration allows for the computation of the maximum superposed arrival rate $\lambda_{\max}$ and the maximum arrival rate of each EV class, $\lambda_{c,\max}$ by using Algorithm 1, which is presented in Figure 5.2. Algorithm 1 uses as input parameters the QoS criterion for the waiting time, the battery capacities, the $SoCA_c$ CDFs and the market shares of the EV classes, as well as the number of CSs and the power rate they provide. At the first stage, the charging time distribution of each class and the system's superposed charging time distribution are derived. The second stage refers to a loop that calculates the maximum superposed arrival rate using the waiting time upper limit as a termination condition. Finally, the third stage determines the maximum arrival rate of each class based on the result of stage 2 and the probabilities k_c.

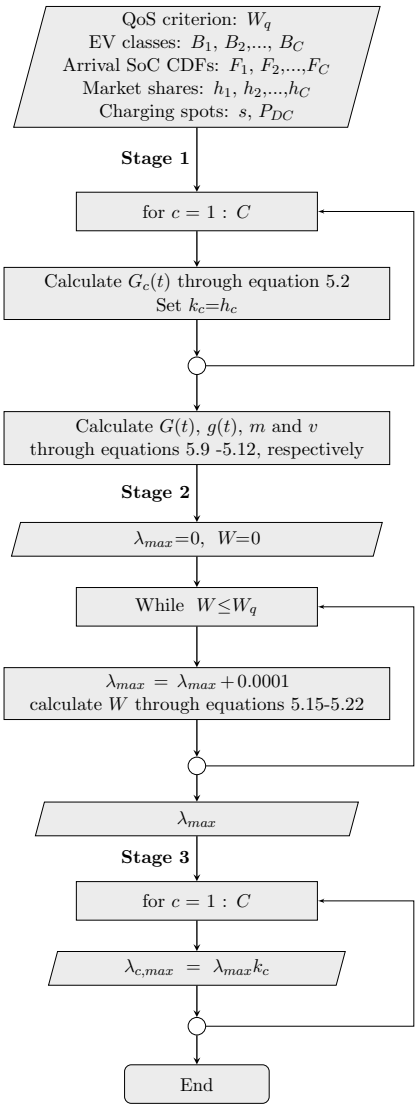

Figure 5.2: Flowchart of Algorithm 1.

Next, the operator's mean revenue R during a time interval τ is calculated under the assumption that the arrival rates are equal to their maximum values. It is also considered that the duration τ is long enough so that the queuing system reaches the steady state. The aforementioned concept may represent a peak traffic period during a typical day. As it is noticed in section 5.3, the total load of the system represents the mean number of occupied CSs in the steady state. Hence, the mean power P_{EVs} drawn by the EVs over the interval τ is given by the product of the mean number of occupied CSs ($a_{\max} = \lambda_{\max} m$) with their power rate:

$$P_{EVs} = a_{\max} P_{DC} \tag{5.23}$$

Furthermore, the mean energy supplied to the EVs during the interval τ is:

$$E_{EVs} = \tau P_{EVs} \tag{5.24}$$

Finally, the mean revenue R of the operator is calculated in equation 5.25 where r (€/kWh) denotes the price that the FCS operator charges the served EVs.

$$R = rE_{EVs} \tag{5.25}$$

5.4 Charging strategy for increasing the arrival rate capacity

In this section, a charging strategy is presented that can be implemented by the FCS operator in order to increase the maximum arrival rate capacity of the system (i.e. $\lambda^{'}_{\max} > \lambda_{\max}$) while providing the same QoS. According to the proposed strategy the FCS operator provides financial incentives (price discount) to customers that accept to recharge their batteries up to an arranged departure SoC threshold SoC_{thr}, which is lower than the maximum possible departure SoC (i.e. $SoCD_{thr} < 0.8$).

For the derivation of the maximum arrival rates $\lambda^{'}_{\max}$ and $\lambda^{'}_{c,\max}$, in this case, each single class is divided into two additional subclasses c_1 and c_2. Subclass c_1 contains the percentage σ_c of c-class EVs that accept the operator's offer, hence, $k_{c1} = \sigma_c k_c$. On the contrary, subclass c_2 contains the remaining 1-σ_c percentage of c-class EVs that do not accept the offer, hence, $k_{c2} = (1 - \sigma_c)k_c$. The charging time CDF $G_{c1}(t)$ and PDF $g_{c1}(t)$, as well as the mean charging time m_{c1} for the EVs belonging to subclasses c_1 where $c = (1, 2, ..., C)$ are derived through equations (5.2)-(5.4), respectively, by replacing $x_c(t)$ with:

$$x_{c1}(t) = SoCD_{thr} - \frac{P_{DC}}{B_c}t. \tag{5.26}$$

Regarding the charging time CDF $G_{c2}(t)$, PDF $g_{c2}(t)$ and mean m_{c2} of the EVs belonging to subclasses c_2, they have exactly the same form as in the set of equations (5.2)-(5.4). Based on the aforementioned analysis, the maximum arrival rates $\lambda^{'}_{\max}$ and $\lambda^{'}_{c,\max}$, under the proposed charging strategy, are computed by using Algorithm 2 of Figure 5.3. Note that compared to Algorithm 1, Algorithm 2 uses two extra input parameters (i.e. σ_c and $SoCD_{thr}$).

Moreover, the operator's mean revenue R' under the proposed charging strategy is calculated by the following relation:

$$R^{'} = \tau \ P_{DC} \ (1 - d) \ r \sum_{c=1}^{C} a_{c1} \ + \ \tau \ P_{DC} \ r \sum_{c=1}^{C} a_{c2}. \tag{5.27}$$

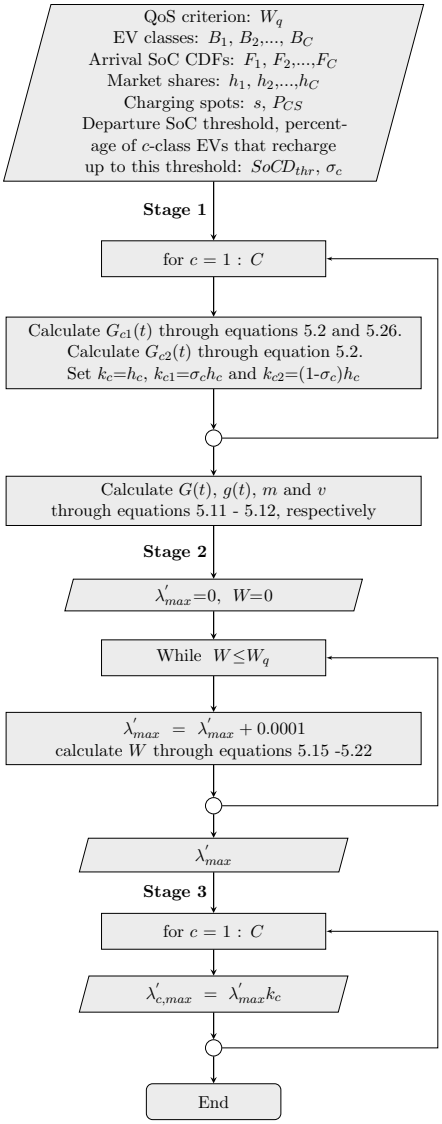

Figure 5.3: Flowchart of Algorithm 2.

As noted in section 5.4, the load of each class (or subclass) represents the mean number of CSs occupied by the EVs belonging to this class (or subclass). Under the proposed strategy the load of subclasses c_1 is $a_{c1} = \sigma_c \lambda'_{c,\max} m_{c1}$, while the load of subclasses c_2 is $a_{c2} = (1 - \sigma_c)\lambda'_{c,\max} m_{c2}$, with $c = (1, 2, ..., C)$. Note also that the EVs belonging to subclasses c_2 are charged with price r, while those belonging to subclasses c_1 are offered a discount d, i.e. $r' = (1 - d)r$. Therefore, the first product in equation (5.27) represents the operator's mean revenue due to the energy supplied to the EVs belonging to subclasses c_1, while the second one represents the operator's mean revenue due to the energy supplied to the EVs belonging to subclasses c_2.

5.5 Numerical results

This section provides analytical and simulation results for the evaluation of the proposed modeling of a FCS as a multi-class M/G/s system. The considered FCS consists of s=5 CSs and the power rate provided by the CHAdeMO and CCS outlets is P_{DC}=50 kW [82]. Depending on the battery sizes, the EVs are divided into C=3 classes, which correspond to the 3 of the most popular EV models of the Spanish market [88]; namely, Nissan Leaf (B_1=24 kWh), BMW i3 (B_2=18.8 kWh) and Mitsubishi i-MiEV (B_3=16 kWh). It is also considered that the random variables SoCA_1, SoCA_2 and SoCA_3 follow the normal CDF with mean 0.25 and standard deviation 0.059. This selection is based on the assumption that the vast majority of EVs seek for fast charging facilities when their batteries' SoC ranges in the interval [0.15, 0.4], which is the 95% confidence interval of the CDF.

The accuracy of the proposed mathematical model is confirmed through the comparison of analytical results with corresponding results from simulation. To this end, a simulator was built in Matlab, which creates events (EV arrivals and departures) based on random numbers. In order to simulate the Poisson arrival process, the simulator considers a large number of EV arrivals i.e. 10^6. For each simulated EV, it records the time of its arrival, the time of its entering for charging and the time of its departure from a CS, in order to determine the EVs' mean waiting time in the queue. Simulation results that are presented in this section are obtained as mean values of 20 runs, which are performed on an Intel Core i7-4712MQ 2.30GHz CPU and 8 GB RAM. For the computation of the queue waiting time, each simulation run lasts 12 minutes, on average. On the contrary, the analytical model computes the queue waiting time in less than 0.2 seconds.

The analytical and simulation results for the EVs' mean waiting time in the queue versus the superposed arrival rate of the system are presented in Figure 5.4. For the derivation of the waiting-time results, 3 different scenarios are considered regarding the values of the probabilities k_c. For each scenario, Table 5.1 summarizes the set of values for k_c and the system's mean charging time, which is calculated through equation (5.11). Scenario 1 considers that the arrival rate of Leaf (class 1), which is the EV model with the biggest battery, is double the arrival rates of i3 (class 2) and i-MiEV (class 3). On the other hand, scenario 3 considers that the arrival rate of i-MiEV, which is the EV model with the smallest battery, is double the arrival rates of the other EV models. For this reason, scenario 1 is

Table 5.1: Parameters for the 3 evaluation scenarios.

Scenario	k_1	k_2	k_3	m (h)
1	0.5	0.25	0.25	0.2277
2	0.25	0.5	0.25	0.2134
3	0.25	0.25	0.5	0.2057

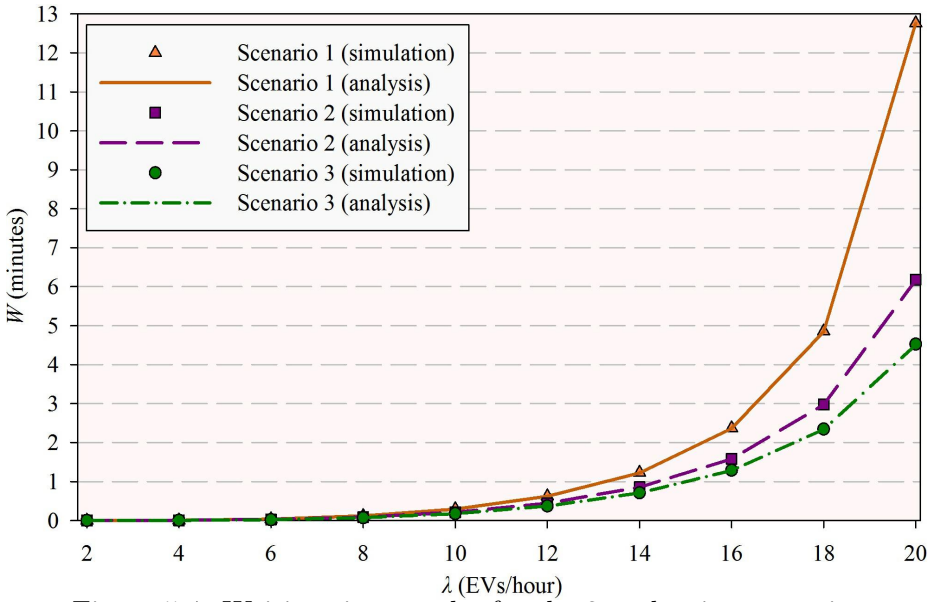

Figure 5.4: Waiting-time results for the 3 evaluation scenarios.

characterized by the longest mean charging time, while scenario 3 is characterized by the shortest one.

As Figure 5.4 indicates, despite the different mean charging time values under the 3 scenarios, the performance of the system is quite similar for arrival rate values up to 14 (EVs/hour). After that point, the waiting time curve becomes steeper with the increase of λ. As noted in section 5.2, a queuing system has a finite queue if the utilization rate is lower than 1 ($\rho < 1$). Therefore, the aforementioned outcome can be interpreted by mapping the arrival rate values to utilization rate values through equation (5.14). The waiting time curve becomes steeper as the utilization rate of the system approaches its limiting value. This is more intense under scenario 1, which is characterized by the highest mean charging time. Finally, it should also be pointed out that the comparison of analytical and simulation results of Figure 5.4 reveals that the accuracy of the proposed queuing model is very satisfactory; in all cases the difference between analysis and simulation is smaller than 1%.

Next, the maximum arrival rates of the EVs are computed given that the mean waiting time in the queue is equal to a maximum acceptable limit W_q=1 min, which is the QoS criterion. In this case, the derivation of the ratios k_c is based on the market shares h_c of the EV classes in Spain [88]. By dividing the population of Leaf with the aggregate population of the 3 EV models, it is derived that $k_1 = h_1 = 0.543$. Following the same process for i3 and i-MiEV, k_2 and k_3 are found to be 0.133 and 0.324, respectively. Given the k_c values, the QoS criterion, and the arrival SoC CDFs, Algorithm 1 computes the maximum value for the superposed arrival rate, which is λ_{max}=13.37 (EVs/h), as well as the maximum arrival rates for the three EV classes, which are $\lambda_{1,max}$=7.26 (EVs/h), $\lambda_{2,max}$=1.78 (EVs/h) and $\lambda_{3,max}$=4.33 (EVs/h). By assuming that the operator's energy tariff is r=0.15 (€/kWh), as

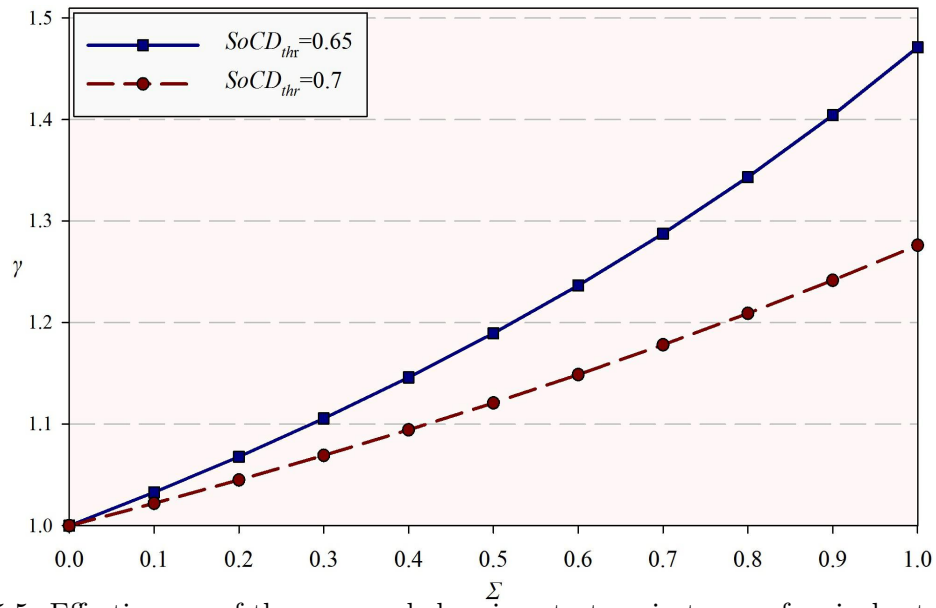

Figure 5.5: Effectiveness of the proposed charging strategy in terms of arrival rate capacity increase.

well as that the EVs' arrival rates are equal to their maximum values during a period of τ=4 h, the FCS operator's revenue during this period is R=91.4 € (equation 5.25).

In what follows, the operator's capability to increase the maximum arrival rate capacity of the system by $\gamma = \lambda'_{\max} \big/ \lambda_{\max}$, while keeping the same QoS level, is examined. This can be achieved by implementing the charging strategy in section 5.4. Crucial for the effectiveness of the proposed charging strategy are the values of parameters σ_c where $c = (1, 2, 3)$, which determine the percentage of the EVs that belong to subclasses c_1. Figure 5.5 presents analytical results for the increase in the arrival rate capacity of the system γ versus the percentages σ_c. For presentation purposes it is assumed that σ_1=σ_2=σ_3=Σ. Furthermore, the performance of the proposed strategy is evaluated by considering two departure SoC thresholds (0.65 and 0.7, respectively). As it was anticipated, the potential of the FCS to serve greater arrival rates providing the same QoS level increases with the increase of Σ. This is due to the fact that the EVs belonging to subclasses c_1 obtain less amount of energy than those belonging to subclasses c_2. Hence, the greater the values of Σ, the shorter the mean charging time of the system becomes. Furthermore, the EVs of subclasses c_1 obtain less energy when $SoCD_{thr}$=0.65 compared to the case where $SoCD_{thr}$=0.7. Therefore, for the same values of Σ, the performance of the proposed strategy is better in the former case.

The proposed charging strategy dictates that the operator makes a discount d to those EVs that accept to recharge up to $SoCD_{thr}$. Figure 5.6 presents the maximum discount d_{max} that the operator is able to make versus the parameter Σ. The values of d_{max} are obtained by setting R'=R. Recall that R is calculated through equation (5.25) and represents the revenue of the operator during a period τ where all EVs recharge up to $SoCD$=0.8 and

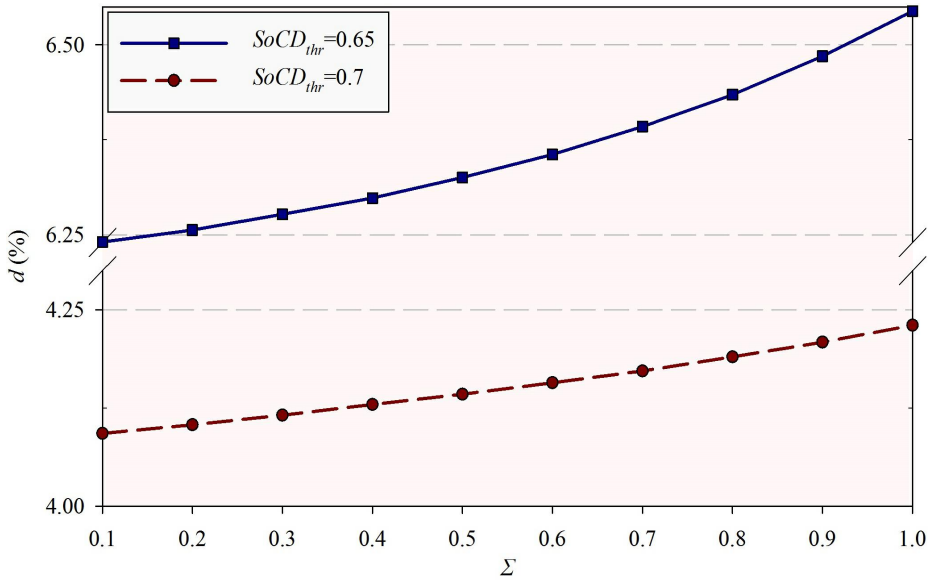

Figure 5.6: Maximum discount the FCS operator can make under the implementation of the proposed charging strategy.

the arrival rates are equal to λ_{max}. On the other hand, $R^{'}$ is calculated through equation (5.27) and represents the revenue of the operator during τ when a percentage of EVs (Σ) recharge up to $SoCD_{thr}$ and the arrival rates are equal to their maximum values ($\lambda^{'}_{c,max}$), as calculated by Algorithm 2.

Without loss of generality, let us interpret the outcomes of Figure 5.6 by comparing the case where all EVs (Σ=100%) recharge up to $SoCD_{thr}$=0.7 with the case where all EVs recharge up to $SoCD$=0.8 (departure SoC when the proposed strategy is not applied). In the former case, each single EV obtains less energy than in the latter. However, the total amount of energy that the operator provides is higher under the $SoCD_{thr}$=0.7 scenario than under the $SoCD$=0.8 one, due to the increase in the EVs' maximum arrival rates (by γ=1.28, Figure 5.5). As a result, the operator can make a discount d_{max}=4.23% (Figure 5.6) in the price that sells energy without financial losses. For the same reason (increase in the maximum arrival rate by γ=1.47), the maximum discount in the case where Σ=100% and $SoCD_{thr}$=0.65 is d_{max}=6.54%. Therefore, although it is reasonable to assume that the EV drivers would more easily accept to recharge their batteries up to $SoCD_{thr}$=0.7 instead of $SoCD_{thr}$=0.65, the FCS operator can make the $SoCD_{thr}$=0.65 case more attractive by providing greater discounts. Finally, it should be noted that any discount lower than d_{max} results in higher operator's revenue. This is shown in Table 5.2, which presents the revenue of the operator versus different discount levels.

Table 5.2: Operator's revenue versus different discount levels.

Case	Revenue (€)						
$SoCD$=0.8	**91.4**						
Discount (%)	1	2	3	4.23	5	6.54	7
Case	Revenue (€)						
$SoCD_{thr}$=0.7, $\Sigma = 100\%$	94.5	93.5	92.6	**91.4**	90.7	89.2	88.8
$SoCD_{thr}$=0.65, $\Sigma = 100\%$	96.8	95.9	94.9	93.7	92.9	**91.4**	91.0

6 Performance evaluation of a multi-standard fast charging station for electric vehicles

In this chapter, a more holistic approach is presented for the derivation of the EV classes' recharging patterns compared to the analysis of the previous chapter. Specifically, the recharging patterns of the EV classes are denoted by the increase of their batteries' SoC, which is considered to be a random variable that may follow any possible distribution function. This consideration enables the utilization of real-case statistical data regarding the amount of energy obtained during a fast charging session, such as the data presented in [89]. Moreover, it contributes to a more flexible analysis because the EVs are not necessarily assumed to recharge their batteries up to the maximum departure SoC level, as in chapter 5. An additional novelty of the present analysis is that the EVs are classified not only by their battery size, but also by the fast charging option (DC or AC) they use. This issue enables the modeling of FCSs that consist of multi-standard CSs containing a CHAdeMO, a CCS and an AC outlet in the same cabinet [90].

Based on the aforementioned novelties, a FCS is modeled as two multi-class M/G/s queues (one for the AC and one for the DC charging queue). The operator's overall daily profit margin, the EVs' mean waiting time in each queue and the tail of the queue waiting time are initially derived under the assumption that a flat-rate pricing policy (FPP) is implemented during the entire duration of the day. Under the FPP, the amount of energy obtained by the EVs is likely to be high because it is mainly determined by the drivers' preferences, rather than actual needs. In turn, this may lead to long waiting times in the queue, especially during peak traffic periods. The flat fee per obtained kWh pricing scheme is one of the most prevalent pricing policies in the existing market of fast charging services [91]-[94], while it also indicates the upper bound of the EVs' queue waiting time.

A different pricing policy is also proposed, where the FCS operator sets energy thresholds and increases the price per obtained kWh for those customers that request amounts of energy greater than the arranged thresholds. The proposed scheduled pricing policy (SPP) is activated during parts of the day where the load of the FCS is high and the queue waiting time rises to unacceptably high levels. The objective of the SPP is to reduce the load of the system and the queue waiting time by regulating both the EVs' arrival rates and recharging patterns.

This chapter is organized as follows. In section 6.1, we derive the FCS operator's daily profit, the EVs' mean waiting time in the queue and the tail of the queue waiting time when the FPP is activated. In section 6.2, the SPP is formulated, while it is also presented the analysis of the FCS when the FPP or the SPP are activated during different parts of the day. Finally, in section 6.3, we evaluate the operation of the FCS and the effectiveness of the SPP by providing numerical examples.

6.1 Fast charging station's operation when the FPP is activated

The FCS is located in a densely populated area and consists of s multi-standard CSs. The CSs are equipped with a CHAdeMO and a CCS outlet that provide the same power P_{DC}, as well as with an AC outlet that provides P_{AC}. According to the technical specifications of the CSs [90], CHAdeMO and CCS outlets of the same CS cannot operate simultaneously. On the contrary, the simultaneous operation of the AC outlet with one of the DC outlets is feasible. For this reason, the EVs that request service by either a CHAdeMO or a CCS outlet form a DC queue, while the EVs that request service by an AC outlet form a separate AC queue. In this section, the operation of the DC system is thoroughly analyzed; due to the fact that the analysis of the AC system follows a similar process, the derivation of the AC performance metrics is described in a more synoptic manner.

6.1.1 EVs' recharging pattern and charging time

The EVs served by the DC outlets (CHAdeMO and CCS) are divided into C_{DC} classes, based on their battery size, B_c with $c=(1,2,...,C_{DC})$. The amount of energy E_c that a c-class EV obtains is defined by the following relation:

$$E_c = \Delta SoC_c B_c \tag{6.1}$$

where ΔSoC_c is the increase in its battery SoC during the fast charging session. Under the FPP, the amount of energy that the EVs obtain depends only on the drivers' preferences and/or estimated needs, since the price does not alternate with the amount of the obtained energy. Therefore, ΔSoC_c is considered to be a random variable that follows a general CDF $F_c(x) = P(\Delta SoC_c \leq x)$, with a corresponding PDF $f_c(x)$. In practice, ΔSoC_c ranges between a minimum and a maximum value $\Delta SoC_{c,\min}$ and $\Delta SoC_{c,\max}$, respectively (i.e. $f_c(x)$ is truncated in the interval $[\Delta SoC_{c,\min}, \Delta SoC_{c,\max}]$).

By taking into account that the charging power P_{DC} is constant during fast charging [83], the charging time T_c of a c-class EV is derived as:

$$T_c = \Delta SoC_c \frac{B_c}{P_{DC}}. \tag{6.2}$$

Based on (6.2), T_c is also a random variable, with a minimum value $T_{c,\min} = \Delta SoC_{c,\min}\,(B_c/P_{DC})$ and a maximum value $T_{c,\max} = \Delta SoC_{c,\max}\,(B_c/P_{DC})$. The CDF of T_c is derived by:

$$G_c(t) = P(T_c \leq t) = P(\Delta SoC_c \leq \tfrac{P_{DC}}{B_c} t) = F_c(x_c(t)) \tag{6.3}$$

where $x_c(t)=(P_{DC}/B_c)t$. Furthermore, the PDF $g_c(t)$ and the mean m_c of T_c are respectively

obtained as follows:

$$g_c(t) = \frac{d}{dt} G_c(t) = \frac{P_{DC}}{B_c} f_c(x_c(t)). \tag{6.4}$$

$$m_c = \int t g_c(t) dt \tag{6.5}$$

6.1.2 Fast charging station's load and operator's daily profit margin

The EVs arrive at the FCS by following a Poisson process, while the mean arrival rates of the EV classes differ during the day, depending mainly on the traffic. For example, the expected arrival rates may be higher during afternoon when people return from their jobs and the traffic is heavy, compared to the arrival rates at night when the majority of the people are at their homes and the traffic is lighter. Therefore, the mean arrival rate of c-class EVs during a time interval I_δ of duration τ_δ is denoted as $\lambda_{c,\delta}$, while the load of c-class EVs during the same interval is defined as:

$$a_{c,\delta} = \lambda_{c,\delta}\ m_c. \tag{6.6}$$

As noted in the previous chapter, in a multi-class queuing system where the arrival process of each class is Poisson, the superposed arrival process is also Poisson. The aggregated mean arrival rate of the system at the time interval I_δ is computed by summing the mean arrival rates the EV classes:

$$\lambda_\delta = \sum_{c=1}^{C} \lambda_{c,\delta}. \tag{6.7}$$

For the same reason (Poisson arrival process), the total load of the system equals the sum of the loads of the EV classes:

$$a_\delta = \sum_{c=1}^{C} a_{c,\delta}. \tag{6.8}$$

Recall also (from section 5.2) that the total load of the system a_δ represents the mean number of busy CSs, while $a_{c,\delta}$ represents the mean number of CSs occupied by c-class EVs at time interval I_δ. Therefore, the mean power charged to the EVs during an interval I_δ is calculated by multiplying the mean number of occupied CSs a_δ by the power output of each CS:

$$P_{V,\delta} = a_\delta P_{DC} \tag{6.9}$$

while the mean energy provided to the EVs is obtained as follows:

$$E_{V,\delta} = \tau_\delta P_{V,\delta} \tag{6.10}$$

When the FPP is activated, the operator charges the served EVs with a constant price R. Therefore, the revenue of the operator during the time interval I_δ is:

$$RVN_\delta = R\ E_{V,\delta} \tag{6.11}$$

In order to compute the operator's expenses (cost of supplied energy) during the same time interval, we make the following considerations: i) the interval I_δ consists of H_δ time slots Z_h of duration d_h, where $h = \{1, 2, \dots H_\delta\}$ and $\tau_\delta = \sum_{h=1}^{\mathrm{H}_\delta} d_h$. ii) During these time-slots, the price R_h that the FCS operator buys energy is constant. The expenses of the operator are then determined by the following relation:

$$EXP_\delta = \sum_{h=1}^{H_\delta} R_h\, d_h\, P_{V,\delta} \tag{6.12}$$

which expresses the sum of products of the mean charging energy $d_h P_{V,\delta}$ during each time slot by the cost of the supplied energy R_h. The revenue and the expenses of the FCS operator during a time interval I_δ are computed through the relations (6.11) and (6.12). By assuming that a day consists of Δ time intervals, the operator's daily revenue and expenses for the DC system are respectively obtained as follows:

$$RVN_{DC} = \sum_{\delta=1}^{\Delta} RVN_\delta. \tag{6.13}$$

$$EXP_{DC} = \sum_{\delta=1}^{\Delta} EXP_\delta. \tag{6.14}$$

Given the battery sizes, the recharging patterns and the arrival rates of the AC classes C_{AC}, as well as the power rate of the AC outlets, the operator's daily revenue RVN_{AC} and expenses EXP_{AC} for the AC system are calculated by following the same process (6.1)-(6.14). Furthermore, the operator's overall profit margin is expressed as the normalized profit:

$$\Gamma = \frac{(RVN_{DC} + RVN_{AC}) - (EXP_{DC} + EXP_{AC})}{RVN_{DC} + RVN_{AC}}. \tag{6.15}$$

6.1.3 EVs' queue waiting time

In this section the QoS metrics of the system i.e. the EVs' mean waiting time in the queue and the tail of the queue waiting time are calculated. The EVs' mean waiting time in the queue in a multi-class M/G/s system is determined based on the analysis presented in the former chapter. The first and foremost step is to derive the CDF of the superposed charging

time of the system T_δ during the interval I_δ:

$$G_\delta(t) = P(T_\delta \leq t) = \sum_{c=1}^{C} k_{c,\delta} G_c(t) \tag{6.16}$$

where $k_{c,\delta} = \lambda_{c,\delta}/\lambda_\delta$ denotes the probability that a c-class EV enters an arbitrary CS. The the mean m_δ and the coefficient of variation v_δ of the superposed charging time distribution are then derived as follows:

$$m_\delta = \int t g_\delta(t) dt, \qquad g_\delta(t) = \frac{d}{dt} G_\delta(t) \tag{6.17}$$

$$v_\delta = \int t^2 g_\delta(t) dt - m_\delta^2 \tag{6.18}$$

while, the utilization rate of the system during the interval I_δ is:

$$\rho_\delta = \frac{\lambda_\delta \; m_\delta}{s} = \frac{a_\delta}{s}. \tag{6.19}$$

The determination of the aforementioned parameters enables the computation of the EVs' mean waiting time in the DC queue $W_{DC,\delta}$ during the time interval I_δ by following the process described in the previous chapter (equations (5.15)-(5.22)).

Besides the mean waiting time in the queue, an additional criterion for assessing the effective operation of a FCS is the tail of the queue waiting time, which denotes the probability that the customers' waiting time in the queue $T_{Q,\delta}$ is longer than a predefined time period T_L. This probability is approximated through the following relation, by incorporating the superposed multi-class metrics m_δ, ρ_δ and a_δ into the single-class analysis presented in [87]:

$$P(T_{Q,\delta} > T_L) = Q(s, \rho_\delta) \; exp\left\{ -\frac{s(1-\rho_\delta) T_L}{m_\delta O_{G,\delta}} \right\} \tag{6.20}$$

$$Q(s, \rho_\delta) = \frac{(\rho_\delta s)^s}{s!(1-\rho_\delta)} \left[\sum_{r=0}^{s-1} \frac{\alpha_\delta^r}{r!} + \frac{\alpha_\delta^s}{s!} \left(1 - \frac{\alpha_\delta}{s}\right)^{-1} \right]^{-1} \tag{6.21}$$

$$O_{G,\delta} = \frac{L_{\delta,M/G/s}}{L_{\delta,M/M/s}} \tag{6.22}$$

where $L_{\delta,M/G/s}$ and $L_{\delta,M/M/s}$ denote the mean number of customers waiting in the queue in an M/G/s and an M/M/s system, respectively, and they are calculated as in section 5.2. Finally, given the battery sizes, the recharging patterns and the arrival rates of the AC classes, as well as the power rate of the AC outlets, the mean waiting time and the tail of the queue waiting time for the AC system are calculated by following the process described in this section regarding the DC system.

6.2 Fast charging station's operation when the SPP is activated

The queue waiting time depends on the EVs' arrival rates and charging times. Taking into account that the FCS is located in a densely populated area, the EVs' arrival rates are expected to be high, especially during peak traffic hours. Furthermore, the charging times depend on the amount of energy obtained during a charging session. Researchers in [95] report that the EV drivers usually overestimate their energy needs. Moreover, under the FPP, the amount of obtained energy is likely to be high because it is mainly determined by the drivers' preferences or/and overestimated needs, rather than actual needs. Therefore, the queue waiting time may rise to unacceptably high levels. In this section we consider that there is a subset $\{\Omega\} \in \{\Delta\}$ of time intervals I_ω, $\omega \in \{\Omega\}$ during which the waiting time W_ω is higher than a maximum allowed for QoS satisfaction limit W_Q. Over these time intervals the operator activates the SPP, which aims at reducing the system's load and queue waiting time by regulating both the EVs' arrival rates and recharging patterns.

The main feature of the SPP is that the FCS operator sets various energy thresholds $E_{thr,j}$ $(j = 1, 2, ..., J)$ for all EVs, which correspond to thresholds in the change of SoC of c-class EVs $\Delta SoC_{c,thr,j} = E_{thr,j}/B_c$. SPP dictates that the EVs are allowed to obtain up to $E_{thr,j}$ kWh at the same price R as in the FPP. However, in case they request to get more than $E_{thr,j}$, they are charged with a higher price $R'_j > R$. The operator determines the $E_{thr,j}$ values depending on the level of the queue waiting time. Specifically, when the waiting time lies on the range $W_{l,j} < W_\omega \leq W_{l,j+1}$, the activated energy threshold is $E_{thr,j}$. As shown in Figure 6.1, higher waiting time levels correspond to the activation of lower energy thresholds. The consideration of multiple thresholds minimizes the effect of an abrupt energy reduction that could result in significant decrease in customers' convenience and comfort. Furthermore, the minimum value of the selected energy thresholds $E_{thr,J}$ can be determined by taking into account statistical data for the EVs' mean covered distance between two consecutive charging events [96]. The aforementioned selection reflects the operator's intention to promote a more sensible recharging pattern during peak traffic periods.

In order to derive the queue waiting time and the operator's profit when the SPP is activated, we divide each EV class into 3 additional subclasses c_1, c_2 and c_3. The rationale of this division, the determination of the arrival rate, as well as the derivation of the recharging pattern and charging time distribution of each subclass are presented in the following section, which refers to the DC system. The same process can be used for the analysis of the AC system.

6.2.1 EVs' subclasses

Under the SPP, the division of each EV class to 3 subclasses is necessary, due to the fact that the price change may affect the number of the EVs that will enter the FCS and the amount

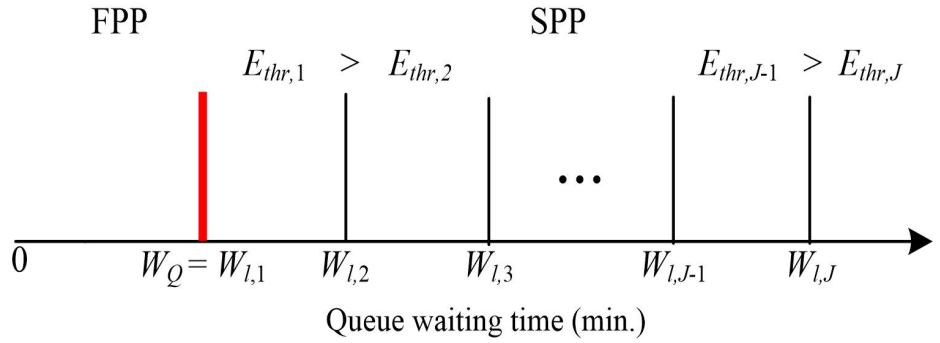

Figure 6.1: Activated energy thresholds depending on the waiting time level.

of energy they will eventually obtain. The proportion of c-class EVs that would request more than $E_{thr,j}$ kWh under the FPP is computed by the integral $\Pi_{c,j} = \int_{\Delta SoC_{c,thr,j}}^{\Delta SoC_{c,\max}} f_c(x)dx$. Due to the price increase under the SPP, we assume that a percentage of those EVs $\Xi_{c,j}$ quit the FCS without recharging, while a percentage $\Sigma_{c,j}$ decide to obtain exactly as much energy as the operator's threshold, in order to avoid the higher price.

Subclass c_1 consists of the remaining $N_{c1,j} = \Pi_{c,j}(1 - \Xi_{c,j} - \Sigma_{c,j})$ percentage of EVs which, despite the price increase, request the same amount of energy as in the FPP because it is necessary for reaching their destination. It should be noted that the proposed SPP dictates that if the EV drivers charge more than the arranged energy threshold, then they have to pay the higher price $R_j^{'}$ for each kWh obtained. Hence, since subclass c_1 drivers decide to charge their EVs under a higher price (because they need more energy for reaching their destination than the arranged threshold), it is considered that they are not strongly motivated to change their recharging pattern. Therefore, the mean arrival rate of subclass c_1 EVs is $\lambda_{c1,\omega,j}{=}N_{c1,j}\lambda_{c,\delta}$, while their recharging pattern is obtained by truncating the function $f_c(x)$ in the interval $[\Delta SoC_{c,thr,j}, \Delta SoC_{c,\max}]$:

$$f_{c_1,j}(x) = \begin{cases} \frac{f_c(x)}{\int_{\Delta SoC_{c,thr,j}}^{\Delta SoC_{c,\max}} f_c(x)dx}, & \Delta SoC_{c,thr,j} \leq x \leq \Delta SOC_{c,\max} \\ 0 & \text{otherwise.} \end{cases} \tag{6.23}$$

The above normalization is necessary so as the integral of $f_{c_1,j}(x)$ to become equal to 1. The charging time PDF $g_{c_1,j}(t)$ of subclass c_1 EVs is derived by following the same procedure as in section 6.1.1 for the derivation of $g_c(t)$ from $f_c(x)$:

$$g_{c_1,j}(t) = \begin{cases} \frac{P_{DC}}{B_c} f_{c_1,j}(x_c(t)), & T_{thr,j} \leq t \leq T_{c,\max} \\ 0 & \text{otherwise} \end{cases} \tag{6.24}$$

where $x_c(t) = (P_{DC}/B_c)t$ and $T_{thr,j} = E_{thr,j}/P_{DC}$. By defining as m_{c_1} the mean of $g_{c_1}(t)$, the load of subclass c_1 is $\alpha_{c_1,\omega,j}{=}\lambda_{c_1,\omega,j}\ m_{c_1,j}$.

Subclass c_2 consists of the proportion $N_{c2,j} = \Pi_{c,j}\Sigma_{c,j}$ of the EVs that decide to obtain exactly $E_{thr,j}$ kWh. For these EVs, it is assumed that requesting more than $E_{thr,j}$ kWh is not indispensable; they can satisfy their urgent needs by obtaining as much energy as the arranged threshold. The mean arrival rate of subclass c_2 EVs is $\lambda_{c2,\omega,j}=N_{c2,j}\lambda_{c,\delta}$, while their recharging pattern and charging time CDF are denoted, respectively, as:

$$F_{c_2,j}(x) = \begin{cases} 1 & x = \Delta SoC_{c,thr,j} \\ 0 & \text{otherwise} \end{cases} \tag{6.25}$$

$$G_{c_2,j}(t) = \begin{cases} 1 & t = T_{thr,j} \\ 0 & \text{otherwise.} \end{cases} \tag{6.26}$$

The mean charging time of subclass c_2 EVs is $m_{c_2,j}=T_{thr,j}$, while the load of subclass c_2 is $\alpha_{c_2,\omega,j} = \lambda_{c_2,\omega,j}m_{c_2,j}$.

Finally, subclass c_3 consists of the proportion $N_{c_3,j}=1-\Pi_{c,j}$ of c-class EVs that would request up to $E_{thr,j}$ kWh under the FPP. This type of EVs do not alternate their recharging pattern under the SPP because they are charged with the same price as in the FPP. The mean arrival rate of subclass c_3 EVs is $\lambda_{c3,\omega,j}=N_{c3,j}\lambda_{c,\delta}$, while their recharging pattern is obtained by truncating the function f_c in the interval $[\Delta SoC_{c,\min}, \Delta SoC_{c,thr,j}]$:

$$f_{c3,j}(x) = \begin{cases} \frac{f_c(x)}{\int_{\Delta SoC_{c,\min}}^{\Delta SoC_{c,thr,j}} f_c(x)dx}, & \Delta SoC_{c,\min} \leq x \leq \Delta SOC_{c,thr,j} \\ 0 & \text{otherwise.} \end{cases} \tag{6.27}$$

Furthermore, the corresponding charging time PDF is:

$$g_{c_3,j}(t) = \begin{cases} \frac{P_{DC}}{B_c} f_{c_1,j}(x_c(t)), & T_{c,\min} \leq t \leq T_{thr,j} \\ 0 & \text{otherwise} \end{cases} \tag{6.28}$$

By defining as m_{c_3} the mean of $g_{c_3,j}(t)$, the load of subclass c_3 EVs is $\alpha_{c_3,\omega,j}=\lambda_{c_3,\omega,j}m_{c_3,j}$.

Having determined the arrival rate and the charging time distribution of each subclass, the mean and the tail of the queue waiting time under the SPP can be derived by following the procedure described in section 6.1.3.

6.2.2 Operator's daily profit margin

In this section the operator's revenue and expenses are initially determined during a time interval I_ω where the SPP is activated. Afterwards, the operator's overall daily profit margin is also computed given that the SPP is activated during the intervals I_ω, $\omega \in \{\Omega\}$, and the FPP is activated during the intervals I_δ, $\delta \in \{\Delta\} - \{\Omega\}$.

Under the SPP, the EVs that belong to subclasses c_1 recharge at price R'_j, while the EVs that belong to subclasses c_2 and c_3 recharge at price R. As it is noted in section 5.2,

the load of each class (or subclass) represents the mean number of CSs occupied by the EVs belonging to this class (or subclass). Hence, the amount of energy provided to the EVs at price $R_j^{'}$ during each time interval I_ω is:

$$E_{V,\omega,j,R_j^{'}} = \tau_\omega P_{DC} \sum_{c=1}^{C} a_{c_1,\omega,j} \tag{6.29}$$

while, the energy provided to the EVs at price R is:

$$E_{V,\omega,j,R} = \tau_\omega P_{DC} \sum_{c=1}^{C} (a_{c_2,\omega,j} + a_{c_3,\omega,j}). \tag{6.30}$$

Therefore, the operator's revenue during the time intervals that the SPP is activated is determined as follows:

$$RVN_{\omega,j} = R\, E_{V,\omega,j,R} + R_j^{'}\, E_{V,\omega,j,R_j^{'}} \tag{6.31}$$

while the daily revenue for the DC system is obtained by:

$$RVN_{DC}^{'} = \sum_{\forall\delta\in\{\Delta\}-\{\Omega\}} RVN_\delta \; + \sum_{\forall\omega\in\{\Omega\}} RVN_{\omega,j} \tag{6.32}$$

where the two summations correspond to the operator's revenue during the time intervals that the FPP or the SPP is activated, respectively.

Furthermore, the operator's expenses during a time interval that the SPP is activated is computed by the following relation:

$$EXP_{\omega,j} = \sum_{h=1}^{H_\omega} R_h\, d_h\, P_{V,\omega,j} \tag{6.33}$$

Note that equation (6.33) has the same form with equation (6.12); the only difference is that $P_{V,\delta}$ (the power charged to the EVs under the FPP) is replaced by the power charged to the EVs under the SPP:

$$P_{V,\omega,j} = P_{DC} \sum_{c=1}^{C} (a_{c_1,\omega,j} + a_{c_2,\omega,j} + a_{c_3,\omega,j}) \tag{6.34}$$

Therefore, the operator's daily expenses for the DC system when the SPP is activated during the intervals I_ω, $\omega\in\{\Omega\}$, and the FPP is activated during the intervals I_δ, $\delta\in\{\Delta\}-\{\Omega\}$ is determined as follows:

$$EXP_{DC}^{'} = \sum_{\forall\delta\in\{\Delta\}-\{\Omega\}} EXP_\delta \; + \sum_{\forall\omega\in\{\Omega\}} EXP_{\omega,j}. \tag{6.35}$$

For the AC system, the operator's daily revenue RVN'_{AC} and expenses EXP'_{AC} when the SPP is activated during specific time intervals over the day are calculated by following the same process. Recall also that the SPP is applied when the queue waiting time is unacceptably high, and that the arranged energy thresholds depend on the level of the queue waiting time. Therefore, the time intervals where the SPP is activated and the arranged energy thresholds for the AC system may be different than those for the DC system.

Based on the aforementioned analysis and considerations, the overall daily profit margin of the FCS operator is computed by the following relation:

$$\Gamma' = \frac{(RVN'_{DC} + RVN'_{AC}) - (EXP'_{DC} + EXP'_{AC})}{RVN'_{DC} + RVN'_{AC}}. \tag{6.36}$$

6.3 Numerical results

In this section, we evaluate the operation of a FCS that consists of s=5 multi-standard CSs. The power output of the DC outlets (CHAdeMO and CCS) is P_{DC}=45 kW, while the power output of the AC outlet is P_{AC}=43 kW [90]. We also consider the four most popular EV models of the Spanish market, which are: i) Nissan Leaf (battery capacity: B_1=24 kWh, fast charging option: DC), ii) BMW i3 (battery capacity: B_2=18.8 kWh, fast charging option: DC), iii) Mitsubishi i-MiEV (battery capacity:B_3=16 kWh, fast charging option: DC) and iv) Renault ZOE (battery capacity: B_1=22 kWh, fast charging option: AC) [88]. Given the fast charging options and the battery capacities of the aforementioned EV models, the DC system consists of C_{DC}=3 EV classes, whereas the AC system consists of C_{AC}=1 EV class.

The operation of the FCS is evaluated during a day, which is considered to be divided into Δ=3 time intervals (TI) I_1=16.00-22.00, I_2=22.00-08.00 and I_3=08.00-16.00. The FCS operator is supplied with energy from a Spanish energy retailer [97]. Table 6.1 summarizes the number of time slots Z_h that each TI contains, and the price R_h of the supplied energy during these time slots. Furthermore, each TI is characterized by a Poisson procedure for the EV arrivals; Table 6.2 presents the mean arrival rates of the EV classes for each TI expressed in number of EVs per hour. It is assumed that during I_1 the traffic is heavy (a great number of people returns from their jobs), and therefore the arrival rates are high. In contrast, during night hours (I_2), the traffic is light, and hence the arrival rates are considered to be low. For the third time interval (I_3), which corresponds to working hours, the arrival rates are assumed to take intermediate values. Given that Leaf is the most popular EV model, its arrival rate is used as reference for the computation of the arrival rates of the other EV models. To this end, λ_1 takes integer values, while the arrival rates of the other EV models are computed by dividing their population by the population of Leaf [88]. Note also that $\lambda_{DC,\delta}$ represents the superposed arrival rate of the whole DC system, and it is computed through equation 6.7, while $\lambda_{AC,\delta}$ tackles the arrival rate of Zoe, which is the only AC class.

Table 6.1: Energy tariffs of the Spanish retailer [97]

Time Intervals	Time slots	Energy price (€/KWh)
I_1= 16.00-22.00	Z_1= 16.00-18.00	0.1
	Z_2= 18.00-22.00	0.119
I_2= 22.00-08.00	Z_1= 22.00-00.00	0.1
	Z_2= 00.00-08.00	0.072
I_3= 08.00-16.00	Z_1= 08.00-16.00	0.1

Table 6.2: Mean arrival rates of the EV classes

TI	Mean arrival rates (EVs/h)				
	λ_1 (Leaf)	λ_2 (i3)	λ_3 (i-MiEV)	$\lambda_{DC,\delta}$	$\lambda_{AC,\delta}$ (Zoe)
I_1	10	2.5	6	18.5	5
I_2	2	0.5	1.2	3.7	1
I_3	6	1.5	3.6	11.1	3

When the FPP is activated during the whole day, the FCS operator charges the served EVs with a constant price R. In this case, we consider that the EVs' recharging patterns $f_c(x)$ with $c=1, 2, 3$, for the DC system and $c=1$ for the AC system follow the Beta PDF. The aforementioned PDF is appropriate for modeling random variables that are limited to intervals of finite length [98], such as the EVs' ΔSoC in an FCS, which is limited to the interval $[\Delta SoC_{c,min}, \Delta SoC_{c,max}] = [0, 0.8]$. The shape parameters α_c, b_c of each Beta PDF, as well as the resulting mean values are summarized in Table 6.3. The values of α_c, b_c have been selected based on the data presented in [89] regarding the recharging pattern of Nissan Leaf in a FCS. The mean value of ΔSoC_1 in Table 6.3 corresponds to the mean energy obtained by the Leaf drivers during a fast charging session (9.3 kWh [89]). Due to lack of data regarding the other EV classes, it is considered that they also obtain 9.3 kWh, on average, during a fast charging session. The resulting recharging patterns of the three DC classes are shown in Figure 6.2. Given the recharging patterns, Table 6.3 also presents the corresponding mean charging times of the EV classes, which are calculated based on the analysis of section 6.1.1. Furthermore, the analysis of section 6.1.2 can be used for the determination of R given the operator's desirable profit margin Γ. Based on the energy tariffs (Table 6.1), the EVs' arrival rates (Table 6.2) and mean charging times (Table 6.3), as well as a desirable daily profit margin of Γ=30%, the price is computed to be R=0.146 (€/KWh).

Table 6.3: Recharging patterns of the EV classes

DC system, P_{DC} = 45 kW						
c	Model	E_c (kWh)	α_c	b_c	mean ΔSoC_c	m_c (EVs/h)
1	Leaf	24	4.3	6.8	0.39	0.21
2	i3	18.8	9.3	9.5	0.49	0.21
3	i-MiEV	16	14	10.1	0.58	0.21
AC system, P_{AC} = 43 kW						
1	Zoe	22	8.8	12	0.42	0.22

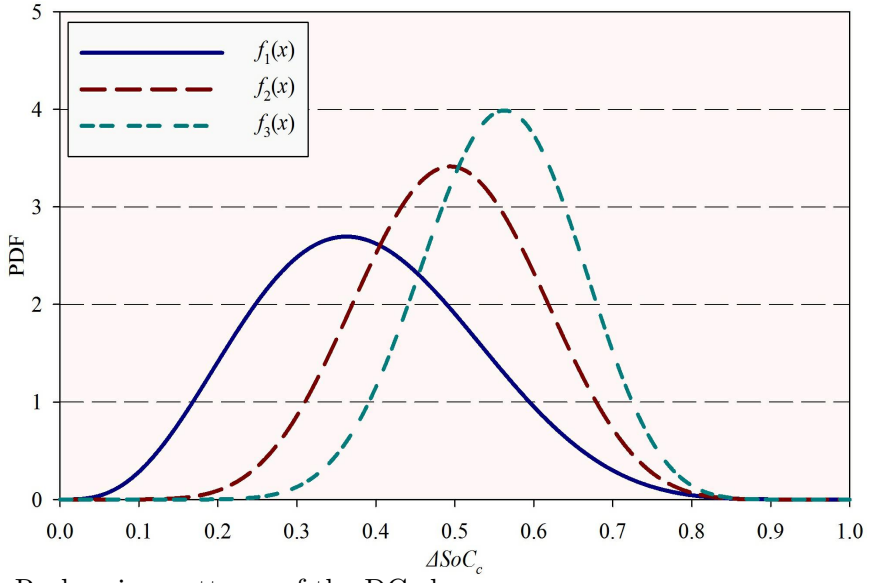

Figure 6.2: Recharging patterns of the DC classes.

Table 6.4: Queue waiting time results

	DC system					**AC system**				
M/G/s	v_δ=0.087	Analysis		Simulation		v_δ=0.063	Analysis		Simulation	
TI	$\rho_{DC,\delta}$	W_δ (min.)	Tail (%)	W_δ (min.)	Tail (%)	$\rho_{AC,\delta}$	W_δ (min.)	Tail (%)	W_δ (min.)	Tail (%)
I_1	0.77	3	25.55	3.03	25.75	0.22	0.013	0.103	0.013	0.103
I_2	0.15	0.003	0.021	0.003	0.021	0.04	0	0	0	0
I_3	0.46	0.29	2.53	0.29	2.54	0.13	0.001	0.01	0.001	0.01
M/M/s	v_δ=1	Analysis		Simulation		v_δ=1	Analysis		Simulation	
TI	$\rho_{DC,\delta}$	W_δ (min.)	Tail (%)	W_δ (min.)	Tail (%)	$\rho_{AC,\delta}$	W_δ (min.)	Tail (%)	W_δ (min.)	Tail (%)
I_1	0.77	5.28	33.91	5.32	34.15	0.22	0.018	0.161	0.018	0.162
I_2	0.15	0.004	0.031	0.004	0.031	0.04	0	0	0	0
I_3	0.46	0.45	4.14	0.46	34.15	0.13	0.002	0.015	0.002	0.015

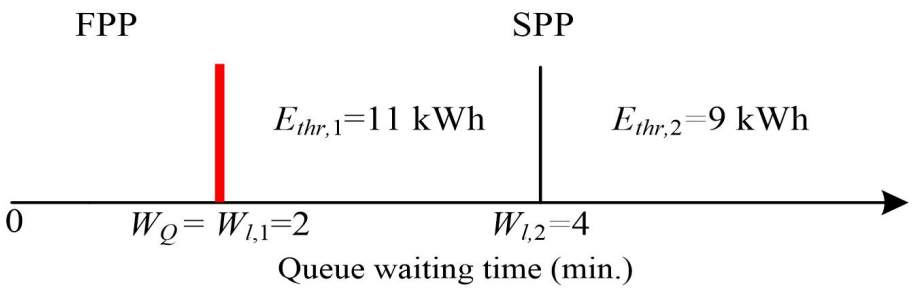

Figure 6.3: Activated energy thresholds depending on the waiting time level.

In what follows, we present analytical and simulation results for the EVs' mean waiting time in the DC and AC queue, as well as the tail of the queue waiting time when the FPP is activated. Recall that the tail of the queue waiting time denotes the probability that the customers' queue waiting time will be longer than a specified time period T_L. For the present numerical evaluation we assume that $T_L = 4$ min.. Table 6.4 compares the results of our multi-class M/G/s model with a corresponding M/M/s model. For a fair comparison of the two models, the recharging patterns of the EV classes in the M/M/s case are considered to follow the exponential distribution with the same mean ΔSoC_c values as in Table 6.3. Furthermore, in both cases, the EVs' arrival rates are given in Table 6.2. The simulation results are obtained by our EV simulator that considers the same arrival and charging procedures with the corresponding analytical models. For the derivation of the analytical results, the arrival rates $\lambda_{DC,\delta}$ and $\lambda_{AC,\delta}$ are mapped to utilization rate values $\rho_{DC,\delta}$ and $\rho_{AC,\delta}$, respectively, by using equation 6.19. Table 6.4 also contains the coefficient of variation of the superposed charging time distribution v_δ, which is derived through equation 6.18. The results prove the high precision of our model, since the difference between analysis and simulation is less than 1%. Furthermore, the results indicate that the M/M/s model overestimates the queue waiting time. This is because the sensitivity introduced by v_δ is not taken into account. In the M/M/s model $v_\delta = 1$, by definition. Another advantage of our model is the utilization of real-case statistical data for the EVs' recharging patterns [89], which is not possible when the M/M/s model is applied.

We proceed by assessing the effectiveness of the proposed SPP in terms of EVs' waiting time reduction. As shown in Figure 6.3, we consider that the FCS provides high QoS when the EVs' mean waiting time in the queue is less than W_Q=2min. Based on this QoS criterion and the results presented in Table 6.4, the AC system operates effectively during the entire duration of the day when the FPP is implemented. On the other hand, the EVs' mean waiting time in the DC queue exceeds the targeted value during the time interval I_1. The FCS operator can activate the SPP during this specific interval in order to reduce both the EVs' mean waiting time in the DC queue and the tail of the queue waiting time. Since the queue waiting time during is 3 mins., the selected energy threshold according to Figure 6.3 is $E_{thr,1}$=11 kWh.

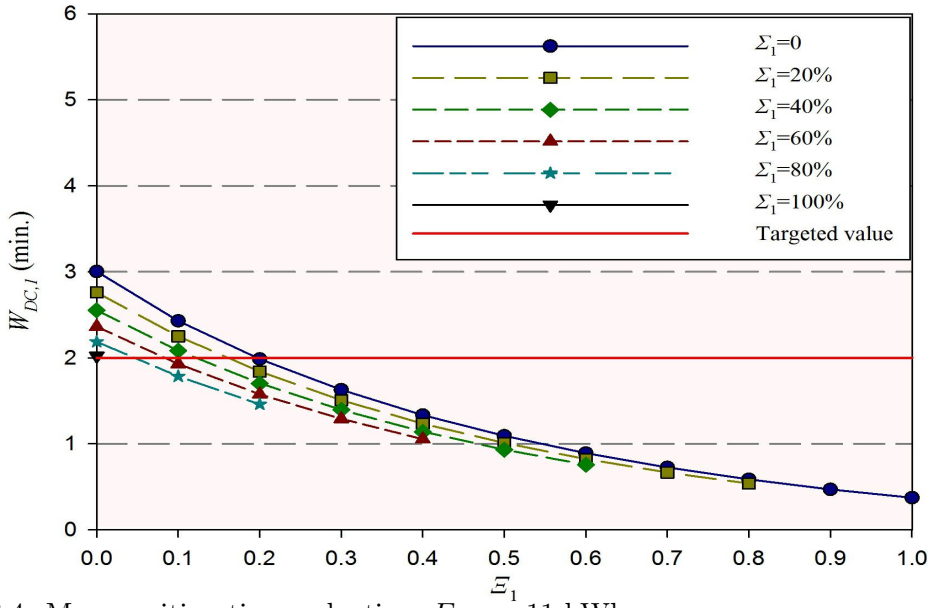

Figure 6.4: Mean waiting time reduction, $E_{thr,1}$=11 kWh.

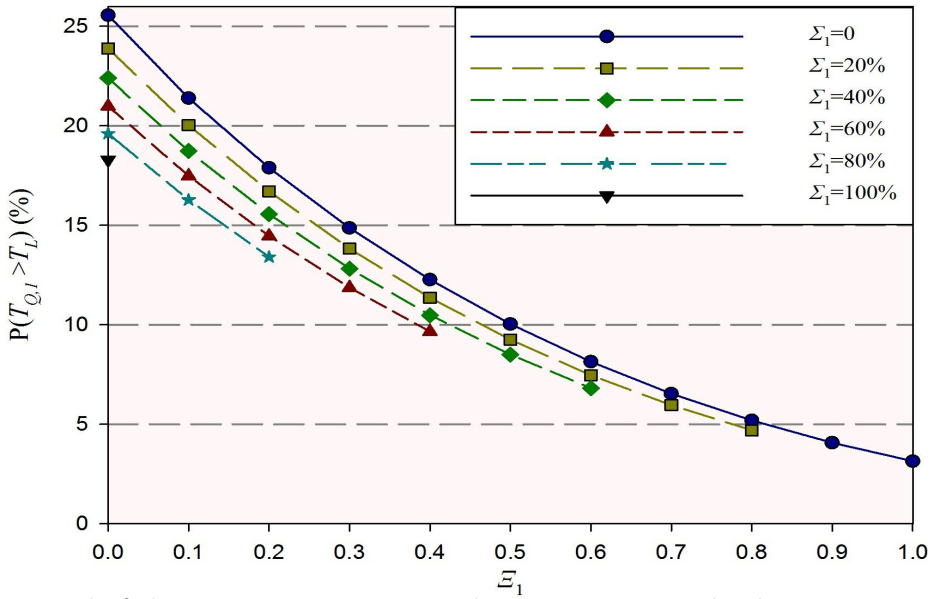

Figure 6.5: Tail of the queue waiting time reduction, $E_{thr,1}$=11 kWh.

Figures 6.4 and 6.5 evaluate the effectiveness of the proposed SPP versus the parameters $\Xi_{c,j}$ and $\Sigma_{c,j}$. Recall that $\Xi_{c,j}$ denotes the amount of the EVs of each class that quit the FCS without recharging, while $\Sigma_{c,j}$ denotes the amount of the EVs of each class that decide to obtain as much energy as the selected energy threshold. For presentation purposes, we assume that $\Xi_{1,1}$=$\Xi_{2,1}$=$\Xi_{3,1}$=Ξ_1 and $\Sigma_{1,1}$=$\Sigma_{2,1}$=$\Sigma_{3,1}$=Σ_1. It should also be noted that the case where Σ_1=Ξ_1=0 corresponds to the queue waiting time when the FPP is applied. According to figure 6.4, as the amount Σ_1 of the EVs that decide to obtain less energy under the SPP compared to the FPP case increases, the queue waiting time is reduced. This is due to the decrease of the system's superposed charging time, which based on equation 6.19 leads to lower utilization rate values. According to figure 6.5, the utilization rate and the queue waiting time are further reduced with the increase of Ξ_1, which reflects the EVs' arrival rate reduction.

Next, it is considered that the EVs' arrival rates are 10% higher than those presented in Table 6.2, which result in a queue waiting time during the interval I_1, $W_{DC,1}$ = 5.7 mins.. In this case, the operator sets the energy threshold to be equal to its minimum value. Specifically, it is considered that the $E_{thr,2}$ value is selected by taking into account the EVs' mean traveled distance between two consecutive charging events and the energy consumption of the EV class with the largest battery capacity. In [96], the mean traveled distance is reported to be 45 km, while the average energy consumption of a Nissan Leaf EV, according to real-case tests, is 0.2 kWh/km [99]. By multiplying the the mean traveled distance with average energy consumption, the energy threshold is set to be equal to 9 kWh. Figure 6.6 evaluates the effectiveness of SPP for this energy threshold.

The aforementioned case studies prove that given the expected level of the queue waiting time, under the FPP, the operator can effectively reduce it to acceptable limits by activating the SPP and by appropriately selecting different energy thresholds.

We now proceed to the determination of the operator's daily profit margin $\Gamma^{'}$ when the SPP is activated during the interval I_1 and the FPP is activated during the intervals I_2 and I_3. It should be noted that the EVs' arrival rates are assumed to be equal to the values provided by Table 6.2, and hence the energy threshold is set to be $E_{thr,1}$ = 11 kWh. We also consider that under the SPP, the price $R_1^{'}$ for those EVs that obtain more than $E_{thr,1}$ = 11 kWh is set to be 5% higher than R. Figure 6.7 presents the profit margin $\Gamma^{'}$ versus the $\Sigma_1 - \Xi_1$ pairs of Figures 6.4 and 6.5. It is observed that the activation of the SPP during the time interval I_1 leads to higher profit margins, compared to the case where the FPP is activated during the whole day. On the one hand, this is because the operator charges the EVs that obtain more than $E_{thr,1}$ kWh, i.e. those belonging to subclasses $c_{1,1}$, with a higher price. On the other hand, it is also observed that $\Gamma^{'}$ gradually rises with the increase of the EVs Ξ_1 that quit the FCS. This outcome can be interpreted as follows: greater values of Ξ_1 correspond to lower amount of energy drawn by the EVs during the interval I_1. This, in turn, leads to both lower operator's revenue and expenses. Despite the decrease in revenue,

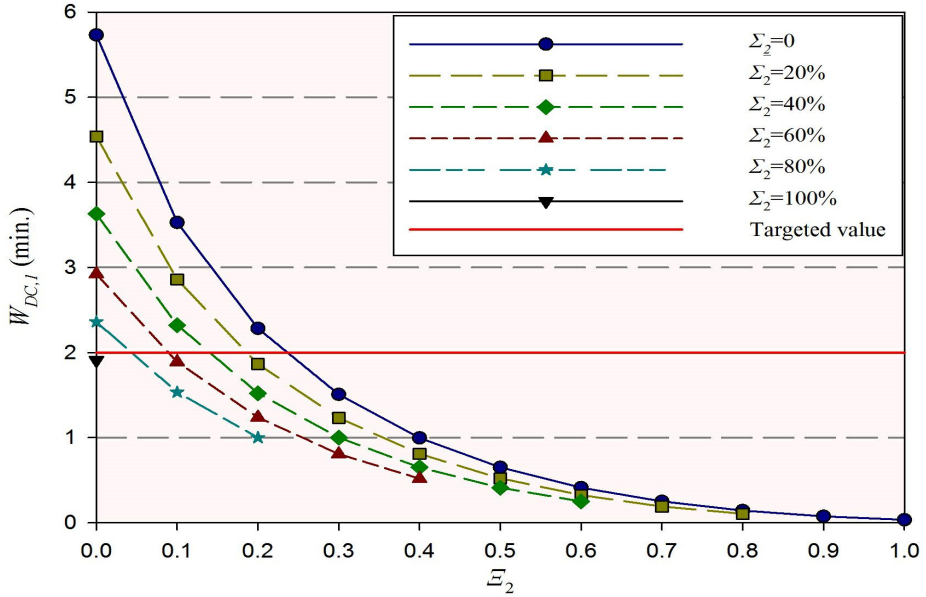

Figure 6.6: Mean waiting time reduction, $E_{thr,2}$=9 kWh.

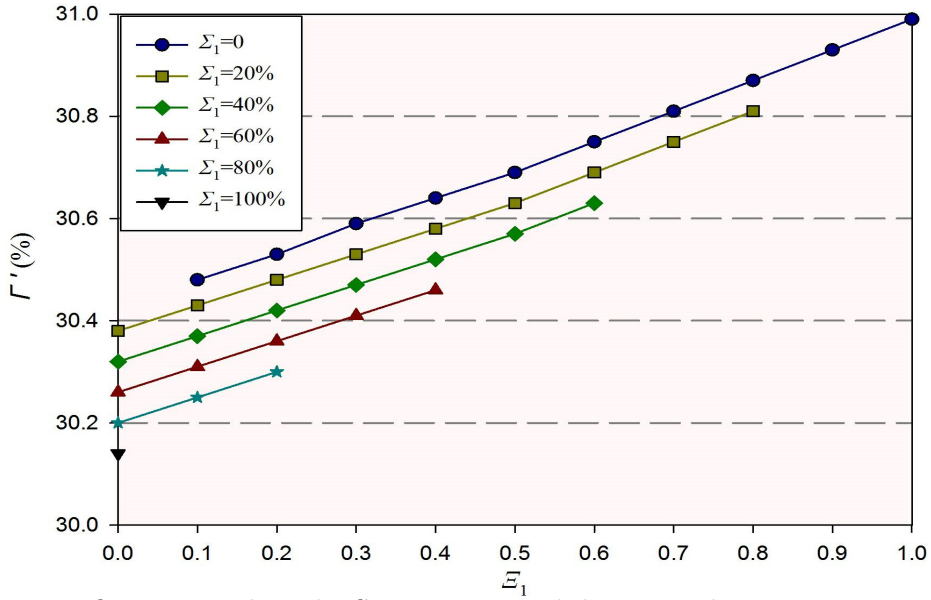

Figure 6.7: Profit margin when the SPP is activated during peak energy cost.

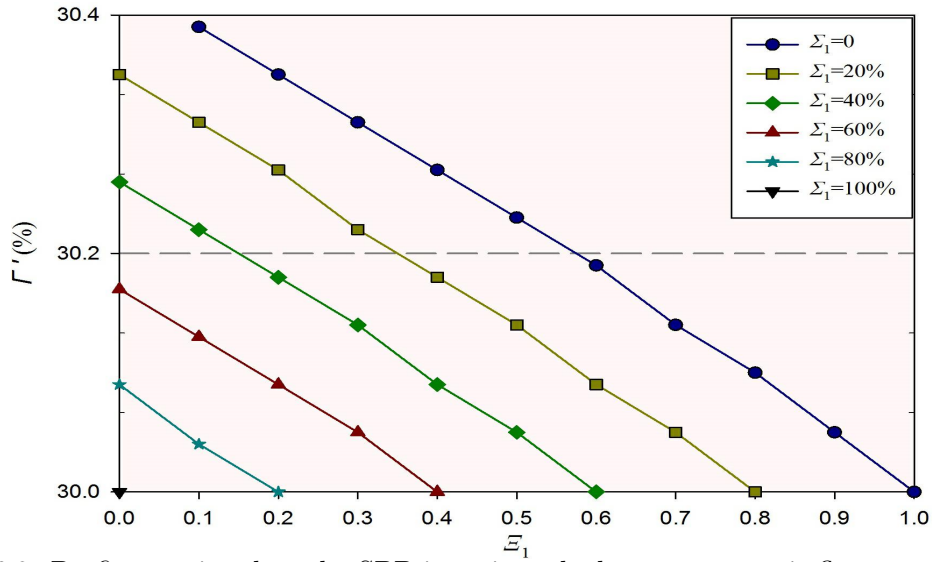

Figure 6.8: Profit margin when the SPP is activated, the energy cost is flat-rate.

the fact that the operator buys energy at a higher price over the interval I_1, compared to the intervals I_2 and I_3 (Table 6.1), combined with the decrease in the energy need to be bought during this specific interval, result in higher daily profit margins.

The aforementioned outcome is derived when the activation of the SPP coincides with the peak energy price period (Table 6.1). We also consider another case study where the operator buys energy at a constant price during the whole day. As Figure 6.8 shows, in this case, the profit margin $\Gamma^{'}$ is higher than $\Gamma = 30\%$ (profit margin when the FPP is applied during the whole day) as far as there are EVs belonging to subclasses $c_{1,1}$ ($\Xi_1 + \Sigma_1 < 1$). This is because those EVs obtain more than $E_{thr,1}$ kWh, and hence they are charged with a higher price when the SPP is activated.

The scenarios examined in this section refer to the operation of a single FCS, which consists of 5 CSs. Next, we consider that the same operator owns two additional neighboring FCSs, consisting of 4 and 8 CSs, respectively. It is also assumed that the arrival rates of the former (4 CSs station) are 40% lower, while the arrival rates of the latter (8 CSs station) are 40% higher than the arrival rates presented in Table 6.2. In this new case study, it is considered that the EV drivers visiting the initial FCS have three choices; a) charge up to $E_{thr,1}$ at price R, b) charge more than $E_{thr,1}$ at price $R_1^{'}$, or c) visit one of the neighboring FCSs and obtain as much energy as they want at price R. For this new case study, the performance of the two additional FCSs when all customers quit the initial FCS ($\Xi_1 = 1$) seeking for being served to the neighboring stations is evaluated. Figure 6.9 presents the queue waiting time during the interval I_1 versus the parameter U, which denotes the percentage of EVs that leave the initial FCS and join any of the additional FCSs. It is observed that the small FCS can accommodate up to 25% of the drivers coming from the initial station, while the large FCS can accommodate up to 75%. Hence, by optimally routing the EV drivers with high energy needs to the proper stations, the operator can keep the queue waiting time in all stations lower than the QoS criterion.

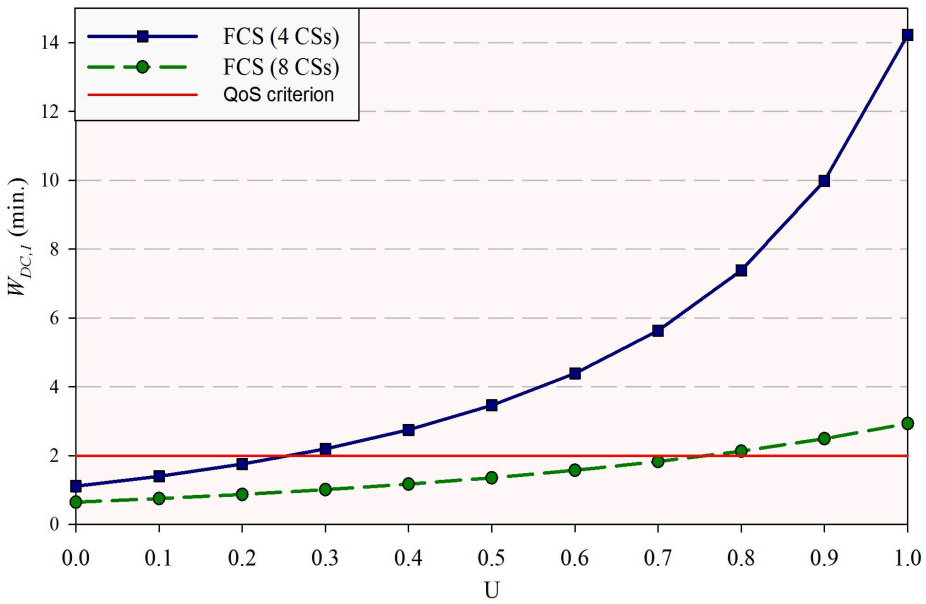

Figure 6.9: Waiting time in the two additional FCSs.

7 Thesis conclusions and future works

This chapter completes the dissertation by summarizing our main contributions and providing some potential research lines for future investigation. In particular, section 7.1 contains the most significant concluding remarks, while section 7.2 outlines the open research issues related to our contributions.

7.1 Concluding remarks

The major contributions of this thesis are divided into two main parts. The first part is confined to chapters 3 and 4, which determine the optimal sizing and operation planning of MGs by using the MILP optimization technique, while the second part includes chapters 5 and 6, which analyze the operation of FCSs for EVs by using queuing theory models.

Chapter 3: This chapter demonstrates the advantages of cooperation among neighboring urban buildings that form a MG and are able to exchange energy in order to achieve reduced energy costs. A MILP optimization model is proposed that targets to determine the optimal capacities of the buildings' equipment (PVs, inverters and ESSs), as well as the optimal power operation plan of the MG, by incorporating the buildings' power consumption patterns, the electricity prices and the carbon emission taxes. The cooperative scheme is compared with the case where the buildings optimize their equipment sizes and power operation plan individually (energy exchanges do not take place). The obtained results indicate that energy exchanges affect the equipment sizing and vice versa, since the optimal capacities to be installed are higher under the cooperation scenario. On the one hand, this leads to higher installation, maintenance and replacement costs. On the other hand, the energy supplying and carbon emission costs are much lower, and hence the cooperative scheme's total cost is lower than the sum of the buildings' total costs when they are optimized individually.

Chapter 4: The analysis of chapter 3 has two main limitations. The first one is that the energy exchanges take place only among buildings that are connected to the low voltage of the same distribution transformer. A more flexible and efficient topology is proposed in chapter 4 where the various buildings are interconnected through a DC bus. In this way, neighboring buildings that are fed by different distribution transformers can exchange energy without needing to use the medium voltage lines of the distribution system. The second limitation of the analysis in chapter 3 is the formulation of the objective function, which minimizes the total cost of the system. By doing so, some MG participants may achieve more savings than other members. In chapter 4 the objective function is formulated based on the Nash bargaining method, which maximizes the deviation of the buildings' costs from their maximum cost (i.e. the cost when they are optimized individually). In this way the coalition savings are equally distributed among the participating members. Moreover, the analysis of

chapter 4 takes into account the operation of V2B systems, which provides extra flexibility on the MGs' power management. Finally, a significant contribution of this chapter is that examines the possibility of more buildings to be part of an already existing coalition several years after its formation. This event improves the energy exchange potential in the MG and it is profitable for both the old and new participants. However, it is proved that participating in the MG from the beginning is a more profitable choice. In addition, there is a maximum lag beyond which joining in an already established coalition becomes fully unattractive.

Chapter 5: This chapter analyzes the operation of a FCS as a multi-class M/G/s system. The customers' mean waiting time in the queue, the EVs' charging load, and the operator's revenue are computed with high precision, as the comparison of analytical and simulation results indicates. The main advantages of the proposed analysis are: a) the classification of the various EV models by their battery size, and b) the derivation of the charging time distribution of each class based on the state of charge of its battery when arriving at the charging station. The proposed model is also used to compute the maximum arrival rate capacity of the FCS, given a maximum value for the queue waiting time. Firstly, the number of efficiently served customers and the operator's revenue are computed under the assumption that the EVs' charging demands are uncontrolled. Moreover, a charging strategy is formulated, which enables the operator to increase its revenue and the arrival rate capacity of the FCS by motivating customers to reduce their energy demands.

Chapter 6: The model of chapter 5 is limited to the analysis of EV classes that use DC power, while it is also assumed that customers recharge their batteries up to the maximum level. Going one step forward, this chapter takes into account EVs that use both DC and AC outlets, and hence the FCS consists of two separate queues. In addition, a more realistic approach is adopted for modeling the EVs' recharging patterns, which are denoted by the increase in their batteries' charging level. Based on the random arrival rates and recharging patterns of the DC and AC classes, the proposed model determines the mean waiting time in each queue, as well as the operator's overall profit margin. The system is firstly evaluated under the assumption that the EVs are allowed to obtain as much energy as they want at a flat-rate price. In this case the queue waiting time may rise to unacceptably high levels during peak-traffic hours. The impact of a different pricing policy on the queue waiting time is also examined. According to this policy the operator sets fixed energy thresholds and penalizes those customers that request amounts of energy greater than the arranged thresholds. The activation of the proposed pricing policy during peak-traffic periods leads to not only lower queue waiting times, but also higher profits margins for the FCS operator.

7.2 Future works

The main contributions presented in this dissertation are precursors of several new research lines for future investigation.

The cooperative scheme of chapter 3 considers that the buildings are equipped with PVs, and ESSs, while the scheme of chapter 4 takes also into account the presence of V2B systems. Although these units satisfy the customers' electrical demands, sources that satisfy the buildings' thermal and cooling loads are not taken into account. For example, CHP units that provide both electrical and thermal energy can increase the self-sufficiency of the MGs in winter months. In addition, the heat output of CHP units can be used as a source of energy to drive a cooling system, such as an absorption chiller, increasing the MGs' self-sufficiency in summer months. Such units will be taken into account in our future work.

Chapters 3 and 4 examine the energy exchange potential being created by neighboring residential, public and commercial buildings, however, the presence of industrial loads is not taken into account. The cooperation of multiple urban MGs with MGs located in industrial areas of the cities will be examined in a future work. In this case, the energy transfer losses should be taken into consideration due to the long distances among the sites.

The cooperation of public charging stations, equipped with RES, with neighboring urban MGs is also an interesting topic for future investigation. For example, the charging spots and the RES of a FCS can be connected to the DC bus of the MG topology presented in chapter 4. In this case, a multi-objective optimization scheme will be formulated where the MGs' implementation and operating costs, the utilization of RES, as well as the charging station's operator profits and the EV users' QoS are jointly optimized.

Chapters 5 and 6 evaluate the operation of a single FCS in terms of customers' QoS and operator's profits. The mathematical modeling and performance evaluation of a network of FCSs will be part of a future work. The impact of such a network on the distribution system will be examined by considering technical objectives, such as the minimization of load variance and power losses, and the preservation of voltage quality.

Finally, although a deterministic model can be effectively used for describing the long-term operation of MGs when the optimal sizing problem is examined (as in chapters 3 and 4), a stochastic model is required for describing the short-term (i.e. daily) operation. Therefore, the problem of optimizing the daily cooperation of urban MGs with charging stations for EVs and industrial loads will be described by combining the stochastic model developed in chapter 6 for analyzing the operation of FCSs, with the stochastic modeling of load demands, RES production and price variability. In this scenario, the MPC technique will be integrated into the model, since it is an effective way for mitigating forecast errors. Moreover, the concept of virtual energy transactions will be investigated, since it allows prosumers without physical connection to participate in the energy exchange process. In this scenario, the participating members make bids (offers to buy or sell energy) in the day-ahead market without the intent of delivering or consuming physical energy real-time.

References

[1] H. R. Khosravani, M. D. M. Castilla, M. Berenguel, A. E. Bruano and P. M. Ferreira, "A Comparison of Energy Consumption Prediction Models Based on Neural Networks of a Bioclimatic Building," *Energies*, vol 9, no 1, pp. 57, 2016.

[2] S. Tan, J. Yan, C. Lee, H. Hashim and B. Chen, "A holistic low carbon city indicator framework for sustainable development," *Appl. Energy*, vol 185 pp. 1919-1930, 2017.

[3] C. E. A. Mulligan and M. Olsson, "Architectural implications of smart city business models: an evolutionary perspective," *IEEE Commun. Mag.*, vol 51, no. 6, pp. 80-85, 2013.

[4] J. Liu, J. Wan, D. Jia, B. Zeng, D. Li, C. H. Hsu and H. Chen, "High-Efficiency Urban Traffic Management in Context-Aware Computing and 5G Communication," *IEEE Commun. Mag.*, vol 55, no. 1, pp. 34-40, 2017.

[5] A. Solanas, C. Patsakis, C. Conti, M. Vlachos, I. S. Ramos, V. Falcone and A. Martinez-Balleste, "Smart health: a context-aware health paradigm within smart cities," *IEEE Commun. Mag.*, vol 52, no. 8, pp. 74-81, 2014.

[6] B. P. Koirala, E. Koliou, J. Friege, R. A. Hakvoort and P. M. Herder "A review on the prediction of building energy consumption," *Renew. and Sustain. Energy Rev.*, vol 56, pp. 722-744, 2016.

[7] C. Carvillo, A. Sánchez-Miralles and J. Villar, "Energy management and planning in smart cities," *Renew. and Sustain. Energy Rev.*, vol 55 pp. 273-287, 2016.

[8] H. X. Zhao and F. Magoules, "A review on the prediction of building energy consumption," *Renew. Sustain.*, vol 16, pp. 3586-3592, 2012.

[9] P. Cazzorla, M. Gorner, J. Teter and W. Yi,"Global EV outlook 2016. Beyond one million electric cars, "OECD/IEA, 2016.

[10] T. Trigg and P. Telleen, "Global EV Outlook - Understanding the Electric Vehicle landscape to 2020, ", Clean Energy Ministerial. Report, 2013.

[11] M. Ghofrani, A. Arabali, M. Etezadi-Amoli and M. S. Fadali, "Smart scheduling and cost-benefit analysis of grid-enabled electric vehicles for wind power integration," *IEEE Trans. Smart Grid*, vol 5, pp. 2306-2313, 2014.

[12] E. A. Nanaki and C. J. Koroneos, "Comparative economic and environmental analysis of conventional, hybrid and electric vehicles-the case study of Greece," *Journal of Cleaner Production*, vol. 53, pp. 251-266, 2013

[13] E. T. P. SmartGrids, "Vision and Strategy for Europe's Electricity Networks of the Future," *European Commission* , 2006.

[14] E. Hossain, E. Kabalci, R. Bayindir, R. Perez, "Microgrid testbeds around the world: State of art," *Energy Conversion and Management*, vol. 86, pp. 132-153, 2014

[15] N. Hatziargyriou, "Microgrid Architectures and Control,"Wiley, 2013.

[16] M. van der Kam and W. van Sark,"Smart charging of electric vehicles with photovoltaic power and vehicle-to-grid technology in a microgrid; a case study" *Appl. Energy*, vol 152, pp. 20-30, 2015.

[17] S. Parhizi, H Lofti, A. Khodaei and S. Bahramirad, "State of the art in research on microgrids: A review," *IEEE Access*, vol. 3, pp. 890-925, 2015

[18] A. Tsikalakis and N. Hatziargyriou, "Centralized control for optimizing microgrids Operation," *Power and Energy Society General Meeting*, pp. 1-8, 2011.

[19] M. Yilmaz and P. T. Krein, "Review of battery charger topologies, charging power levels," *IEEE Trans. Power Elec.*, vol. 28, no. 5, pp. 2151-2169, 2013

[20] [Online]. Available: `https://www.nissanusa.com/electric-cars/leaf/charging-range/charging/`, accessed Apr. 26, 2018

[21] [Online]. Available: `http://media.mitsubishicars.com/channels/2017-i-MiEV/?la=1`, accessed Apr. 26, 2018

[22] [Online]. Available: `https://www.kia.com/us/en/content/ev-faqs_2016/welcome`, accessed Apr. 26, 2018

[23] [Online]. Available: `https://www.bmw.com/en/bmw-models/bmw-i/i3/2017/index.html`, accessed Apr. 26, 2018

[24] [Online]. Available: `http://www.plugincars.com/volkswagen-electric-e-golf-blue-e-motion`, accessed Apr. 26, 2018

[25] [Online]. Available: `https://www.renault.co.uk/vehicles/new-vehicles/zoe-250.html`, accessed Apr. 26, 2018

[26] [Online]. Available: `http://www.fueleconomy.gov/feg/findacar.shtml`, accessed Apr. 26, 2018

[27] [Online]. Available: `https://pushevs.com/electric-car-range-efficiency-epa/`, accessed Apr. 26, 2018

[28] L. Zhang, B. Shaffer, T. Brown and G. S. Samuelsen,"The optimization of DC fast charging deployment in California," *Appl. Energy*, vol 157, pp. 111-122, 2015.

[29] P. Sadeghi-Barzani, A. Rajabi-Ghahnavieh and H. Kazemi-Karegar "Optimal fast charging station placing and sizing," *Appl. Energy*, vol 125, pp. 289-299, 2014.

[30] S. Morse and K. Glitman,"Electric vehicles as grid resources," *Vermont Energy Investment Corporation*, 2014.

[31] S. Bakker, P. Leguijt and H. van Lente, "Niche accumulation and standardization - the case of electric vehicle recharging plugs," *Journal of Cleaner Production*, vol 94, pp. 155-164, 2015.

[32] I. Subotic, N. Bodo and E. Levi, "An EV Drive-Train With Integrated Fast Charging Capability," *IEEE Trans. Power Electron.*, vol 31, no. 2, pp. 1461-1471, 2016.

[33] efacec. [Online]. Available: `http://electricmobility.efacec.com/ev-qc45-quick-charger/`, accessed Apr. 26, 2018

[34] Southampton City Council. [Online]. Available: `http://www.southampton.gov.uk/roads-parking/travel/smartcities-card/`, accessed Apr. 26, 2018

[35] Amsterdam Smart City. [Online]. Available: `https://amsterdamsmartcity.com/projects`, accessed Apr. 26, 2018

[36] City of Stockholm. [Online]. Available: urlhttps://international.stockholm.se/city-development/the-smart-city/, accessed Apr. 26, 2018

[37] Dept Business [Online]. Available: `https://www.gov.uk/government/publications/smart-cities-background-paper`, accessed Apr. 26, 2018

[38] Ajuntament de Barcelona. [Online]. Available: `http://ajuntament.barcelona.cat/digital/ca`, accessed Apr. 26, 2018

[39] Agència d'Ecologia Urbana de Barcelona. [Online]. Available: http://bcnecologia.net/, accessed Apr. 26, 2018

[40] P. O. Kriet and M. Salani, "Optimal control of a residential microgrid," *Energy*, vol 42, no 1, pp. 321-330, 2012.

[41] A. Parisio, E. Rikos and G. Luigi "A model predictive control approach to microgrid operation optimization," *IEEE Trans. Control Systems Technology*, vol 22, no 5, pp. 1813-1827, 2014.

[42] Y Zhang, T. Zhang, R. Wang, Y Liu and B. Guo, "Optimal operation of a smart residential microgrid based on model predictive control by considering uncertainties and storage impacts," *Solar Energy*, vol 122, pp. 1052-1065, 2015.

[43] N. Paterakis, I. Pappi, A. Bakirtzis and J. Catalão, "Coordinated operation of a neighborhood of smart households comprising electric vehicles energy storage and distributed generation," *IEEE Trans. Smart Grid*, 2016.

[44] A. Ouammi , H. Dagdougui and R. Sacile, "Coordinated model predictive-based power flows control in a cooperative network of smart microgrids," *IEEE Trans. Smart Grid*, pp. 1-10, 2015.

[45] O. Erdnic, N. Paterakis, N.G. Pappi and A. G. Bakirtzis, "A new perspective for sizing of distributed generation and energy storage for smart households under demand response," *Applied Energy*, pp. 26-37, 2015.

[46] R. Atia, N. Yamada, "Sizing and Analysis of Renewable Energy and Battery Systems in Residential Microgrids," *IEEE Trans. Smart Grid*, vol. 7, no. 3, pp. 1204-1213, 2016.

[47] E. Mehleri, H. Sarimveis, N. Markatos, L. Papageorgiou, "A mathematical programming approach for optimal design of distributed energy systems at the neighbourhood level," *Energy*, vol. 44, no. 1, pp. 96-104, 2012.

[48] S. Singh, M. Singh, S. C. Kaushik "Feasibility study of an islanded microgrid in rural area consisting of PV, wind, biomass and battery energy storage system," *Energy Conversion and Management*, vol. 128, pp. 178-190, Mar. 2016.

[49] M. Shadmand and R. Balog "Multi-objective optimization and design of photovoltaic-wind hybrid system for community smart dc microgrid, " *IEEE Trans. Smart Grid*, vol. 5, no. 5, pp. 2635-2643, Sep. 2014.

[50] M. L. Di Silvestre, G. Graditi, E. R. Sanseverino, "A generalized framework for optimal sizing of distributed energy resources in micro-grids using an indicator-based swarm approach", *IEEE Trans. Ind. Informat.*, vol. 10, no. 1, pp.152-162, Feb. 2014.

[51] D. Zhang, N. J. Samsatli, A. D. Hawkes, D.J.L. Brett, N. Shah, L. G. Papageorgiou"Fair electricity transfer price and unit capacity selection for microgrids," *Energy Economics*, vol. 36, pp. 581-593, 2013.

[52] N. Liu, Q. Chen, J. Liu, X. Lu, P. Li and J. Lei, "A Heuristic Operation Strategy for Commercial Building Micro-Grids Containing EVs and PV System," *IEEE Trans. Ind. Electron.*, vol 62, no 4, pp. 2560-2570, 2015.

[53] X. Guan, Z. Xu and QS. Jia, "Energy-Efficient Buildings Facilitated by Microgrid," *IEEE Trans. Smart Grid*, vol 1, no 3, pp. 243-252, 2010.

[54] M. Gulin, A. Martincevic and V. Lesic, "Multi-level Optimal Control of a Microgrid-supplied Cooling System in a Building," *In PES ISGT-Europe*, 2016, pp. 1-6.

[55] X. Jin, X. Wang, Y. Mu, H. Jia, X. Xu and Y. Qi, "] Optimal Scheduling Approach for a Combined Cooling, Heating and Power Building Microgrid Considering Virtual Storage System," *In proc. IEEE PESGM*, 2016, pp. 1-5

[56] Y. Zhang, N. Gatsis and G. B. Giannakis, "Robust energy management for microgrids with high-penetration renewables," *IEEE Trans. Sustain. Energy*, vol. 4, no. 4, pp. 944-953, Oct. 2013.

[57] S. Bracco, F. Delfino, F. Pampararo and M. Robba, "A pilot facility for analysis and simulation of smart microgrids feeding smart buildings," *Sustainable Energy*, vol. 58, pp. 1247-1255, 2016.

[58] M. Hosseinzadeh and F. R. Salmasi , "Robust optimal power management system for a hybrid AC/DC micro-grid ," *IEEE Trans. Sustain. Energy*, vol. 6, no. 3, pp. 675-687, Jul. 2015.

[59] G. Graditi, M. Di Silvestre, R. Gallea and E. Riva Sanseverino, "Heuristic-based shiftable loads optimal management in smart micro-grids," *IEEE Trans. Ind. Informat.*, vol. 11, no. 1, pp. 271-280, Feb. 2015.

[60] PVWatts Calculator. [Online]. Available: `http://pvwatts.nrel.gov/`, accessed Apr. 26, 2018

[61] endessa. [Online]. Available: `https://www.endesaclientes.com/one-luz-maxi.html`, accessed Apr. 26, 2018

[62] G. Li, X. P. Zhang, "Modeling of plug-in hybrid electric vehicle charging demand in probabilistic power flow calculations," *IEEE Trans. Smart Grid*, vol. 3, no. 1, pp. 492-499, 2012.

[63] S. Bae and A. Kwasinski, "Spatial and temporal model of electric vehicle charging demand," *IEEE Trans. Smart Grid*, vol. 3, no. 1, pp. 394-403, Mar. 2012.

[64] H. Liang, I. Sharma, W. Zhuang and K. Bhattacharya "Plug-in electric vehicle charging demand estimation based on queueing network analysis," *in Proc. IEEE PES Gen. Meet.*, Washington, pp. 1-5, Mar. 2014.

[65] Q. Gong, S. Midlam-Mohler, E. Serra, V. Marano and G. Rizzoni, "PEV charging control for a parking lot based on queuing theory" *in Proc. ACC 2013*, Washington, pp. 1124-1129, 2013.

[66] D. Said, S. Cherkaoui and L. Khoukhi, "Queuing model for EVs charging at public supply stations," *in Proc. IWCMC*, pp. 65-70, 2013.

[67] C. Farkas and L. Prikler, "Stochastic modelling of EV charging at charging stations," *in Proc. ICREPQ*, pp. 28-30, 2012.

[68] A. Gusrialdi, Z. Qu, MA. Simaan, "Scheduling and cooperative control of electric vehicles' charging at highway service stations," *In Proc. IEEE 53rd An. Conf. Decision and Control (CDC)*, Dec. 2014, pp. 6465-6471.

[69] G. Michailidis, M. Devetsikiotis, S. Bhattacharya, A. Chakrabortty and F. Granelli "Local energy storage sizing in plug-in hybrid electric vehicle charging stations under blocking probability constraints" *In Proc. IEEE SmartGridComm,*, pp. 78-83, 2011.

[70] I. S. Bayram, G. Michailidis, M. Devetsikiotis, "Unsplittable load balancing in a network of charging stations under QoS guarantees," *IEEE Trans. Smart Grid*, vol. 6, no. 3, pp. 1292-1302, May 2015.

[71] I. S. Bayram, A. Tajer, M. Abdallah, K. Qaraqe, "Capacity planning frameworks for electric vehicle charging stations with multiclass customers," *IEEE Trans. Smart Grid*, vol. 6, no. 4, pp. 1934-1943, 2015.

[72] J. S. Vardakas, "Electric vehicles charging management in communication controlled fast charging stations," *In Proc. IEEE CAMAD*, Dec. 2014, pp. 115-119.

[73] K. Yunus, D. La Parra, H. Zelaya and M. Reza, "Distribution grid impact of Plug-In Electric Vehicles charging at fast charging stations using stochastic charging model," *in Proc. 14th Eur. Conf. Power Electron. Appl. (EPE)*, Birmingham, U.K., Aug. 2011, pp. 1–11.

[74] M. Alizadeh, A. Scaglione, J. Davies and K. S. Kurani, "A scalable stochastic model for the electricity demand of electric and plug-in hybrid vehicles,", *IEEE Trans. Smart Grid*, vol. 5, no.2, pp.848-860, 2014.

[75] P. Fan, B. Sainbayar, S. Ren, "Operation Analysis of Fast Charging Stations With Energy Demand Control of Electric Vehicles", *IEEE Trans. Smart Grid*, vol. 6, no.4, pp.1819-1826, Jul. 2015.

[76] S. Backhaus, G. W. Swift, S. Chatzivasileiadis, W. Tschudi, S. Glover, M. Starke, J. Wang, M. Yue, D. Hammerstrom, "DC Microgrids Scoping Study-Estimate of Technical and Economic Benefits," *Los Alamos National Laboratory*, Mar., 2007.

[77] Clean Technica. [Online]. Available: `https://cleantechnica.com/2015/05/07/tesla-powerwall-price-vs-battery-storage-competitor-prices-residential-utility-scale/`, accessed Apr. 26, 2018

[78] I. Zenginis, J. S. Vardakas, N. Zorba and C. Verikoukis, "Analysis and quality of service evaluation of a fast charging station for electric vehicles," *Energy*, vol. 112, pp. 669-678, Oct. 2016.

[79] I. Zenginis, J. S. Vardakas, N. Zorba and C. Verikoukis, "Performance Evaluation of a Multi-standard Fast Charging Station for Electric Vehicles," *IEEE Trans. Smart Grid,* 2017.

[80] [Online]. Available: `https://www.ipcc.ch/pdf/special-reports/sroc/Tables/t0305.pdf`, accessed Apr. 26, 2018

[81] T. Barker, S. Junankar, H. Pollitt, P. Summerton "Carbon leakage from unilateral environmental tax reforms in Europe, 1995-2005," *Energy Policy*, vol. 35, pp. 6281-6292, 2007.

[82] efacec. [Online]. Available: `https://www.chargepoint.com/files/Efecec_QC_50_DC_fast_charger_datasheet.pdf`, accessed Apr. 26, 2018.

[83] H. Hoimoja, A. Rufer, G. Dziechciaruk, and A. Vezzini, "An ultrafast EV charging station demonstrator," *in Proc. IEEE SPEEDAM*, pp. 1390-1395, Jun. 2012.

[84] Bhat, U. Narayan, "An introduction to queueing theory: modeling and analysis in applications," *Springer Science & Business Media*, 2008.

[85] Gautam, Natarajan, "Analysis of queues: methods and applications," *CRC Press*,2012.

[86] H. Akimaru and K. Kawashima, "Teletraffic Theory and Applications," *Springer Verlag*, Berlin, Germany, 1993.

[87] T. Kimura, "Approximations for multi-server queues: system interpolations," *Queueing Systems*, vol. 17, no. 3-4, pp. 347-382, 1994.

[88] motorpasion. [Online]. Available: `https://www.motorpasion.com/otros/ventas-en-espana-de-coches-y-furgonetas-electricas-en-2014`, accessed Apr. 26, 2018.

[89] J. Smart and D. Scoffield, "Workplace Charging Case Study: Charging Station Utilization at a Work Site with AC Level 1, AC Level 2, and DC Fast Charging Units," *Idaho National Laboratory*, 2014.

[90] efacec. [Online]. Available: `http://electricmobility.efacec.com/wp-content/uploads/2016/10/CS119I1307D1_QC45.pdf`, accessed Apr. 26, 2018.

[91] [Online]. Available:`http://www.plugincars.com/quick-charge-providers-choosing-billing-system-proves-tough-127731.html`, accessed Apr. 26, 2018.

[92] [Online]. Available:https://chargedevs.com/features/dc-fast-charging-billing-models-and-encouraging-efficient-usage/, accessed Apr. 26, 2018.

[93] [Online]. Available:http://www.blinknetwork.com/membership-faqs.html, accessed Apr. 26, 2018.

[94] [Online]. Available:https://fastned.nl/en/choose-your-priceplan, accessed Apr. 26, 2018.

[95] G. Tal, M. Nicholas and J. Davies, J. Woodjack, "Charging Behavior Impacts on Electric Vehicle Miles Traveled: Who Is Not Plugging In?," *Transportation Research Record: Journal of the Transportation Research Board*, Vol. 2454, pp. 53-60, 2014.

[96] J. Smart, W. Powell and S. Schey, "Extended Range Electric Vehicle Driving and Charging Behavior Observed Early in the EV Project," *SAE Techn. Paper*, 2013.

[97] [Online]. Available:https://www.somenergia.coop/es/tarifas-de-electricidad/#tarifa3, accessed Apr. 26, 2018.

[98] Eugene, D. Hahn, "Bayesian Methods for Management and Business: Pragmatic Solutions for Real Problems,"2014.

[99] [Online]. Available:http://www.consumerreports.org/cro/news/2011/09/nissan-leaf-full-test-results-are-in/index.htm, accessed Apr. 26, 2018.